

Treball Final de Grau

**Pre-design of an air cooling system used by a solar chimney.
Simulation with ANSYS® Fluent.**

**Pre-diseño de un Sistema de refrigeración de aire utilizado para
una chimenea solar y simulación con ANSYS® Fluent**

Bruno García Galindo

June 2017



**UNIVERSITAT DE
BARCELONA**

Aquesta obra està subjecta a la llicència de:
Reconeixement–NoComercial–SenseObraDerivada



<http://creativecommons.org/licenses/by-nc-nd/3.0/es/>

*Nuestras vidas realmente no nos pertenecen,
pertenecen al mundo, y a pesar de nuestros
esfuerzos por darle un sentido a éste, el mundo es
un lugar que va más allá de nuestro
entendimiento.*

Paul Auster

A mi familia

CONTENTS

SUMMARY	i
RESUM	iii
1. INTRODUCTION	1
2. OBJECTIVES	5
3. MATERIALS AND METHODS	7
3.1. GEOGRAPHIC LOCATION	7
3.2. LOCATION OF THE DESGIN IN THE FACILITY	8
3.3. HEAT EXCHANGER	9
3.4. PROCEDURE USING EMPIRIC EQUATIONS	10
3.5. PROCEDURE USING ANSYS®	13
3.5.1. Design of the geometry	14
3.5.2. Meshing of the design	15
3.5.3. Calculation of the solution	16
4. RESULTS	19
4.1. RESULTS USING EMPIRIC METHODS	19
4.2. RESULTS USING ANSYS®	23
4.3. RESULTS FOR DESIGN 13	26
4.4. RESULTS FOR DESIGN 14	35
4.5. COMPARISON BETWEEN THE EMPIRIC EQUATIONS AND ANSYS®	41
4.5.1. Comparison of arrangement A	41

4.5.2. Comparison of arrangement B	44
4.6. COMPARISON OF THE ANSYS® FINAL DESIGNS	46
5. CONCLUSIONS	49
6. RECOMMENDATIONS	51
6.1. DESIGN RECOMENDATIONS	51
6.2. SIMULATION RECOMENDATIONS	51
REFERENCES AND NOTES	53
ACRONYMS	55

APPENDICES **DVD**

The APPENDICES are located in the DVD attached (file name: *TFG García Galindo, Bruno 2016-17 P APPENDIX.pdf*)

[This electronic version has all the appendices at the end of the memory](#)

SUMMARY

Passive ventilation systems are being proposed as an alternative method to mechanical ventilation systems in view of their potential benefits in terms of operational cost, energy requirement and carbon dioxide emission.

Solar chimney is a passive ventilation system, which relies on solar energy. A significant amount of research has been done on solar chimney since the 1990s. Solar chimneys are generally tall wide structures constructed facing the sun, with a dark coloured matt surface, designed to absorb solar radiation. As the chimney becomes hot, so it heats the air inside it. The hot air rises up the chimney and is vented out of the top, drawing more air in at the bottom of the chimney.

Due to the complexity that presents the design of a solar chimney, the present work focuses on the design of the inlet of the system, where a heat exchanger will be placed so as to refrigerate the air coming from the outside of the building. The heat exchanger components are found in DIY stores.

The first stage of this work is focused on the determination using empiric models of the heat exchanger necessary to refrigerate air from the outside of the building using a staggered tube bench filled with water at 18 °C. The different inlet temperatures tested are 34 °C, 30 °C and 26 °C, reached in summer in the city of Barcelona. With the tube diameters used, 8 mm and 12 mm, the total number of tubes necessary to refrigerate the air is 20 in both cases. Subsequently, the results obtained are compared with a heat exchanger designed using ANSYS®.

In a second stage, on the basis of the data obtained from the empiric equations, different heat exchangers are designed and modelled using ANSYS® software, proposing two final designs, which are tested in different initial conditions. All of the designs proposed provide a considerable ΔT in order to make the temperature inside the building comfortable though some of them has a considerable ΔP .

RESUMEN

Los sistemas de ventilación pasiva han sido propuestos como un método alternativo a los sistemas de ventilación mecánica debido a sus beneficios en cuanto a costes de operación, requerimiento energético y emisiones de dióxido de carbono.

La chimenea solar, tema ampliamente estudiado desde 1990, es un sistema de ventilación pasiva que se basa en el aprovechamiento de la energía solar. En ella, el aire es calentado por acción de la radiación solar, creando una corriente ascendente que arrastra el aire proveniente del interior del edificio, creando una ventilación natural desde una toma de aire hasta su salida por la chimenea.

Debido a la complejidad que presenta el diseño de una chimenea solar, este trabajo se presenta como una parte del total, más concretamente, en la entrada de este sistema, donde se pretende instalar un intercambiador de calor que enfríe el aire que proviene del exterior. Este intercambiador está compuesto principalmente por piezas comerciales que se pueden encontrar en una ferretería.

Para ello, la primera parte del presente trabajo se centra en la determinación, mediante modelos empíricos, del intercambiador de calor necesario para refrigerar aire del exterior mediante el uso de un banco de tubos con agua que se encuentra a 18 °C. Se han ensayado tres condiciones de temperatura: 34 °C, 30 °C y 26 °C que pueden ser alcanzadas en los meses de verano en la ciudad de Barcelona. Con los dos diámetros de tubo utilizados (8 mm y 12 mm) se han obtenido un total de 20 tubos ambos diámetros. Posteriormente, los resultados obtenidos son comparados con un intercambiador de calor diseñado con el software ANSYS®.

En una segunda parte, y a partir de los datos obtenidos mediante ecuaciones empíricas, se diseñan diversos intercambiadores de calor y se modelizan con el software ANSYS®; de estos, se proponen dos diseños finales, que son testados en diferentes condiciones iniciales para evaluar su comportamiento sobre el aire. Todos los diseños propuestos consiguen una ΔT considerable que permite que la temperatura en el interior del edificio sea confortable, aunque algunos acarrearán una pérdida de presión considerable.

1. INTRODUCTION

Natural ventilation is an important sustainable building design strategy, and has attracted a strong growing interest because of its potential advantages over mechanical ventilation in terms of energy requirement, economic and environmental benefits. Mechanical ventilation systems are also associated with carbon dioxide emissions, which has a negative impact on the environment. Therefore, natural ventilation is being proposed as a means of saving energy to provide quality air and adequate thermal comfort [1].

Natural ventilation is provided either by thermal buoyancy or by wind. On one hand, wind driven ventilation is solely dependent on wind direction and wind intensity, which are two unpredictable factors that make design considerations very challenging and difficult. On the other hand, buoyancy driven ventilation depends on the temperature difference between the inside and outside of the building. It takes place even in hot summer windless days.

Several strategies have been developed to enhance natural ventilation; one of these strategies for enhancing buoyancy driven ventilation is the use of solar chimney for buildings [1]. A solar chimney is a type of passive solar heating and cooling system used to improve the natural ventilation of buildings by using convection of air heated by solar energy among other applications. It is designed to maximize ventilation effect by maximizing solar gain, thereby creating a sufficient temperature difference between the inside and the outside of the building to drive an adequate airflow rate.

The solar chimney has to be higher than the roof level, it has to be constructed on the wall facing direction of the sun with a dark coloured matt surface designed to absorb solar radiation. During the day, the solar radiation heats the chimney and the air within creating an updraft air in it. The suction created at the chimney base is useful to ventilate and refrigerate the building.

Solar chimneys are also used for heating, much like a trombe wall¹. If the top exterior vents are closed, the heated air is not exhausted out the top. At the same time, if high interior vents are opened to let the heated air into occupied spaces, it will provide convective air heating. This works even on cold and relatively cloudy days. It is useful for locations with hot summers and cold winters, switching between cooling and heating by adjusting which vents are open and closed [2] (Figure 1)

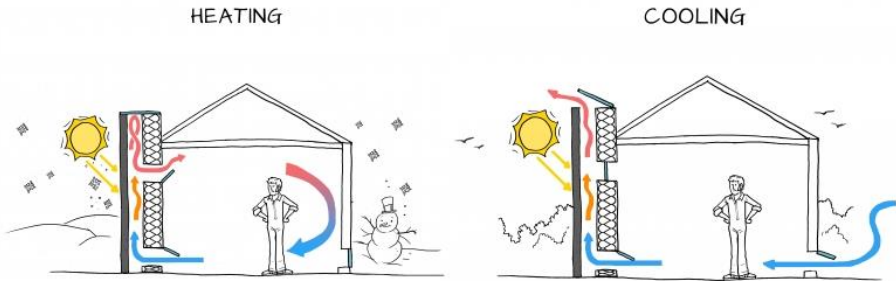


Figure 1. Example of how solar chimneys provide either heat or cool spaces [2]

Different variations in solar chimney design are likely to be found, due to different factors such as the location, climate, orientation, size of the space to be ventilated [1]. However, the basic elements such as solar collector, transparent cover, and apertures (inlet and outlet) are the part of every design (refer to Figure 2)

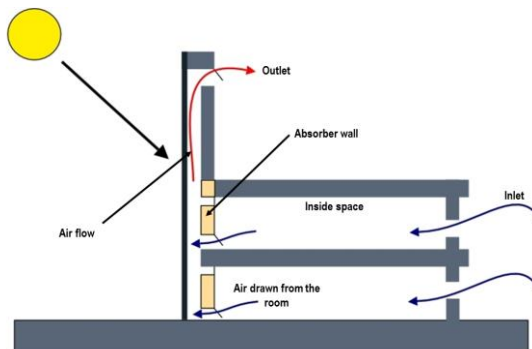


Figure 2. Schematic of solar chimney with vertical absorber geometry [3]

¹ **Trombe wall.** A Trombe wall is a system for indirect solar heat gain. It consists of a dark coloured wall of high thermal mass facing the sun, with glazing spaced in front to leave a small air space. The glazing traps solar radiation like a small greenhouse.

Due to the complexity of the geometry design and the afterwards analysis of the results, CFD (Computational Fluid Dynamics) modelling is commonly used to predict the flow pattern inside the chimney as well as in the space (room) adjoining the solar chimney. The existing CFD models predict velocity and temperature profiles along with other flow characteristics accurately, however, these models do not consider the thermal energy storage in the walls [4]. Nevertheless, the use of CFD modelling in solar chimney study has been increasing. These studies have greatly contributed to the current understanding of solar chimney, and are classified into three categories.

- a) Study based on small scale models
- b) Study based on large scale and full size models
- c) Study based on controlled indoor environment

The purpose of this work is focused in the inlet of the solar chimney (see Figure 2), where a heat exchanger will be placed next to the water supply connection in a load-bearing wall of the building. Thanks to the solar chimney damper, the air enters the building by the inlet of the heat exchanger, and, in its way through, is naturally cooled. The design of the heat exchanger will be carried out in two phases.

In a first stage, different designs of the heat exchanger will be proposed following the empiric equations in [5], [6]. The heat exchanger consists of a cross flow staggered tube bench, where the air is cooled using the mains of the building. It is important to notice that the geometry of the tubes has to be determined, as well as the arrangement that provides the best cooling for the air, considering the limitation of the space available. Once the heat exchangers have been designed, different simulations will be carried out making use of the ANSYS® software in order to compare the results obtained with the empiric equations.

In a second stage, on the basis of the results obtained from the empiric model, different designs for the heat exchanger will be proposed in order to achieve the maximum cooling for the air. For this purpose, the inclusion of elements such as horizontal, vertical and triangular baffles will be needed to guide the airflow properly in the heat exchanger.

It is important to notice though, that the heat exchanger is, at all times, linked with the whole solar chimney system. Because of this, the designs proposed may have variations according to the needs of the system. In addition to that, different improvements for the heat exchanger design are recommended. Finally, two heat exchanger designs are proposed, compared and discussed.

2. OBJECTIVES

The purpose of this study is to describe and pre-design different cross flow heat exchangers integrated in a load-bearing wall to decrease the inlet temperature of the air in a facility using a solar chimney and the mains water.

Determine using the bibliography the minimum number of tubes necessary to acclimatize air from the street using different inlet conditions. Compare the results obtained with the cases simulated using ANSYS®

The acquisition of knowledge of the ANSYS® software in order to simulate the different designs proposed using the Geometry, Mesh and Fluent tools. Be capable of judging the results and stabling conclusions with the different simulations carried out.

Determination of the configurations that provide the best heat exchanging conditions at the entrance of the facility, providing the least pressure drop, the simplest geometry and a minimum ΔT of 3 °C.

Furthermore, this work is a small part of a bigger project where different parts of the installation are studied separately and afterwards, joined together and optimised. Therefore, the final designs proposed may have variations depending on the needs of the rest of the system.

3. MATERIALS AND METHODS

This section shortly introduces the necessary fundamentals and methods for understanding the process setup, the geographic location of the building, the location of the heat exchanger in the building, the empiric models used for the heat exchanger and the software used to do the rigorous simulation.

3.1. GEOGRAPHIC LOCATION

In this work, the heat exchanger will be located in the shady part of a building, to provide the coolest air possible. The building is assumed located in the city of Barcelona, with Mediterranean climate. The temperature data has been provided by the *Departament de Física Aplicada de la Universitat de Barcelona*. Considering July as the hottest month of the year, the temperatures of everyday has been used to find the different inlet temperatures for the different cases studied, as illustrated in Figure 3.

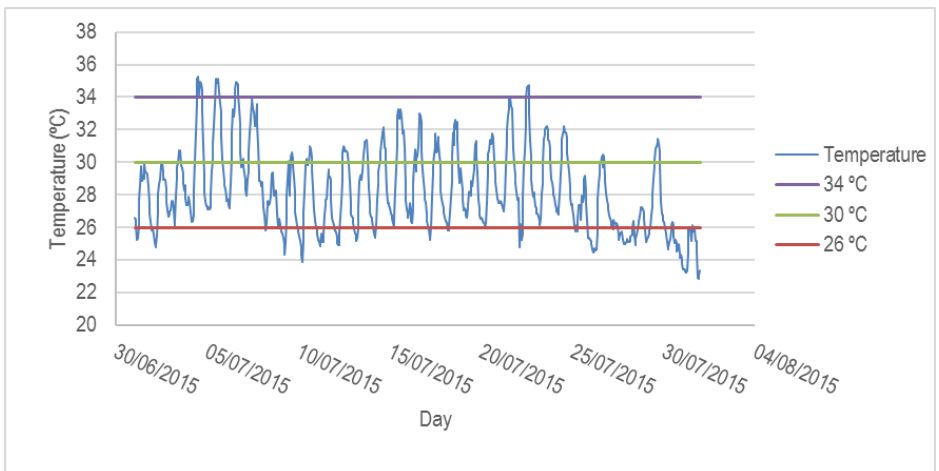


Figure 3. Average temperature of everyday of July in 2015

The inlet temperatures chosen for the design of the heat exchanger are listed below.

- 34 °C, which is the maximum temperature reached in the past years
- 30 °C as an approximation for the average temperature reached during daylight time
- 26 °C as an approximation of the average temperature reached in the night time.

3.2. LOCATION OF THE DESIGN IN THE FACILITY

The inlet previous to the heat exchanger consist of a typical opening in a load-bearing wall of a building, used to ventilate the air in a room. Here, the air flows by natural convection due to the chimney damper (Figure 4).



Figure 4. Plate covering in a house

Different inlet areas are found depending on the base and height of the transversal opening and the plate covering the entrance of the system. Making a research on different DIY (Do It Yourself) webs and shops, three different types of metal plate are chosen for this study (Figure 5).



Figure 5. From left to right. 15 x 30 cm, 25 x 25 cm, 20 x 20 cm metal plate

Taking into account the velocity inlet, which depends on the inlet area, different velocity inlets are found when the volumetric flow (q) is constant [7]. Evidence for this is in Table 1, where the base on each case is constant, thus the height of the inlet at a constant wide determines the velocity inlet (v_i). The higher the height, the lower the velocity inlet is.

Table 1. Inlet dimensions for the heat exchanger

Base (m)	Height (m)	Area (m ²)	q (m ³ /s)	v_i (m/s)
0.066	0.300	0.0198	0.099	5.0
0.066	0.250	0.0165	0.099	6.0
0.066	0.200	0.0132	0.099	7.5

3.3. HEAT EXCHANGER

The refrigeration system of the heat exchanger is composed by a series of staggered tubes filled with water by a bypass made from the water mains of the facility, next to the water supply.

It is very important to notice that the water has to be kept, as long as the climate conditions allow it, below 20 °C. Legionella is latent in temperatures below 20 °C, from 20 °C to 45 °C multiplies, over 50 °C does not multiply, and up to 70 °C dies. Therefore, the temperature of 18 °C is chosen for the refrigeration system [8].

Different commercial diameter tubes have been tested in the early stage of this work from different DIY stores, (Appendix 1. Tube geometry for the different cases located in the DVD attached). Due to the small space available, and, in order to increase the total area, the minor diameters for commercial tubes chosen were 8 mm and 12 mm made of copper due to its well-known heat transfer properties (see Figure 6). Higher tube diameter increment costs and the space needed, and lower diameter tubes increase the pressure drop of the water. In the cases studied, the temperature of the tube wall will be considered stationary at 18 °C.



Figure 6. On the right. 8 mm diameter tube. On the left. 12 mm diameter tube

3.4. PROCEDURE USING EMPIRIC EQUATIONS

Heat transfer by convection is due to fluid motion. A cold fluid adjacent to a hot surface receives heat which it imparts to the bulk of the cold fluid by mixing with it [9]. The motion of the fluid is an essential part of convective heat transfer. A key step in calculating the rate of heat transfer by convection is the calculation of the heat-transfer coefficient, h .

The present work is focused on the study of the flow through a tube bench. The equations to determine the average values for the heat-transfer coefficient by convection are different depending on the disposition of the tube bench. Therefore, two different arrangements are found, the aligned and the staggered, sketched in Figure 7.

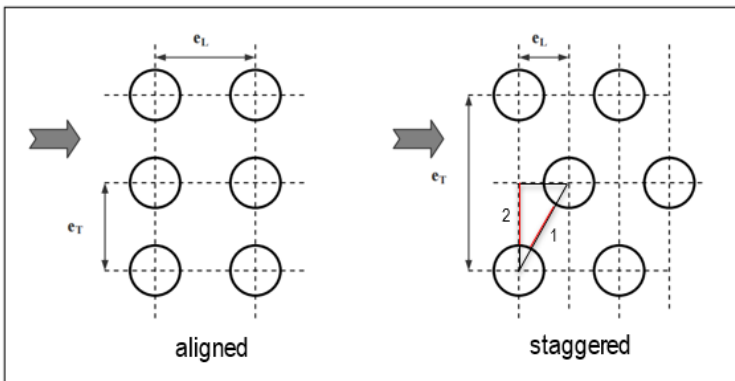


Figure 7. Disposition of the tube bench [6]

The arrangement of the tube bench is determined by the longitudinal (e_L) and transversal (e_T) tube pitch. At first, different arrangements were taken to determinate the influence of the pitch; eventually, a disposition where e_T was two times e_L was chosen, making the tubes form an isosceles triangle.

For the present resolution, a staggered tube arrangement has been chosen in order to minimize the bypass created in the aligned tube bench. For this arrangement, different empiric equations are found based on Nusselt number (Nu), the diameter of the tube (D), the Reynolds number (Re) and the mass flow density (G) evaluated as the mass flow divided by the minimum area between tubes. The Reynolds and mass flow density are calculated using.

$$Re_{max} = \frac{G_{max} \cdot D}{\mu} \quad (1)$$

$$G = \frac{mass\ flow}{minimum\ area} = v \cdot \rho \quad (2)$$

where

G_{max} = mass flow rate per unit of the minimum area, $kg/m^2 \cdot s$

D = diameter of the tube, m

μ = viscosity of the fluid, $kg/m \cdot s$

ρ = density of the fluid, kg/m^3

v = velocity of the fluid, m/s

The minimum area has to be chosen between the one formed by the tubes of the same row and the other formed by tubes that do not belong to the same row (see Figure 7). The distance shown in Figure 7 where 1 and 2 are be calculated with.

$$d_1 = \sqrt{(e_T/2)^2 + e_L^2} - D \quad (3)$$

$$d_2 = (e_T - D)/2 \quad (4)$$

If the relation shown in equation (5) is accomplished

$$\sqrt{(e_T/2)^2 + e_L^2} - D < (e_T - D)/2 \quad (5)$$

Then, the minimum area is determined by the diagonal space between opposite tubes.

$$A_{min} = \sqrt{(e_T/2)^2 + e_L^2} - D \quad (6)$$

In which case the mass flow density is.

$$G_{max} = \frac{e_T/2}{\sqrt{(e_T)^2 + e_L^2} - D} \cdot G \quad (7)$$

If not, the mas flow density is.

$$G_{max} = \frac{e_T}{e_T - D} \cdot G \quad (8)$$

If the fluid outside the tubes is air, over ten or more tube rows, Grimison [5] recommends using the equation below.

$$Nu = a \cdot Re_{max}^m \cdot f \quad (9)$$

where.

Nu = Nusselt number

Re = Reynolds number

Where the values of a and m are function of e_T and e_L , and the tube arrangement, and f is a correction value [5]. Furthermore, when the number of rows or tubes is lesser than 10, the Nusselt obtained must be multiplied by a factor indicated in [5].

Once the Nusselt is obtained, the value of h is found with.

$$h = \frac{Nu \cdot k}{D} \quad (10)$$

where.

k = thermal conductivity of the material, W/(m·K)

The heat transferred by the air is calculated using.

$$\dot{Q} = w \cdot c_p \cdot \Delta T \quad (11)$$

where

\dot{Q} = heat flux, W

w = mass flow, kg/s

c_p = heat capacity, J/kg·°C

ΔT = temperature increment from the initial temperature to the final, °C

And the minimum area is calculated with.

$$\dot{Q} = A_{min} \cdot h \cdot \Delta T \quad (12)$$

Calculating then.

$$\frac{S}{L} = 2 \cdot \pi \cdot r \quad (13)$$

where

S = section of the tube, m²

L = length of the tube, m

r = radius of the tube, m

The total length of the tube is calculated dividing equation (12) per equation (13), obtaining the perimeter of the tube. The number of tubes is the division between the total length of the tubes and the height of one tube.

The pressure drop, ΔP in pascals (Pa), when gases go through a tube bench is calculated with equation (14).

$$\Delta P = \frac{2 \cdot f' \cdot G_{max}^2 \cdot N}{\rho} \left(\frac{\mu_w}{\mu_b} \right)^{0.14} \quad (14)$$

where

N = number of transversal rows

ρ = density evaluated in the conditions of the free stream, kg/m³

μ_b = average viscosity of the free stream, kg/(m·s)

μ_w = viscosity in the wall, kg/(m·s)

f' = empiric friction factor proposed by Jacob [5], calculated using equation (15).

$$f' = \left(0.25 + \frac{0.118}{\left(\frac{e_T - D}{D} \right)^{1.08}} \right) \cdot Re_{max}^{-0.16} \quad (15)$$

3.5. PROCEDURE USING ANSYS®

Almost all solar chimney studies are aimed on finding optimum design solutions for enhancing natural ventilation, taking into consideration different design parameters [1]. The existing CFD models predict velocity and temperature profiles along with other flow characteristics accurately. ANSYS® provides simulation software to predict the behaviour of a product in a real environment. The ANSYS® Fluent is a computational fluid dynamics software tool that simulates fluid flows in a virtual environment [10]. It is divided in three main tools called modules.

- Pre-processing where the geometry is created and meshed
- Processing where the boundary conditions are set and the calculation is run

- Post-processing where the results are displayed in the geometry as property contours or in tables.

The methodology used in order to find the best design for the heat exchanger has been an iterative process illustrated in Figure 8.

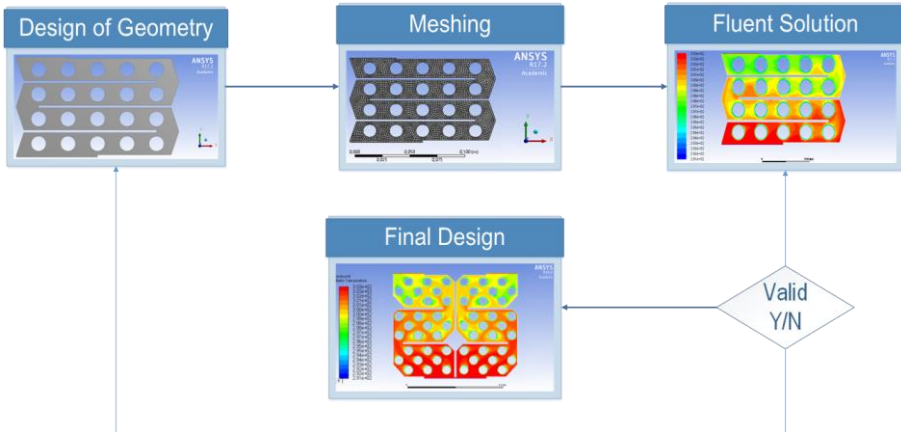


Figure 8. Iteration process for the design

3.5.1. Design of the geometry

In first place, the design is drawn using the Geometry software. Every design consist of a single sketch made in the XY plane, drawing a body named *air* with rectangular shape. The different tubes are made drawing a row of circles, and using the *Copy Paste* command the tube bench is created. To adjust the dimensions and location for each tube, the command *General* in the *Dimensions* tab is used. Once each row is copied and aligned, by clicking on the *Generate* button the software creates a hole in the design.

The horizontal and vertical baffles are drawn using rectangles with the commands *Dimensions* and *Generate*. The triangular baffles, used to guide the air through the design, are made by drawing the two sides of a triangle and then drawing the hypotenuse. Afterwards, using the command *Trim*, the sides of the triangles are eliminated, and using the command *Generate*, the drawing is updated.

3.5.2. Meshing of the design

Secondly, the meshing has to be generated. It is important to emphasize that the presence of circles in the geometry causes a distortion in the mesh, which implies the use of quadrilaterals and triangles, prioritizing quadrilaterals as long as the geometry allows it.

The shape checking is CFD due to the nature of the system. The different parts of the design must be indicated in the mesh by clicking on each part and creating a *Named selection* in order to determine afterwards the boundary conditions of the design. The named selections used for the designs are described below.

- **PipeN**. Indicates the number of each tube present in the design. Indicating this named selection allows the afterwards determination of the boundary conditions and the material used in the Fluent software.
- **Inletair**. Indicates the location of the inlet in the design. By indicating this named selection, the inlet conditions are set in the Fluent software such as temperature or velocity.
- **Outletair**. Indicates the location of the outlet in the design. This named selection is used in the Fluent software to indicate the conditions in the outlet, such as pressure or temperature.
- **DeflectorN**. Indicates the number of deflectors present in the design. This named selection allows the identification of the material, its temperature or the heat that exchanges.

Once all the *Named selections* are indicated, by clicking on the *Update* button, the program generates a default mesh in the conditions described. The time necessary to generate the mesh depends on the complexity of the geometry and the relevance used. The final result of the meshing is illustrated in Figure 9.

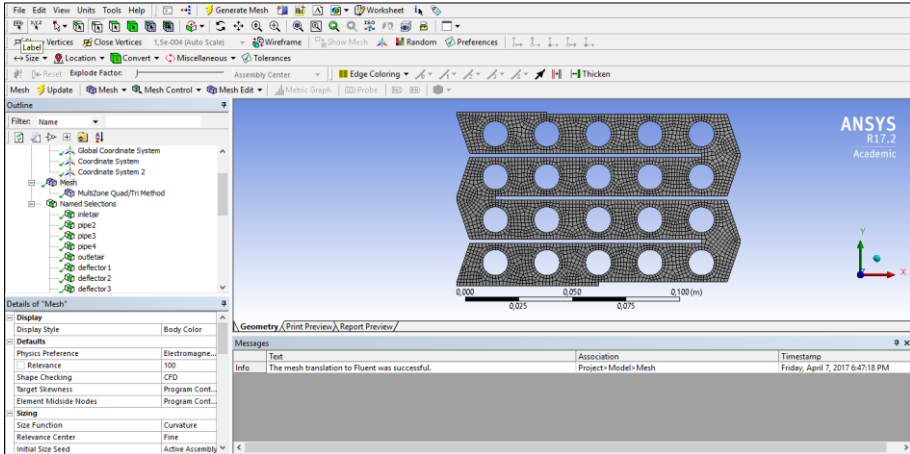


Figure 9. Example of a meshing system

3.5.3. Calculation of the solution using Fluent

Using the Fluent tool and setting the boundary conditions, different solutions are found (refer to nomenclature of the studied conditions to see the cases studied).

In order to choose a model for the simulation, the Energy and the Standard k-epsilon turbulent model are chosen. In some cases, the iterations do not converge, the problem might be in the mesh or the internal resolution of the program using the mesh generated

The materials chosen for the simulation are air for the fluid and copper for the walls and baffles. The properties of both are shown in the table below where the density of the air is considered as an ideal gas.

Table 2. Materials properties for the simulation

Material	Density (kg/m ³)	Specific Heat (J/kg·K)	Thermal conductivity (W/m·K)
Air	1.2	1006.4	0.02
Copper	8978.0	381.0	387.60

The boundary conditions of the system are set according to these statements.

- The deflectors are considered as a stationary adiabatic (heat flux = 0) wall made of copper.

- In the inlet, the velocity magnitude and the temperature are considered constant. The different values chosen are found in the nomenclature of the studied conditions.
- The pressure and the temperature determine the outlet. For this case, the gauge pressure is considered zero (absolute pressure of 1 atm) and the outlet temperature changes depending every simulation.
- The pipes are considered as a stationary wall made of copper, at a constant temperature of 18 °C.

Once the boundary conditions are set, the solution is found using an iterative process. The residuals of each iteration appear in the console panel and has an absolute criterion, which means that the software will continue iterating until the value of the residual in the iteration is equal or lesser than this absolute criterion.

Table 3. Absolute criteria for the simulations

Residual	Continuity	x-velocity	y-velocity	Energy	k	Epsilon
Absolute criterion	10^{-3}	10^{-3}	10^{-3}	10^{-6}	10^{-3}	10^{-3}

A solution is considered valid when.

- The value of the outlet temperature is equal or differ 0.1-0.2 K from the temperature set in the boundary conditions. If the outlet temperature found is lower than the temperature set in the boundary conditions, the result is considered valid. This is because the system is even more capable of cooling the air. However, this temperature cannot be lower than the temperature of the tubes.
- The pressure drop value is considered acceptable when it is lower than $6.0 \cdot 10^4$ Pa, in such way that would not affect negatively the velocity of the air.

In order to find the value of a property, the *Surface Integral* window included in *Reports* is used. Here, the values for different properties are found for the different named selections such as velocity, pressure, temperature, density, etc.

4. RESULTS

4.1. RESULTS USING EMPIRIC METHODS

As stated in the Procedure using empiric methods section, a staggered tube bench is chosen for the heat exchanger. Two different arrangements are selected, listed in *Table 4*.

Table 4. Values of the disposition of the tubes in the tube bench

Arrangement	D (m)	e _T (m)	e _L (m)	d ₁ (m)	d ₂ (m)	e _T /D	e _L /D	a	m
A	0.012	0.024	0.012	0.0050	0.006	2.00	1.00	0.460	0.568
B	0.008	0.020	0.010	0.0061	0.006	2.50	1.25	0.521	0.559

The values of a and m are obtained from [5], d_1 and d_2 are obtained from equations (3) and (4). When the values are not indicated in the table, an interpolation is made. Notice that in the first case $d_2 > d_1$, therefore, equation (7) has to be used. Furthermore, in the second case $d_1 > d_2$ and equation (8) has to be used to determine the value of G_{\max} .

For this case of study, the volumetric flow rate is shown in equation (16) used by [7].

$$q = 0.099 \frac{m^3}{s} \quad (16)$$

The initial tube length considered is 1 m. Once the geometry is stated, the inlet and outlet temperatures has to be set, which also implies the need to know the thermodynamic properties of the air, which are obtained from [6] and are shown in Appendix 1. Tube geometry for the different cases. Table 5 shows the different cases carried out, also indicated in the nomenclature of the studied conditions sheet.

Table 5. Temperature and velocity for the different simulations

Case n°	T _i (°C)	T _o (°C)	v _i (m/s)
1	26	23	2.5
2	34	27	2.5
3	30	25	2.5

The different values of G and G_{\max} using equations (2), (7) and (8) for the two different dispositions named as A for the 12 mm diameter tube and B for the 8 mm diameter tube are shown in Figure 10.

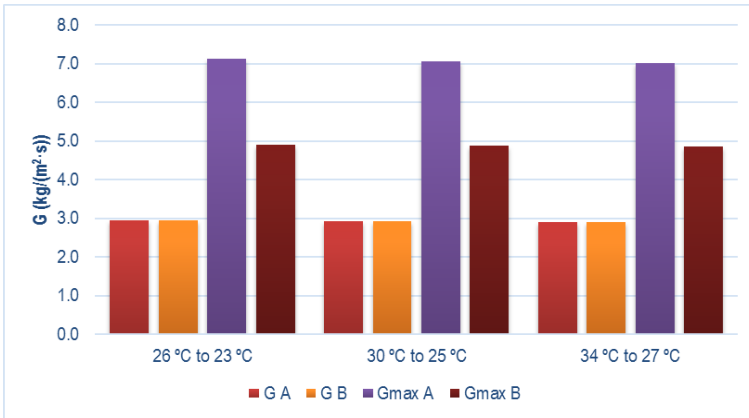


Figure 10. Values of G and Gmax

Notice that the values of G are all the same because the velocity inlet and the density of the fluid remain constant at the inlet. The values of G_{\max} are function of the geometry of the tube and G. With the values of G_{\max} , the maximum Reynolds number is calculated. The values of the Reynolds number for each case are shown in Figure 11.

When velocity is constant, the Reynolds number depends on the density and viscosity of the gas. Lower temperatures increase the Reynolds number making viscosity lower. On the other hand, higher temperatures decrease the viscosity making the Reynolds number lower. The differences now between A and B are because of the diameter.

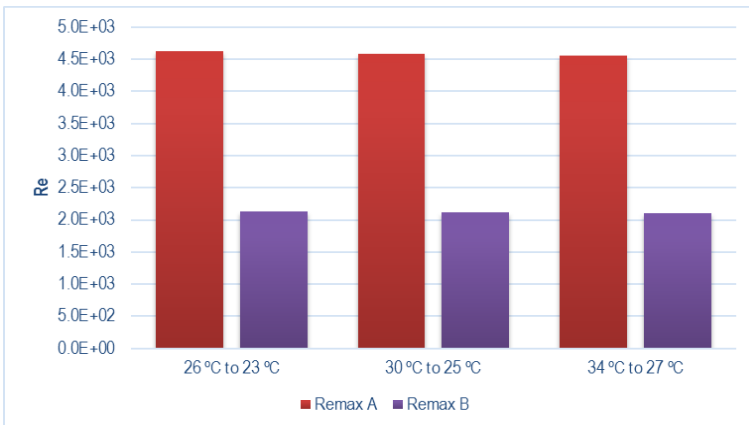


Figure 11. Reynolds number for each case

Once the Reynolds number is determined, the Nusselt number is calculated with equation (9), and the individual heat transfer coefficient using equation (10). The values of the individual heat transfer coefficient are shown in Figure 12.

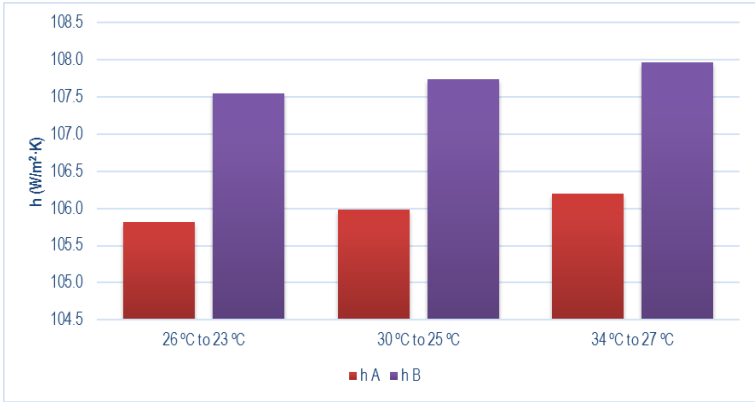


Figure 12. Values of h for each case

The heat transfer coefficient is function of the Nusselt and k. When the temperature is increased, k is also increased. On the other hand, when the temperature is decreased, k values are also decreased.

Using the thermodynamic properties of the air and the equations (11), (12), (13) (see Appendix 1. Tube geometry for the different cases), the heat exchanged and the minimum number of tubes are found and the results are shown Figure 13 in and Figure 14.

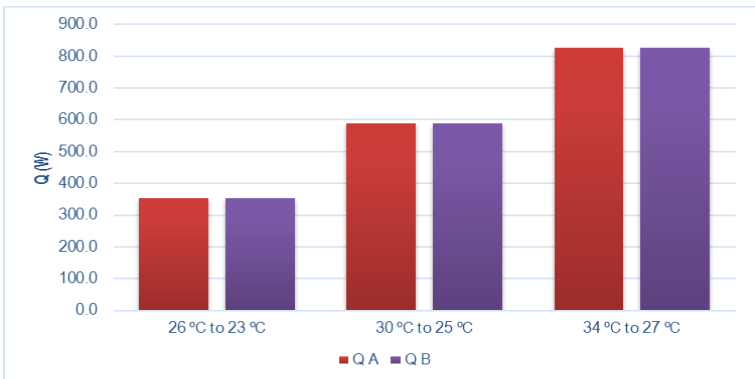


Figure 13. Heat exchanged by the water

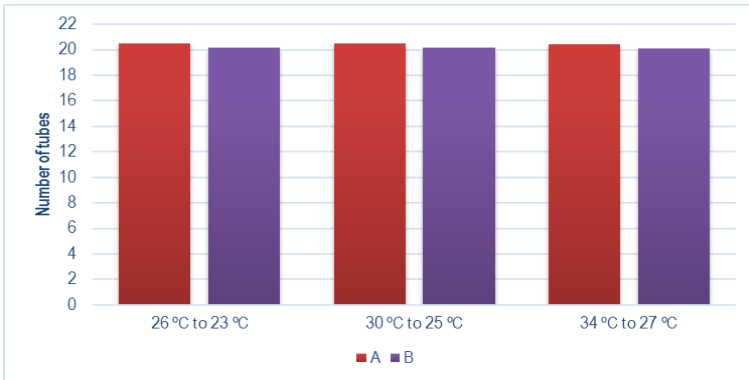


Figure 14. Minimum number of tubes

For different values of temperature maintaining the velocity constant, the heat exchanged increases when the ΔT increases. The minimum number of tubes for both arrangements is 20.

Making use of equation (14) the friction factor is calculated, and equation (15) gives the value of the pressure drop in the system. As shown from Figure 15, the pressure drop of A is higher than B in all cases because of the diameter of the tubes.

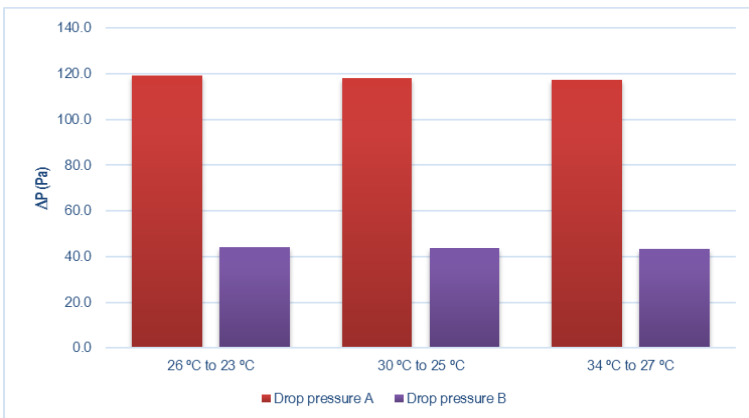


Figure 15. Pressure drop on each case

4.2. RESULTS USING ANSYS®

The previous design of the system was meant to be a classic tube bench (see Appendix 2. ANSYS® results for each simulation) with 20 tubes divided in five rows. Figure 16 shows the results of the simulation for the temperature contours.

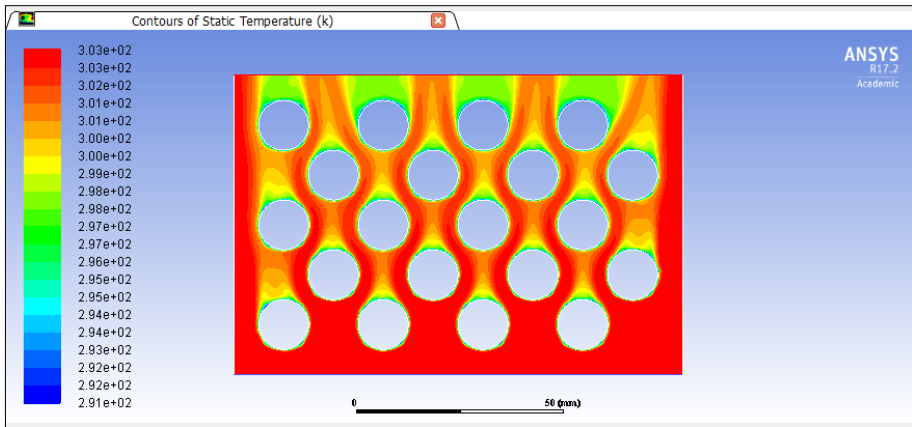


Figure 16. Temperature contours of Design 1

The temperature profile shows that the air is cooled, but the temperature of 298.15 K is only reached after the last row of tubes, even though there is also presence of air that is still at the inlet temperature (303.15 K). It should be noted that the flow path that the air follows is also visible and is indicated by the decreasing temperatures that goes through each tube. To decrease the average outlet temperature, two more rows were added to the design. However, the outlet temperature was still too close to the inlet temperature (see Appendix 2. ANSYS® results for each simulation).

Finally, it was possible to decrease the outlet temperature by adding baffles between each row of tubes, forcing the airflow to cross each tube as illustrated in Figure 17.

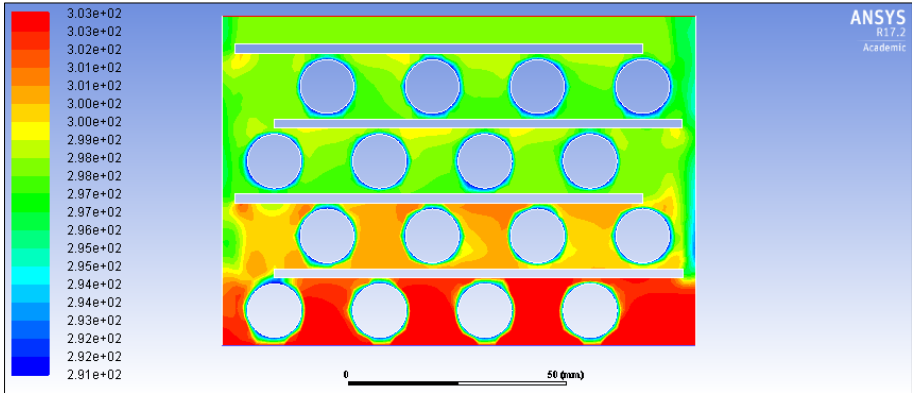


Figure 17. Design 4 including horizontal deflectors

Comparing Figure 16 and Figure 17 it is shown that once the baffles are added, the outlet temperature is highly decreased. Due to the space created between the wall of the heat exchanger and the baffle, the air is expanded and cooled. However, this space creates an important pressure drop. Afterwards, different designs were made changing the geometry of the baffles, adding vertical and triangular baffles and reducing the diameter of the tube (see Appendix 2. ANSYS® results for each simulation).

Because of the pressure drop due to the small space between the baffle and the wall, it was decided to join the baffles to the wall of the heat exchanger. In this way, the whole volumetric airflow must cross each row of the heat exchanger in order to reach the outlet.

It was found that low heat was exchanged in the first and last row of tubes, especially on the first two tubes of the first row, and the last two tubes of the last row. By placing barriers at the inlet and outlet, a better heat exchange was provided. For the inlet, the barrier covered the whole inlet except the first tubes on one side, forcing the air to strike directly to them and enhance the heat exchanged. The outlet was placed on the opposite side of the entry from the penultimate row. All these considerations are taken care on Design 10 shown in Figure 18.

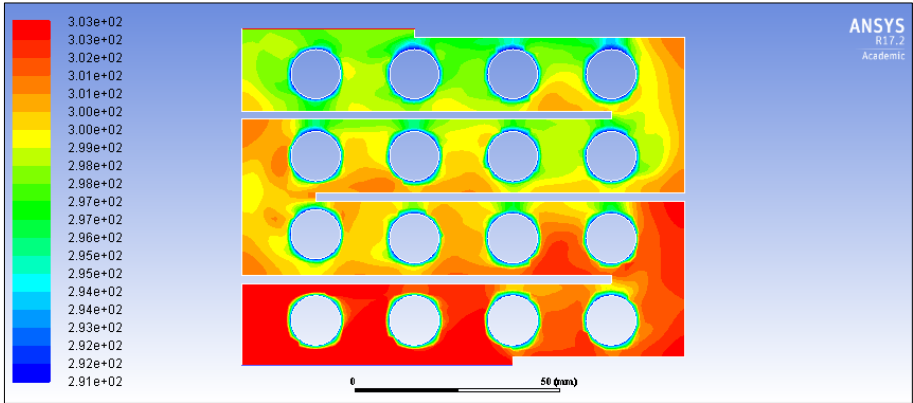


Figure 18. Design 10 with the baffles joined to the walls

Because of this new design, dead spaces appeared in the corners (see Figure 18), creating spaces where hot air was stuck without being renovated. Therefore, the calculation of the solution was in most of the cases unstable, because the mass balance in the system did not converged. One example is shown in Figure 19.

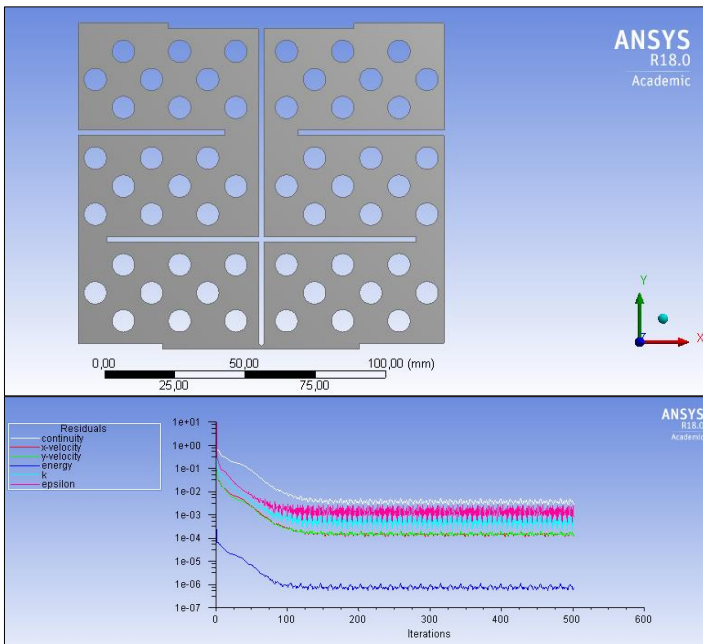


Figure 19. Example of a non converging design

In order to reduce the impact of these dead spaces, triangular baffles were added in the corners of the heat exchanger. In view of the above, an iterative process was carried out to determine the dimensions of the baffle.

1. An initial length was assigned to sides of the triangle using the Geometry software.
2. The design was then meshed.
3. Making use of the fluent, the temperature contours were represented in order to find dead spaces.

Evidence of this process is in Figure 20. These baffles also increased the mixing of the gas by guiding it to the subsequent row, increasing the heat exchanged. After these considerations, two different final designs are proposed.

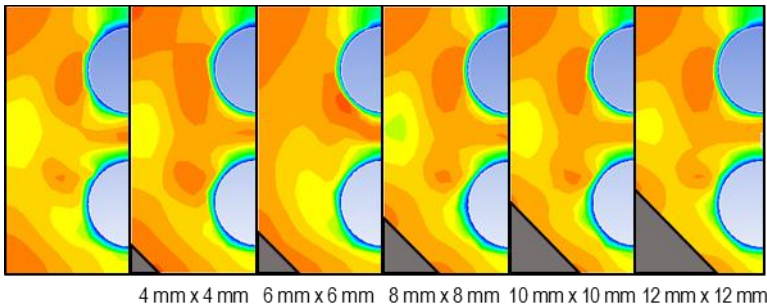


Figure 20. Influence of the triangular baffle in the design

4.3. RESULTS FOR DESIGN 13

Design 13 is the first final design. In Figure 21, the design is shown using AutoCAD® 2017. It consist of three different parts. on the upper side (grey) is located the inlet, where water enters the system at the refrigeration temperature, is distributed among the tube bench (red), and is collected back at the bottom. The tube bench is divided in five rows; each row has four 12 mm diameter tubes, making twenty tubes. Horizontal and triangular baffles guide the airflow from one row to the next increasing mixing and enhancing the heat exchanged as shown in Figure 22.

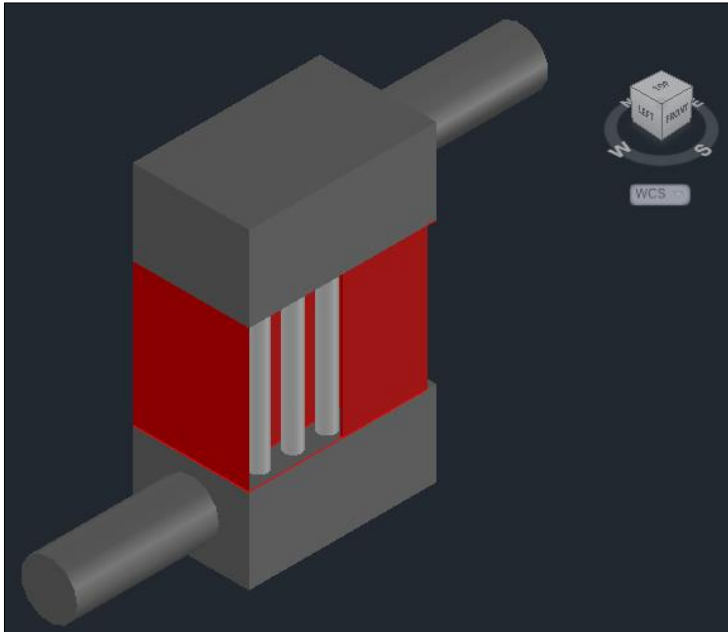


Figure 21. Heat exchanger using Design 13

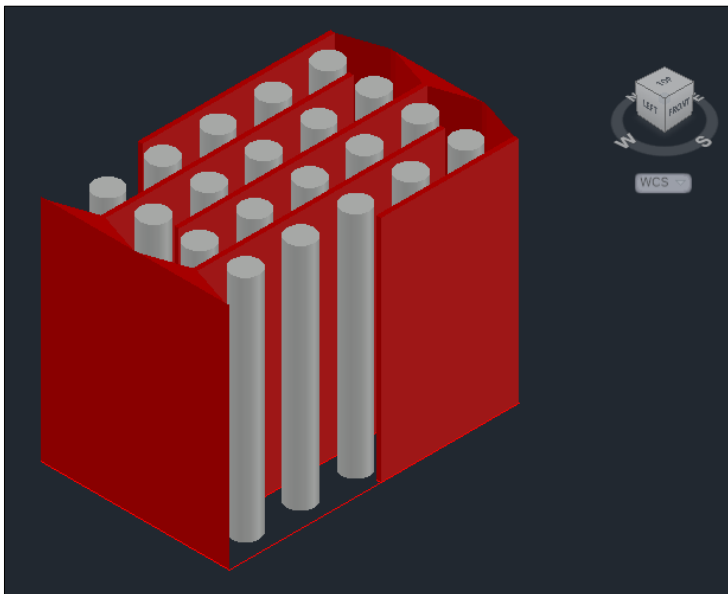


Figure 22. Design 13 using AutoCAD 2017®

The distances of the design are shown in Figure 23 in mm.

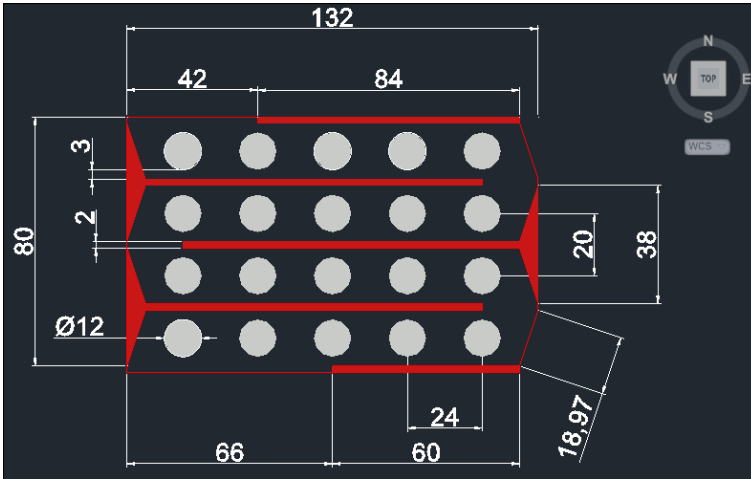


Figure 23. Dimensions of Design 13 in mm

Making use of the Geometry tool included in ANSYS® 17.2 the design is made following the dimensions indicated in Figure 23 and is illustrated in Figure 24.

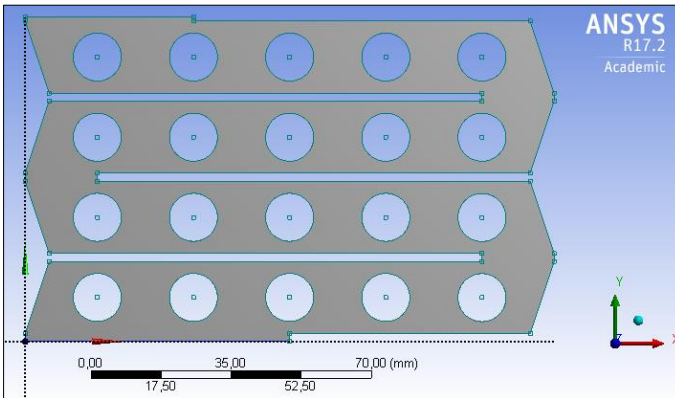


Figure 24. Design 13 using the Geometry software

In order to determine the influence of the mesh in the solution obtained, specifically on the outlet temperature, different element sizes were tested. When the element size was reduced, the number of nodes increased and the outlet temperature found was the same as the given using the default meshing. If the element size was lower than a threshold though, the software was not

able to find a solution as shown in Table 6 with red numbers (for the non-converging solutions see Appendix 5. Non-converging results).

Moreover, when the element size was increased, the number of nodes remained constant and the software found the same outlet temperature in all cases.

Table 6. Meshing comparison for different element sizes

Case n°	Element Size	Nodes	T _o (K)
1	9.00E-04	28,442	No solution
2	1.00E-03	23,219	No solution
3	1.15E-03	17,469	No solution
4	1.20E-03	15,653	No solution
5	1.25E-03	14,602	297.5
Default	1.55E-03	11,018	297.5
6	5.00E-03	11,018	297.5
7	9.90E-02	11,018	297.5

It seems plausible that ANSYS® detects the minimum number of nodes to solve the system as shown in Table 6.

By making use of the Fluent software, setting the boundary conditions and the inlet and outlet conditions, different solutions are found (refer to Nomenclature of the studied condition for the different simulations carried out and to Appendix 3. Final design 13 using ANSYS®). The procedure is the same in all five cases, therefore, the case number 3 (303 K to 298 K at 5 m/s) will be used as a guide and explained below.

As stated above, the calculation consist of an iterative process. While the calculation is running, the software displays a graphic where the X-axis correspond on the number of iterations and the Y-axis to the residuals of the calculations as illustrated in Figure 25.

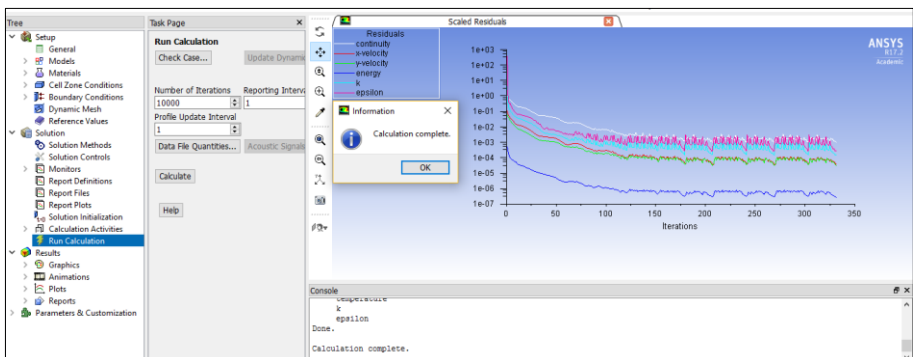


Figure 25. Calculation of the solution

The results for the simulation are shown using contours below. In order to understand the behaviour of the air in the system, it is important to determine the velocity contour, shown in Figure 26.

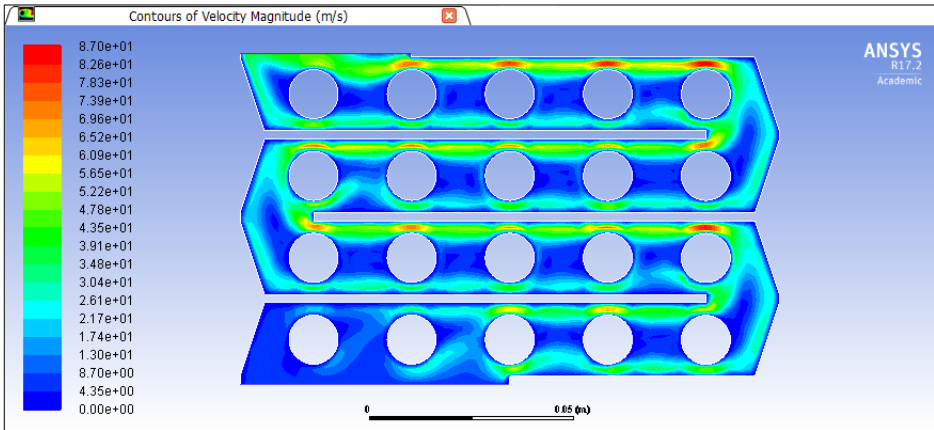


Figure 26. Velocity contour in Design 13

The velocity at the inlet is constant at 5 m/s, shown in a dark blue colour. The air enters the system, guided by the triangular baffle strikes into the first two tubes. At the next three tubes, the air is conducted between the tube and the horizontal baffle. Here, due to the small size of the baffle-tube space, the velocity is increased, creating preferential paths and lower velocity zones between the tubes.

By the time the air crosses the first row, the lower path strikes to the triangular baffle and is conducted to the first tube of the second row, where the flow is again divided in two different paths. The third row has a similar behaviour as the second row, with two different paths, and lower velocity zones between tubes. For the last row, it was found that adding a barrier and placing the outlet at the end of the row, the outlet temperature decreased. This is because the air is forced to cross the entire tube bench in order to reach the outlet. If there was no barrier, most of the air will escape once it reached the end of the third row, and only a small part would continue through the last row.

It is important to emphasize that the first tube of the second, third and fourth row are the ones where the heat exchanged is higher because of the turbulence created. The first row will be the one that provides the lower heat exchange because the air is not conducted yet.

In order to provide a better understanding of the velocity in the system, the vector contour is displayed in Figure 27.

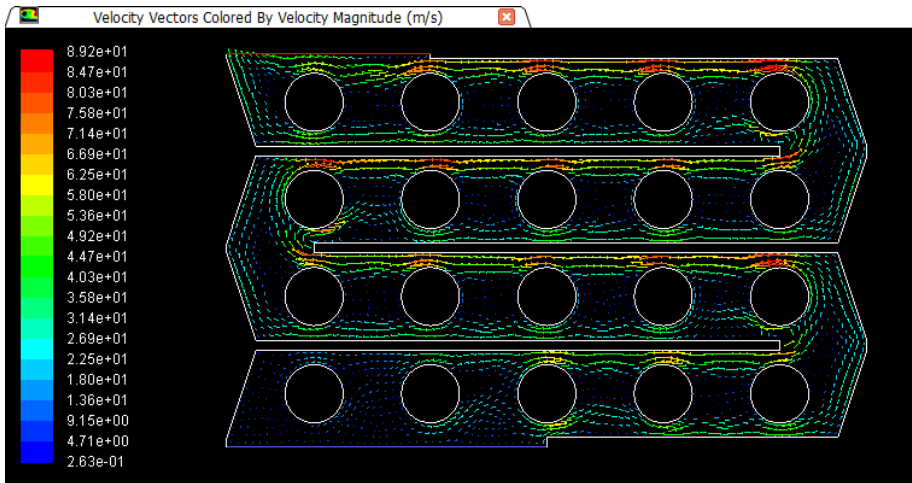


Figure 27. Velocity vectors in Design 13

The temperature profile is detailed in Figure 28. The air enters the system at 303.15 K, and strikes directly to the first two tubes and half of the third. Thanks to the triangular baffles located in the left side of the inlet, the air is conducted to the right and is cooled, generating a small zone of lower temperature at the first tube, increased in the second one.

In the fourth and fifth tube, the air strikes and due to its velocity creates a small bag of cold air in the space between the tubes. The air that crosses the first space (at the right), strikes to the triangular baffle and changes its direction to strike again to the first tube of the second row, dividing the flow on the upper and lower side of the tube.

In the second row, the air is gradually cooled from 302 K to 300 K creating zones of lower temperature between tubes. Once again, the air strikes to the triangular baffles changing its direction and striking to the first tube of the third row. Notice that the tendency of the temperature profile in the second and third row are similar.

The triangular baffle at the end of the last row prevents the creation of dead spaces and guides the airflow to the outlet, achieving a temperature drop of 3 K.

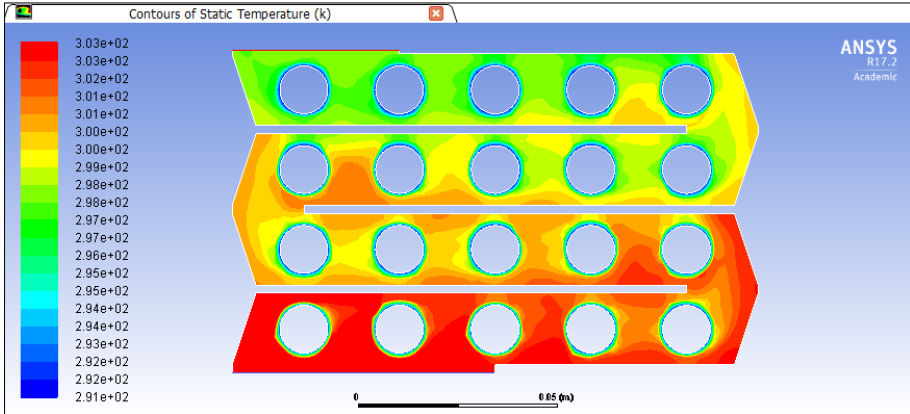


Figure 28. Temperature profile of Design 13

The pressure gauge contour is displayed in Figure 29. Notice that the pressure decreases whether the air goes through each row. Every time the air changes its direction, the pressure is decreased. In addition, in the spaces between tube and deflector, the pressure is highly decreased due to the expansion of the gas.

In the outlet, the pressure is highly reduced due to significant expansion of the gas. For this design, the ΔP existing is considerable, about 10^4 Pa.

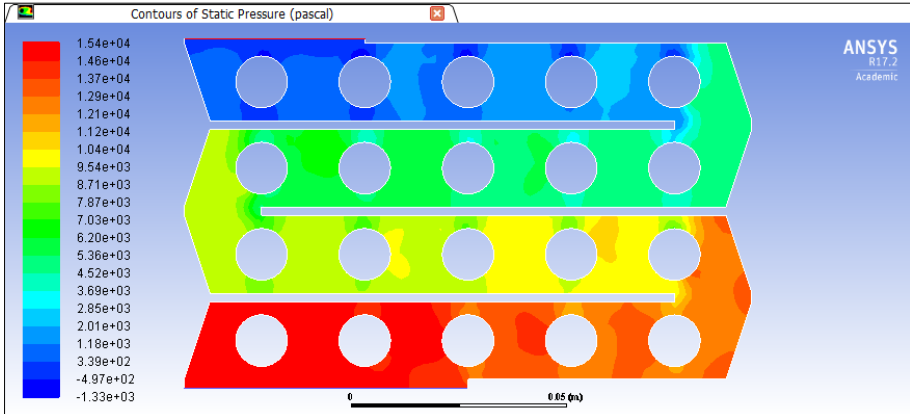


Figure 29. Pressure contour of Design 13

Another important aspect in the results of the simulations, are the values of the heat transfer coefficient, displayed in Figure 30.

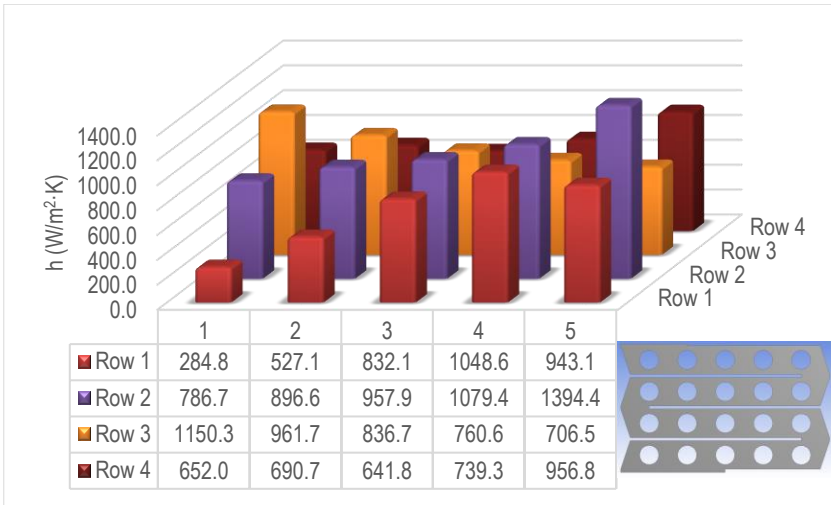


Figure 30. h values for Design 13

Notice that the graphic is made following the geometry of the design. Therefore, the inlet is located on the left side of the first row; the air then flows from left to right. In the second row, the air flows from right to left and subsequently. The outlet is located on the left side of the fourth row.

In the first row, the values of h increase from left to right, due to the increase of the velocity and therefore, the increase of the turbulence. In the second row, the values of h decrease from right to left, the first tube of the row has a higher value because receives all the air from the first row and the turbulence is higher. The same behaviour is observed in the third row and the last row where the values decrease gradually.

The cases carried out with the final design are found below, and are distinguished in two types.

- Cases where the velocity inlet remain constant and the inlet temperature is changed (case 1 to 3).
- Cases where the inlet temperature remain constant and the velocity inlet is changed (case 3 to 5). The results of these simulations are given in Table 7.

Table 7. Results for the cases carried out in Design 13

Case nº	v_i (m/s)	V_o (m/s)	T_i (K)	T_o (K)	ΔT (K)	ΔP (Pa)	\dot{Q} (W)
1	5.0	30.0	299.2	295.3	3.8	$1.53 \cdot 10^4$	452.3
2	5.0	30.0	307.2	300.2	6.9	$1.47 \cdot 10^4$	817.9
3	5.0	30.0	303.2	297.5	5.6	$1.49 \cdot 10^4$	662.2
4	6.0	31.9	303.2	297.4	5.7	$2.41 \cdot 10^4$	677.9
5	7.5	47.2	303.2	296.6	6.5	$4.96 \cdot 10^4$	771.8

The cases where the inlet temperature was changed, it was found that when the difference between the inlet temperature and the temperature of the tubes was increased, the value of the ΔT between the inlet and the outlet temperature increased and thus, the heat exchanged. This is because of the temperature gradient existing.

When the inlet temperature remains constant, an increase of the velocity inlet corresponds with a greater turbulence, therefore, an increase of the pressure drop and an improvement of the heat exchanged, achieving higher ΔT and \dot{Q} whenever the velocity is increased (see Appendix 3. Final design 13 using ANSYS®).

4.4. RESULTS FOR DESIGN 14

Design 14 is the second design, shown using AutoCAD® 2017 in Figure 31. The design consist of three different parts, on the upper side, the refrigeration water inlet (grey), in the middle, the tube bench with the deflectors (orange) and, at the bottom, the outlet of the refrigeration water (grey).

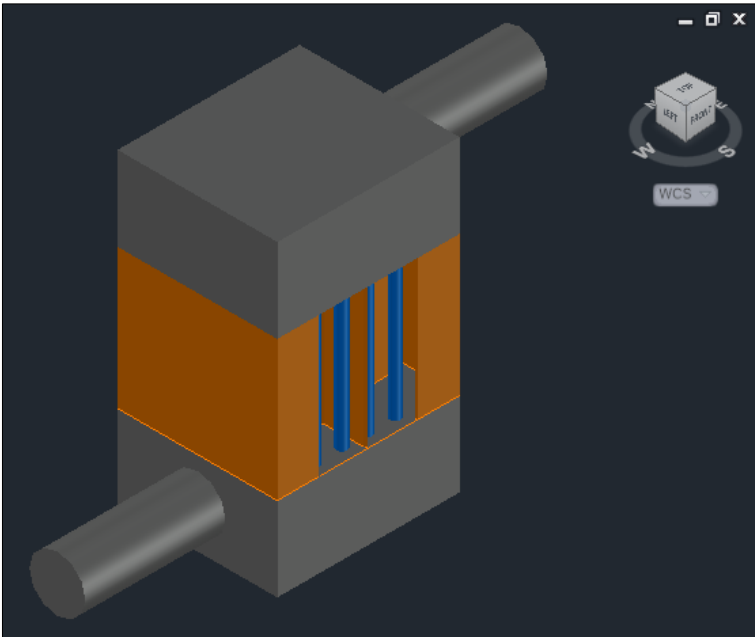


Figure 31. Final design for Design 14

In Figure 32 the design is illustrated without the refrigeration inlet and outlet. The tube bench is divided using a vertical deflector in two symmetric parts. Each part is divided by horizontal deflectors, making six zones. Each zone consist of a three row staggered tube bench, with three 8 mm diameter tubes on each row. Both the inlet and outlet have horizontal barriers to guide the airflow and enhance the heat transfer. The dimensions of the design are shown in Figure 33.

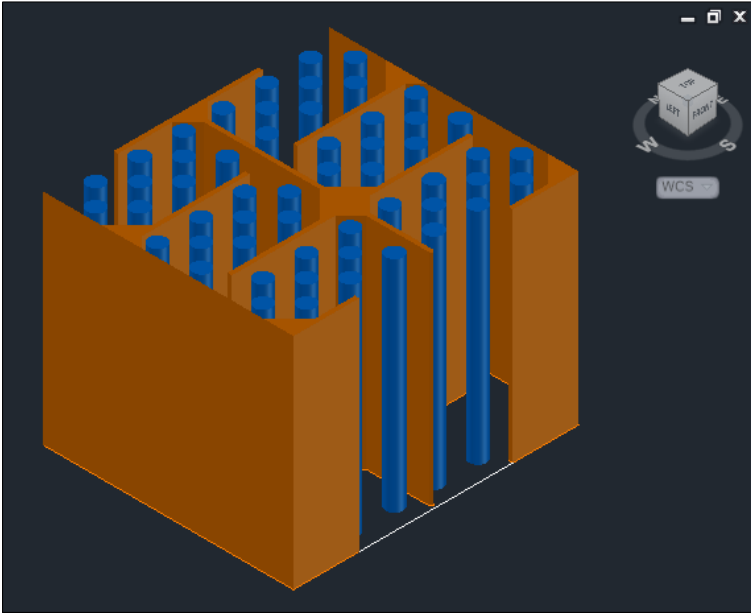


Figure 32. Design 14 using AutoCAD

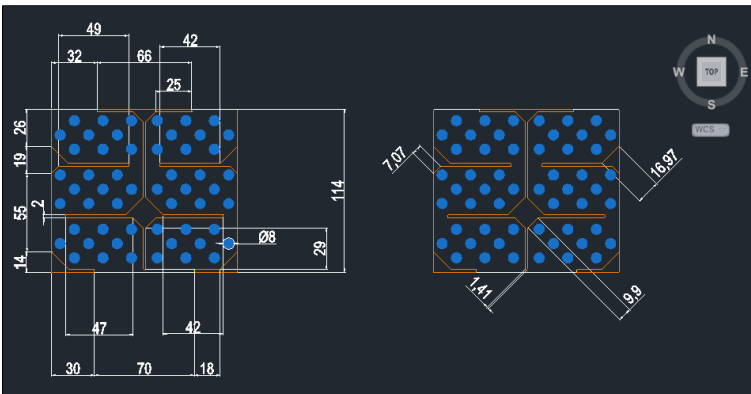


Figure 33. Dimensions of Design 14

Making use of the Geometry software included in ANSYS® 18.0, the design is made following the dimensions indicated in Figure 33.

The procedure is the same as followed with Design 13, drawing first a rectangle and then, modifying it by inserting the horizontal and vertical baffles. The triangular baffles are drawn using the *Dimensions* and *Trim* commands.

All the tubes are made perforating the rectangle, copying a 3-row tube bench and then pasting it in the spaces between deflectors. Using the *Dimensions* tool the horizontal and vertical dimension for each row of tubes are adjusted. The result is shown in Figure 34.

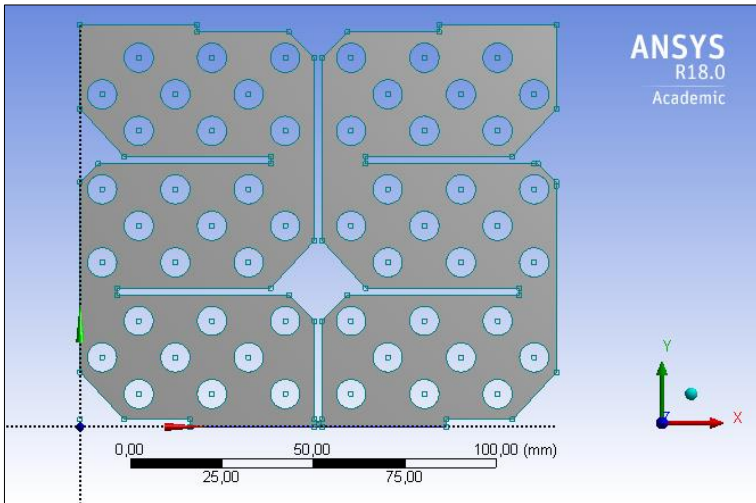


Figure 34. Design using Geometry software

The mesh is generated following the same steps as followed in Design 13.

Making use of the Fluent tool, setting the boundary conditions, different solutions are found (see nomenclature of the studied conditions). The procedure is the same in all five cases; therefore, case n° 3 (303-298 K at 5m/s) will be used as guide (Appendix 4. Final design 14 using ANSYS®).

In order to understand the behaviour of the air in the system, it is important to determine the velocity contours, illustrated in Figure 35. The velocity in the inlet is constant at 5 m/s and is divided by a vertical deflector to the left and right side. The air then flows through both tube benches, striking on the horizontal deflector and changing its direction to the first exit, increasing its velocity.

In the second tube bench, two different paths are created, one that goes vertically and strikes on the triangular baffle and then goes straight to the exit, and another where the air crosses the entire tube bench before arriving to the exit.

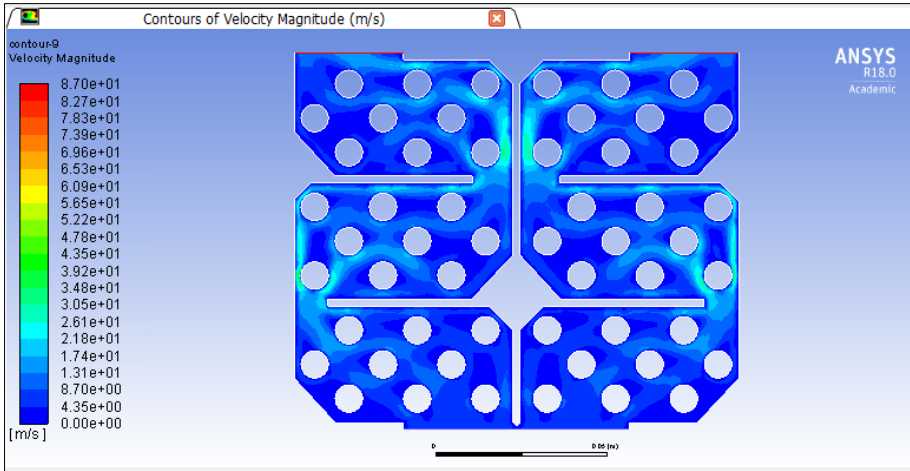


Figure 35. Velocity contour for Design14.

The same behaviour is observed in the third tube bench, where part of the airflow goes straight to the exit and the other part crosses the entire tube bench. The zones where the velocity is higher are an indicative of a higher heat exchange. Therefore, it seems plausible that the higher values of the heat transfer coefficient will be located in the tubes where the air has the maximum velocity.

The vector profile is shown in Figure 36 in order to help understanding the behaviour of the velocity.

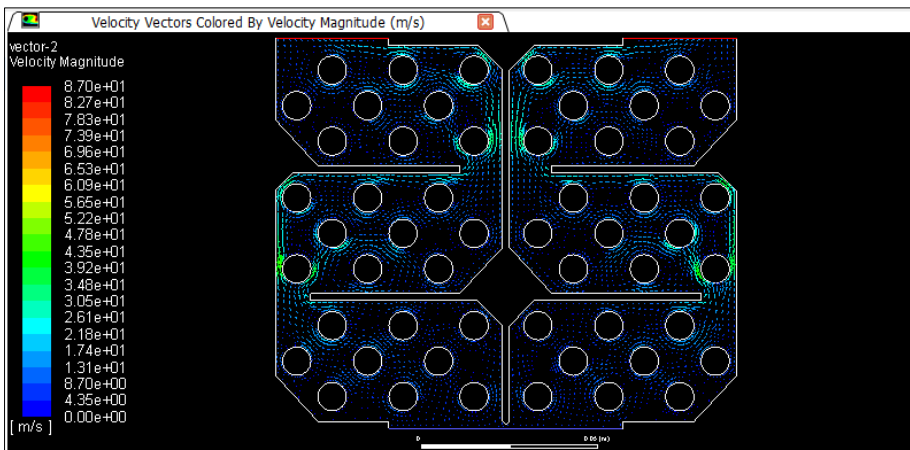


Figure 36. Vector velocity contour

The temperature contour is detailed in Figure 37. The air enters the system at 303 K and is rapidly divided in two parts. Here, the temperature profile is well defined, after each tube; a low temperature trail appears coincident with the velocity contour. The air is progressively cooled among the six zones present in the design.

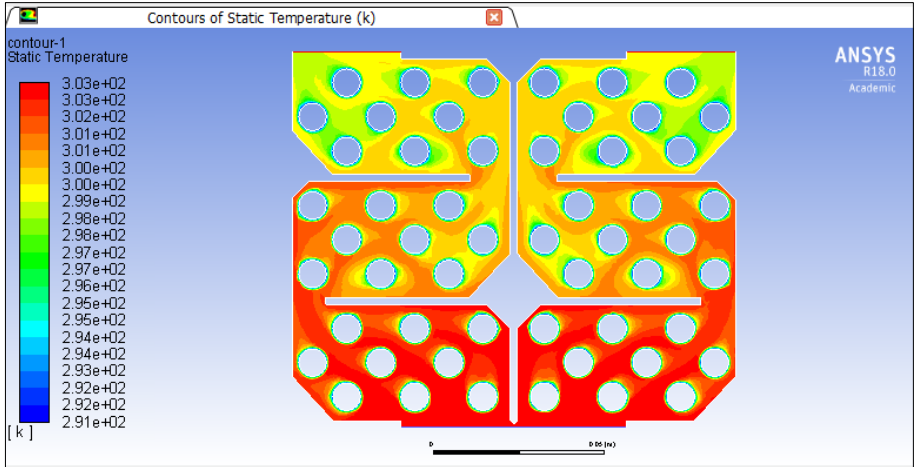


Figure 37. Temperature contour for Design 14

The pressure contours are shown in Figure 38. For this design, the ΔP is distributed in the different zones. Every time the air crosses to another zone, its pressure drops. The ΔP for this design is lower than for Design 13.

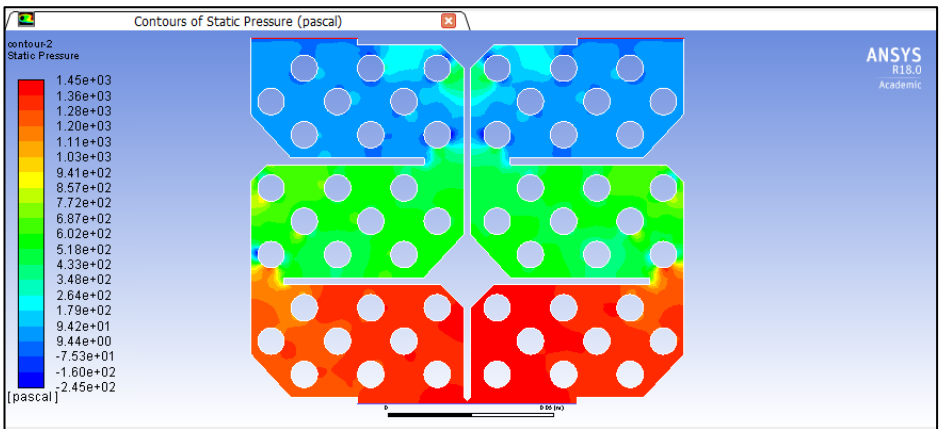


Figure 38. Pressure contour for Design 14

The values of the heat coefficient transfer for this case are detailed in Figure 39. As expected, the highest values for the heat transfer coefficient are located where the highest velocity is reached, this is, in the first and sixth tube of the fourth, fifth and sixth row, and the third and fourth tube of the seventh, eighth, and ninth row. The rest of the values tend to increase but are lower in all cases.

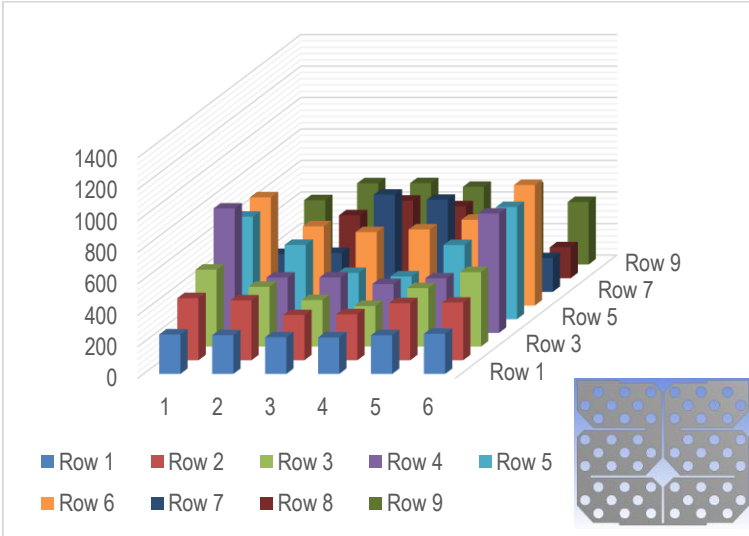


Figure 39. Heat transfer coefficient values for Design 14

The results of each case are given in Table 8.

Table 8. Results for the simulation

Case n°	v_i (m/s)	v_o (m/s)	T_i (K)	T_o (K)	ΔT (K)	ΔP (Pa)	\dot{Q} (W)
1	5.0	5.2	299.2	296.5	2.7	$1.4 \cdot 10^3$	318.6
2	5.0	5.2	307.2	301.8	5.4	$1.4 \cdot 10^3$	637.3
3	5.0	5.2	303.2	299.1	4.0	$1.4 \cdot 10^3$	478.0
4	6.0	6.3	303.2	299.2	4.0	$2.0 \cdot 10^3$	468.3
5	7.5	7.8	303.2	299.5	3.7	$3.1 \cdot 10^3$	434.2

The cases where the inlet temperature was changed, it was found that when the difference between the inlet temperature and the temperature of the tubes was increased, the value of the ΔT between the inlet and the outlet temperature increased, and, therefore, the heat exchanged was also increased. This is because of the temperature gradient existing.

When the inlet temperature remains constant, an increase of the velocity inlet does not increment the ΔT as could be noticed from cases 4 and 5. This is due to the geometry of the design, which causes the apparition of preferential paths, increasing only the heat exchanged in a few tubes. The same behaviour can be found in the heat exchanged values where cases 4 and 5 are lower than case 3.

4.5. COMPARISON BETWEEN THE EMPIRIC EQUATIONS AND ANSYS®

In an attempt to establish a comparison between the empiric model described in the bibliography and the results found using the ANSYS® software, two different simulations were carried out, corresponding on Design 1 and Design 2. The ΔT , ΔP and the heat transfer coefficient values will be compared for each case.

4.5.1. Comparison of arrangement A

Disposition A consists of a staggered tube bench with five rows of four tubes each, making a total of twenty tubes (see Appendix 2. ANSYS® results for each simulation).

The ΔT values are displayed in Figure 40. In all cases, the ΔT of the empiric case are higher than the ΔT found with the ANSYS® software. However, the same tendency is observed in all three cases.



Figure 40. ΔT for each case studied

As for the ΔP , it was found that the simulations carried out with ANSYS® had a lesser pressure drop than the empiric calculations. Prove of that is shown in Figure 41. For both cases the ΔP remains practically constant when the temperature inlet is changed.

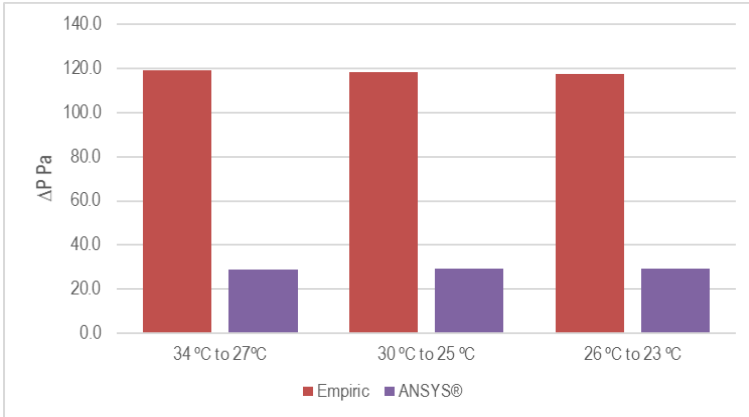


Figure 41. ΔP for each case studied

The values of h for the different cases studied are shown in Figure 42. Making use of the empiric equations, a constant value of h is found in all three cases. Making use of the ANSYS® software, the value of the heat transfer coefficient is calculated for each tube; the values shown in the figure consist of an average value for all the tubes. By examining the values for each simulation, it could be concluded that when the difference between the inlet temperature and the tube temperature is increased, the value of h is increased.

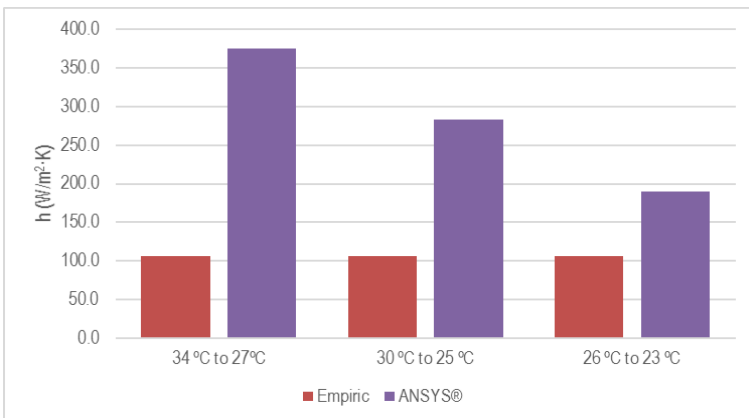


Figure 42. h values for each case studied

As for the heat exchanged values, Figure 43 shows that for the empiric equations, the heat exchanged is in all cases higher than the heat exchanged found in the simulations using ANSYS®. This is because the heat exchanged value is directly related to the ΔT value, and, as stated above, the ΔT values found in the empiric equations were higher than the ones found with ANSYS®

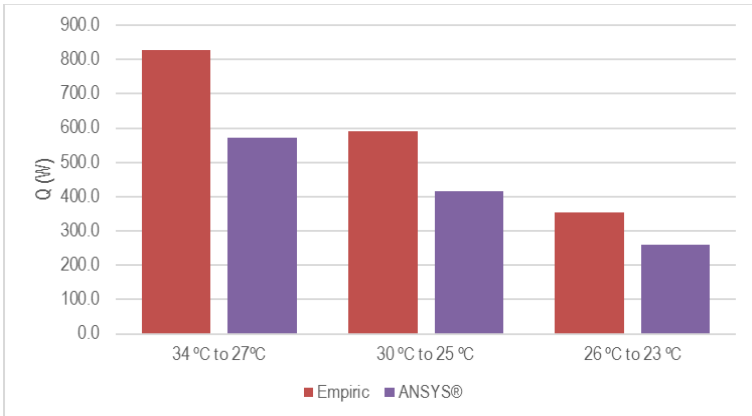


Figure 43. Heat exchanged values for each case studied

4.5.2. Comparison of arrangement B

Disposition B consists of a staggered tube bench with four rows of five tubes each, making a total of twenty tubes (see Appendix 2. ANSYS® results for each simulation).

The ΔT values are displayed in Figure 44. The ΔT values found using the empiric equations are in all cases higher than the values found using the ANSYS® software, the same behaviour as found for arrangement A.

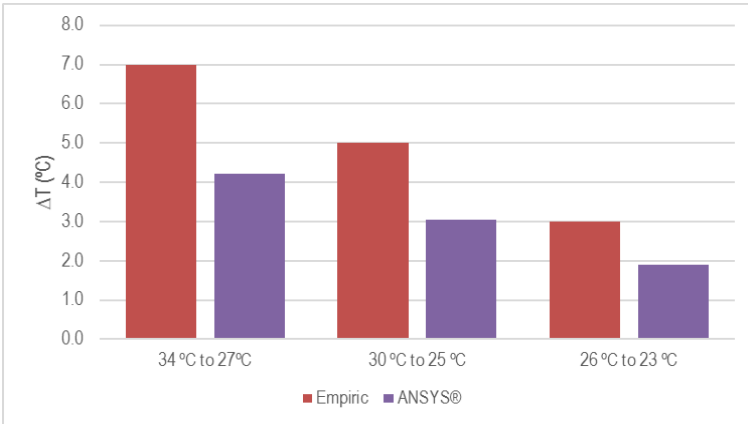


Figure 44. ΔT for each case studied

The ΔP values are shown in Figure 45. Following the same tendency described in arrangement A, the ΔP in the empiric case is higher than the found using the ANSYS® software. However, all values remain constant for each simulation carried out.

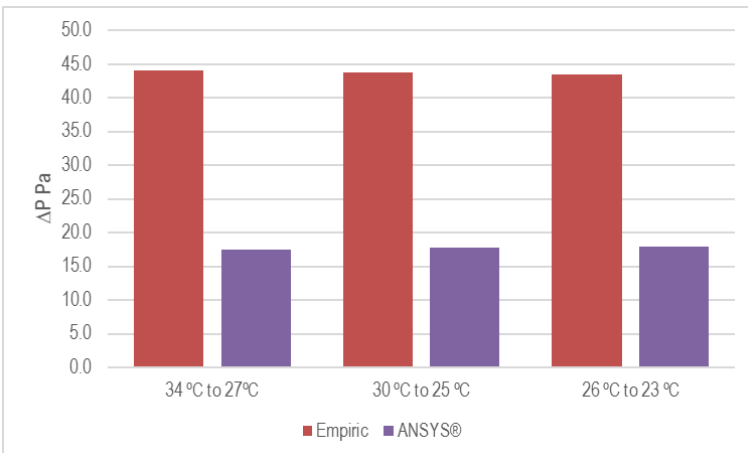


Figure 45. ΔP for each case studied

As for the heat transfer coefficient values, it was found that in each simulation, the values found using the ANSYS® software decreased when the difference between the inlet temperature and the temperature of the tube were similar, but, in all cases these values were higher than the values found using the empiric equations.

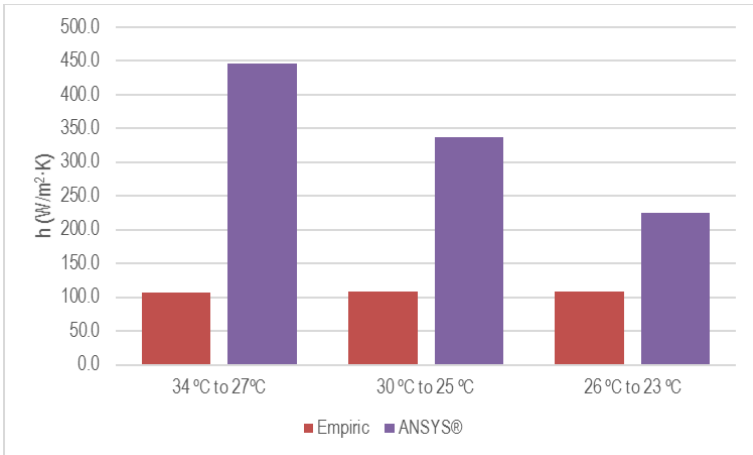


Figure 46. h values for each case studied

As for the heat exchanged, the values are higher when the ΔT is higher. Therefore, for the empiric equations, it was found that the heat exchanged was higher than the calculated using ANSYS® (Figure 47).

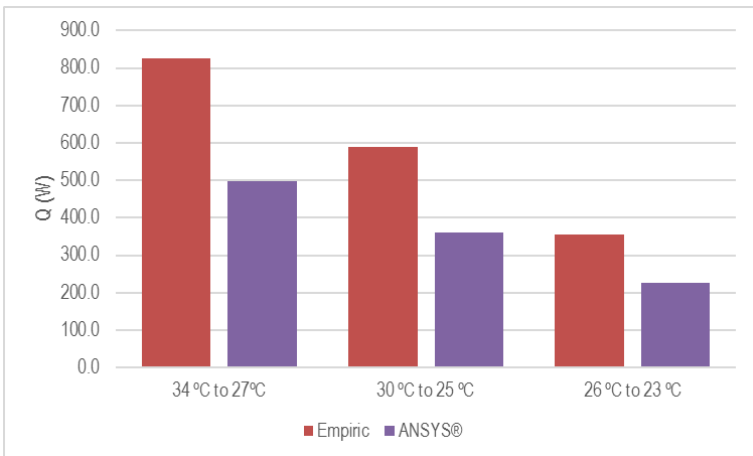


Figure 47. Heat exchanged values for each case studied

4.6. COMPARISON OF THE ANSYS® FINAL DESIGNS

Once the final designs are determined, it is important to establish a comparison between them. The most important factors to attend are the temperature and the pressure. Thus both temperature and pressure contours are detailed in an attempt to establish the differences found in each design.

Figure 48 shows the temperature profile for both designs. The outlet temperature in Design 13, on the left is lower than the outlet temperature in Design 14, on the right. This is because in Design 13, the air is forced to go through every tube following a single path while in Design 14, the air is distributed among each independent tube bench and the flow is not conducted, creating preferential paths and zones where the heat exchange is lower.

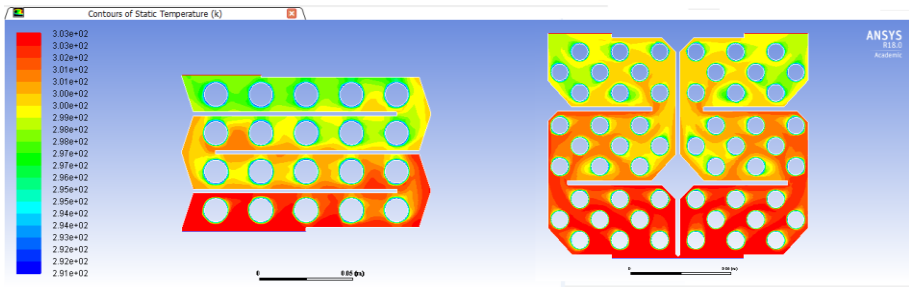


Figure 48. Temperature contour for both final designs

An examination of the pressure profile illustrated in Figure 49 shows that Design 13 has a higher pressure drop than Design 14 due to the disposition of the tubes and the baffle-tube space.

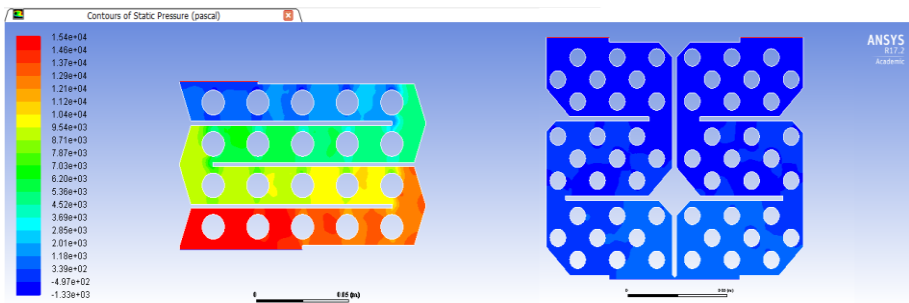


Figure 49. Pressure contour for both final designs

In Design 13, the zones where the pressure drop is increased are located on each change of row, where the air changes its direction and strikes directly on the first tube of each row and in the space between the tube and the deflector, where the air is expanded.

In Design 14, the pressure drop is less pronounced because of the disposition of the tubes in each zone, where the highest pressure drop is located in the spaces between tube benches

5. CONCLUSIONS

The minimum number of tubes determined using empiric models is 20 when the air wants to be refrigerated from 30 °C to 25 °C for both dispositions presented.

The minimum number of tubes necessary using the ANSYS® software is approximately the same as found using the empiric models.

Even though the triangular baffles provide a more complex design in terms of the geometry and costs, they had been a crucial part in the search for valid solutions.

Each one of the models design provide a ΔT considerable in order to make the temperature inside the building comfortable.

All the designs proposed when the inlet temperature was 30° C has a ΔT higher than 3 °C, though when the simulation was carried out in another conditions, only two designs are considered valid.

Different heat exchangers has been pre-designed and described, two of them considered as the final designs. The outlet temperature reached with Design 13 is lower than expected in all the cases studied, though the pressure drop existing in the design is considerable. On the other hand, Design 14 does not refrigerate as much as Design 13 but its pressure drop is less pronounced in all the cases studied.

The complete modelling of the heat exchanger has not been proposed yet because the solar chimney has not being modelled. Once the solar chimney damper sets the inlet conditions, the proper design of the heat exchanger will be carried out.

6. RECOMMENDATIONS

The present section focuses on what the next steps should be after this work, as well as the simulations that could be carried out hereinafter.

6.1. DESIGN RECOMMENDATIONS

In terms of the design of the heat exchanger, it would be recommendable to include cooling fins in the tubes of the heat exchanger to determine the minimum outlet temperature reached even though the material has to be changed to stainless steel. New designs could also be proposed changing the geometry of the heat exchanger or the geometry, number and shape of the tubes, for example, spiral tubes.

6.2. SIMULATION RECOMMENDATIONS

In terms of the simulation of the heat exchanger, the humidity of the air could be used as a variable in the simulation as well as the fouling to determine how these parameters affect the outlet temperature and the heat exchanged.

The present work has been carried out in stationary conditions, assuming that the water within the tubes is constantly flowing and at the same temperature. It would be desirable to simulate the heat exchanger in transient conditions, when the mains of the building are not being used, to see the evolution of the temperature of the water inside the tubes and the outlet temperature of the air.

The simulation of the two final designs has been carried out in two dimensions. It would be interesting though, to simulate the heat exchanger in a 3D model to determine if the results match with the obtained in this work as well as determine the friction of the air with the walls, the appearance of dead spaces and the optimal height.

In order to determine the viability of the process, the simulation of the solar chimney plus the heat exchanger inlet could be carried out.

REFERENCES AND NOTES

- [1] R. Khanal and C. Lei, “Solar chimney — A passive strategy for natural ventilation,” *Energy Build.*, vol. 43, no. 8, pp. 1811–1819, 2011.
- [2] “Stack Ventilation and Bernoulli’s Principle | Sustainability Workshop.” [Online]. Available: <https://sustainabilityworkshop.autodesk.com/buildings/stack-ventilation-and-bernoullis-principle>. [Accessed: 23-Mar-2017].
- [3] “Solar chimney - Designing Buildings Wiki.” [Online]. Available: https://www.designingbuildings.co.uk/wiki/Solar_chimney. [Accessed: 25-Mar-2017].
- [4] A. Dimoudi, “Solar Chimneys in Buildings—The State of the Art,” *Adv. Build. Energy Res.*, vol. 3, no. 1, pp. 21–44, 2009.
- [5] J. P. Holman, *Transferencia de Calor*, 8th ed. Aravaca, Madrid: McGraw-Hill, 1998.
- [6] R. H. P. Don W. Green, *Perry’s chemical engineers Handbook*, 8th ed. Kansas: McGraw-Hill, 2008.
- [7] X. Zhou, J. Yang, B. Xiao, and G. Hou, “Experimental study of temperature field in a solar chimney power setup,” *Appl. Therm. Eng.*, vol. 27, no. 11–12, pp. 2044–2050, 2007.
- [8] Gobierno Español, *Real Decreto 140/2003, de 7 de febrero, por el que se establecen los criterios sanitarios de la calidad del agua de consumo humano*. Pub. L. BOE nº 45, 2003, pp. 1–27.
- [9] D. Q. Kern, *Process Heat Transfer*, ISE. Tokyo: McGraw-Hill, 1983.
- [10] “Simulation Driven Product Development | ANSYS.” [Online]. Available: <http://www.ansys.com/>. [Accessed: 24-May-2017].

ACRONYMS

\dot{Q}	Heat flux (W)
3D	Three dimensions
A	Name for the first arrangement
A_{\min}	Minimum Area (m ²)
B	Name for the second arrangement
CFD	Computational fluid dynamics
C_p	Heat capacity (J/kg·°C)
D	Diameter (m)
d_1	Distance 1 (m)
d_2	Distance 2 (m)
DeflectorN	Deflector number
DIY	Do it yourself
e_L	Longitudinal pitch (m)
e_T	Transversal pitch (m)
f	Correction factor (Adimensional)
f	Empiric friction factor (Adimensional)
G	Mass flow density (kg/m ² ·s)
G_{\max}	Maximum mass flow density (kg/m ² ·s)
h	Heat transfer coefficient (W/m ² ·K)
k	Thermal conductivity (W/m·K)
L	Length (m)
N	Number of transversal rows
Nu	Nusselt number (Adimensional)
P_i	Pressure inlet (gauge, Pa)
PipeN	Pipe number
P_o	Pressure outler (gauge, Pa)

q	Volumetric flow rate (m^3/s)
r	Radius (m)
Re	Reynolds (Adimensional)
Re_{max}	Maximum Reynolds (Adimensional)
S	Section (m^2)
T_i	Inlet temperature (K or $^{\circ}\text{C}$)
T_o	Outlet temperature (K or $^{\circ}\text{C}$)
v_i	Velocity inlet (m/s)
v_o	Velocity outlet (m/s)
w	Mass flow (kg/s)
w_r	Mass flow for the refrigerant (kg/s)
ΔP	Pressure drop (Pa)
ΔT	Temperature drop (K or $^{\circ}\text{C}$)
ΔT_{ml}	Logarithmic mean temperature difference (Adimensional)
μ	Viscosity ($\text{kg}/\text{m}\cdot\text{s}$)
μ_b	Average viscosity of the free stream ($\text{kg}/\text{m}\cdot\text{s}$)
μ_w	Viscosity in the wall ($\text{kg}/\text{m}\cdot\text{s}$)
ρ	Density (kg/m^3)

APPENDICES

APPENDIX 1. TUBE GEOMETRY FOR THE DIFFERENT CASES

The different tube diameters used in the previous calculations are listed below.

Table 1. D = 4.8 mm

Geometry conditions.

e_T (m)	e_L (m)	D (m)	d_1 (m)	d_2 (m)
0.012	0.006	0.005	0.004	0.004

Air properties

v (m/s)	μ (kg/(m·s))	ρ (kg/m ³)	k (W/(m·K))	v (m/s)
2.3	1.91E-05	1.1	0.03	2.3

Calculation of the Reynolds

G (kg/(m ² ·s))	G_{max} (kg/(m ² ·s))	Re
2.5	4.2	1050.7

Calculation of h

a	m	N° of rows	Correction factor	Nusselt	h (W/(m ² ·K))
0.5	0.6	6	0.9	23.9	132.0

Calculation of the area.

T_i (°C)	T_o (°C)	w (kg/s)	C_p (J/kg·°C)	ΔT (°C)	\dot{Q} (W)	ΔT_{ml}	A (m ²)
30	25	0.02	717.6	5	59.9	7.2	0.06

Calculation of the number of tubes

Perimeter (m)	Length (m)	Height (m)	N° of tubes
0.02	4.2	0.2	21

Table 2. D = 8 mm

Geometry conditions.

e_T (m)	e_L (m)	D (m)	d_1 (m)	d_2 (m)
0.020	0.010	0.008	0.006	0.006
0.020	0.010	0.008	0.006	0.006
0.020	0.010	0.008	0.006	0.006

Air properties

v (m/s)	μ (kg/(m·s))	ρ (kg/m ³)	k (W/(m·K))	v (m/s)
2.5	1.84E-05	1.2	0.03	2.5
2.5	1.85E-05	1.2	0.03	2.5
2.5	1.86E-05	1.2	0.03	2.5

Calculation of the Reynolds

G (kg/(m ² ·s))	G_{max} (kg/(m ² ·s))	Re
2.9	4.9	$2.13 \cdot 10^3$
2.9	4.9	$2.11 \cdot 10^3$
2.9	4.9	$2.10 \cdot 10^3$

Calculation of h

a	m	Nº of rows	Correction factor	Nusselt	h (W/(m ² ·K))
0.5	0.6	4	0.88	33.2	107.6
0.5	0.6	4	0.88	33.1	107.7
0.5	0.6	4	0.88	33.0	108.0

Calculation of the area.

T_i (°C)	T_o (°C)	w (kg/s)	C_p (J/kg·°C)	ΔT (°C)	\dot{Q} (W)	ΔT_{ml}	A (m ²)
26	23	0.12	1006.9	3	354.0	4.3	0.76
30	25	0.12	1007.1	5	590.0	7.2	0.76
34	27	0.12	1007.1	7	826.0	10.1	0.76

Calculation of the number of tubes

Perimeter (m)	Length (m)	Height (m)	Nº of tubes
0.04	20.2	1	20
0.04	20.1	1	20
0.04	20.1	1	20

Calculation of the pressure drop

f'	ΔP (Pa)
0.27	44.1
0.27	43.8
0.27	43.5

Table 3. D = 12 mm

Geometry conditions.

e_T (m)	e_L (m)	D (m)	d_1 (m)	d_2 (m)
0.02	0.01	0.012	0.005	0.006
0.02	0.01	0.012	0.005	0.006
0.02	0.01	0.012	0.005	0.006

Air properties

v (m/s)	μ (kg/(m·s))	ρ (kg/m ³)	k (W/(m·K))	v (m/s)
2.5	1.84E-05	1.2	0.03	2.5
2.5	1.85E-05	1.2	0.03	2.5
2.5	1.86E-05	1.2	0.03	2.5

Calculation of the Reynolds

G (kg/(m ² ·s))	G_{max} (kg/(m ² ·s))	Re
2.9	7.1	$4.62 \cdot 10^3$
2.9	7.1	$4.59 \cdot 10^3$
2.9	7.0	$4.56 \cdot 10^3$

Calculation of h

a	m	N° of rows	Correction factor	Nusselt	h (W/(m ² ·K))
0.5	0.6	4	0.88	49.0	105.8
0.5	0.6	4	0.88	48.8	106.0
0.5	0.6	4	0.88	48.6	106.2

Calculation of the area.

T_i (°C)	T_o (°C)	w (kg/s)	C_p (J/kg·°C)	ΔT (°C)	\dot{Q} (W)	ΔT_{ml}	A (m ²)
------------	------------	------------	-----------------	-----------------	---------------	-----------------	---------------------

26	23	0.12	1006.9	3	354.0	4.3	0.8
30	25	0.12	1007.1	5	590.0	7.2	0.8
34	27	0.12	1007.1	7	826.0	10.1	0.8

Calculation of the number of tubes

Perimeter (m)	Length (m)	Height (m)	Nº of tubes
0.04	20.5	1	21
0.04	20.5	1	20
0.04	20.4	1	20

Calculation of the pressure drop

f'	ΔP (Pa)
0.28	119.2
0.28	118.3
0.28	117.5

Table 4. D = 15 mm

Geometry conditions.

e_T (m)	e_L (m)	D (m)	d_1 (m)	d_2 (m)
0.027	0.014	0.015	0.004	0.006

Air properties

v (m/s)	μ (kg/(m·s))	ρ (kg/m ³)	k (W/(m·K))	v (m/s)
2.3	1.91E-05	1.1	0.03	2.3

Calculation of the Reynolds

G (kg/(m ² ·s))	G_{max} (kg/(m ² ·s))	Re
2.5	8.3	$6.50 \cdot 10^3$

Calculation of h

a	m	Nº of rows	Correction factor	Nusselt	h (W/(m ² ·K))
0.5	0.6	6	0.94	63.2	111.6

Calculation of the area.

T_i (°C)	T_o (°C)	w (kg/s)	C_p (J/kg·°C)	ΔT (°C)	\dot{Q} (W)	ΔT_{ml}	A (m ²)
30	25	0.02	717.6	5	59.9	7.2	0.1

Calculation of the number of tubes

Perimeter (m)	Length (m)	Height (m)	N° of tubes
0.05	1.6	0.2	8

Table 5. D = 18 mm

Geometry conditions.

e_T (m)	e_L (m)	D (m)	d_1 (m)	d_2 (m)
0.036	0.017	0.018	0.007	0.009

Air properties

v (m/s)	μ (kg/(m·s))	ρ (kg/m ³)	k (W/(m·K))	v (m/s)
2.3	1.91E-05	1.1	0.03	2.3

Calculation of the Reynolds

G (kg/(m ² ·s))	G_{max} (kg/(m ² ·s))	Re
2.5	6.7	$6.30 \cdot 10^3$

Calculation of h

a	m	N° of rows	Correction factor	Nusselt	h (W/(m ² ·K))
0.5	0.6	6	0.94	62.1	91.5

Calculation of the area.

T_i (°C)	T_o (°C)	w (kg/s)	C_p (J/kg·°C)	ΔT (°C)	\dot{Q} (W)	ΔT_{ml}	A (m ²)
30	25	0.02	717.6	5	59.9	7.2	0.1

Calculation of the number of tubes

Perimeter (m)	Length (m)	Height (m)	N° of tubes
0.06	1.6	0.2	8

APPENDIX 2. ANSYS® RESULTS FOR EACH SIMULATION

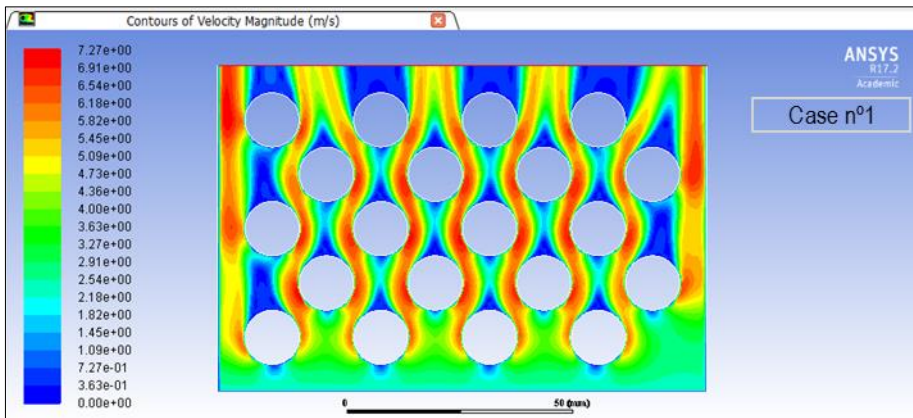
The contours for the different designs are listed below.

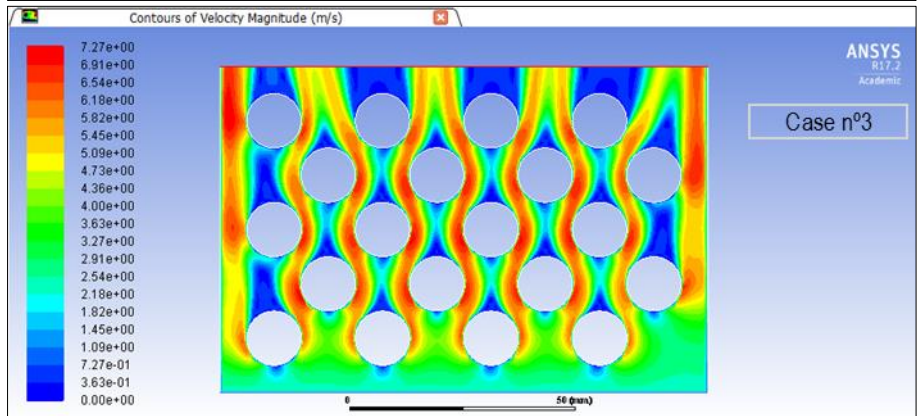
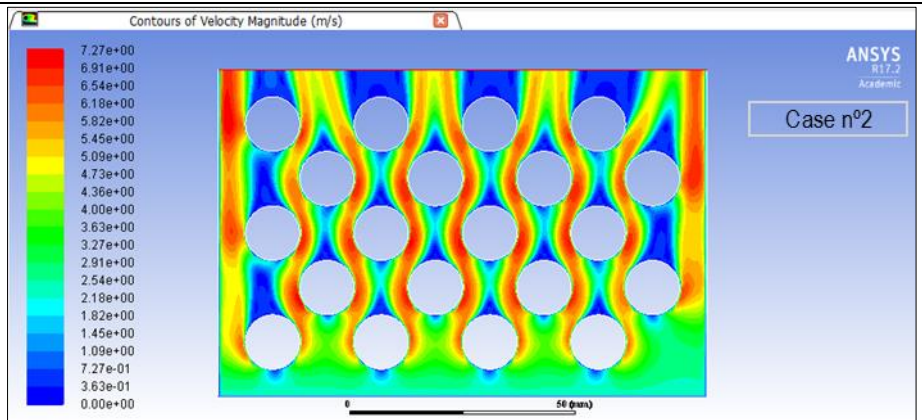
Design 1

Design 1 is the first design made. It consists of a simple staggered tube disposition, following the same dimensions as A arrangement shown in Table 4, with 20 tubes divided in five rows, with four tubes in each row. The diameter of the tube is 12 mm and the separation between tubes is 20 mm. The vertical distance between tubes of the same row is 10 mm. For this design, three different cases were studied and are shown and compared below.

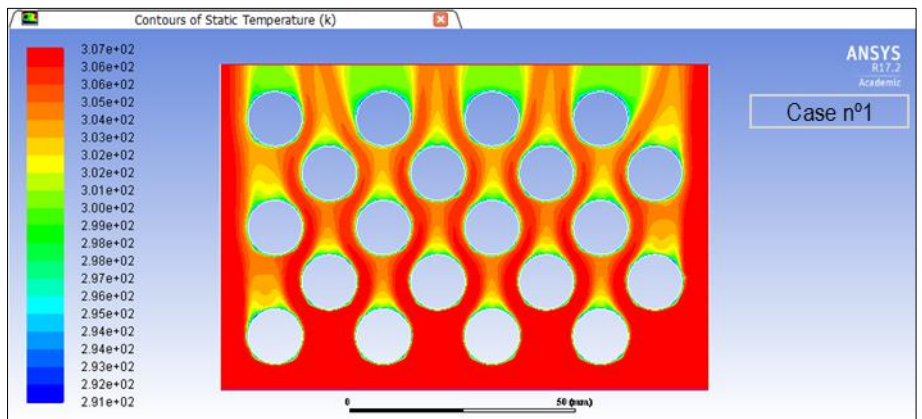
n° Design	Case n°	Mesh n° of nodes	v_i (m/s)	v_o (m/s)	T_i (°C)	T_o (°C)	ΔT (°C)	ΔP (Pa)
1	1	47,226	2.5	2.8	34.0	29.2	4.8	290.0
	2	47,226	2.5	2.8	30.0	26.5	3.5	290.0
	3	47,226	2.5	2.8	26.0	23.8	2.2	300.0

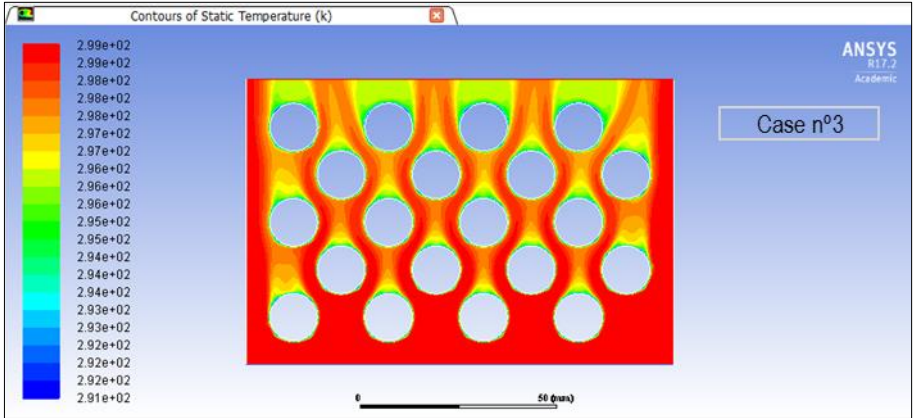
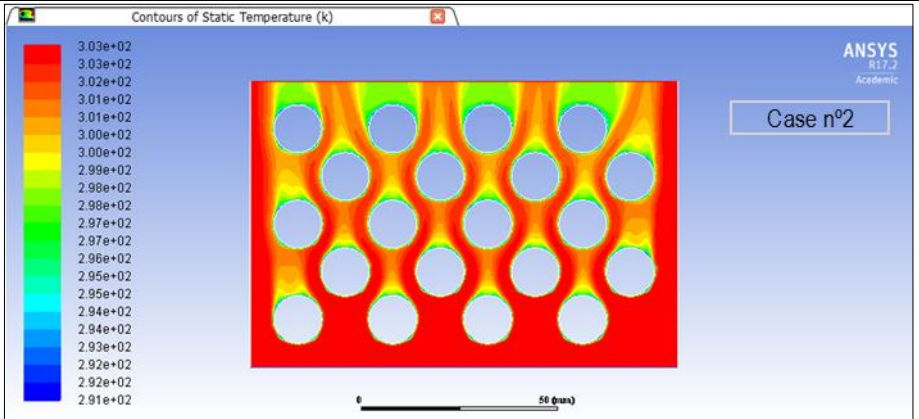
For the velocity contour, it is possible to identify the preferential paths created by the air, and the two main preferential paths created on the left and right sides. Different low velocity zones are created behind each tube indicated by a blue colour. When the temperature is changed, the velocity profile remains stable for all three cases as shown in the figures below.



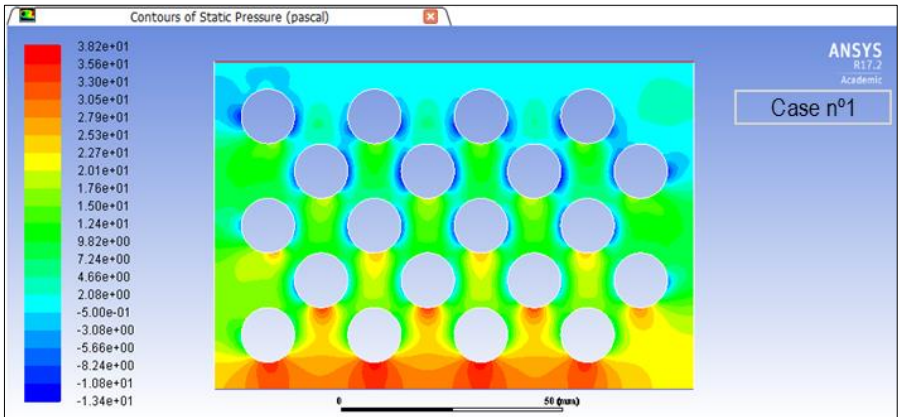


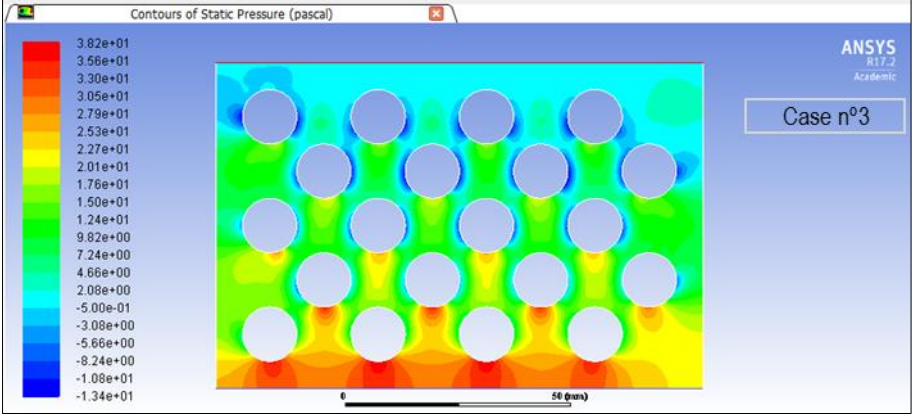
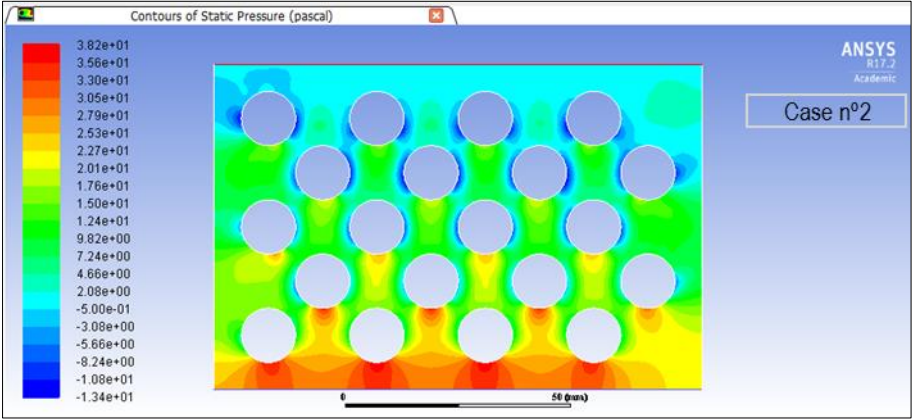
As for the temperature profile, the design is not able to cool the air in the three cases. This is mostly due to the preferential paths created at both sides of the design where the air is barely cooled.





The pressure contour shows that the pressure drop remains practically constant when the inlet temperature is changed.



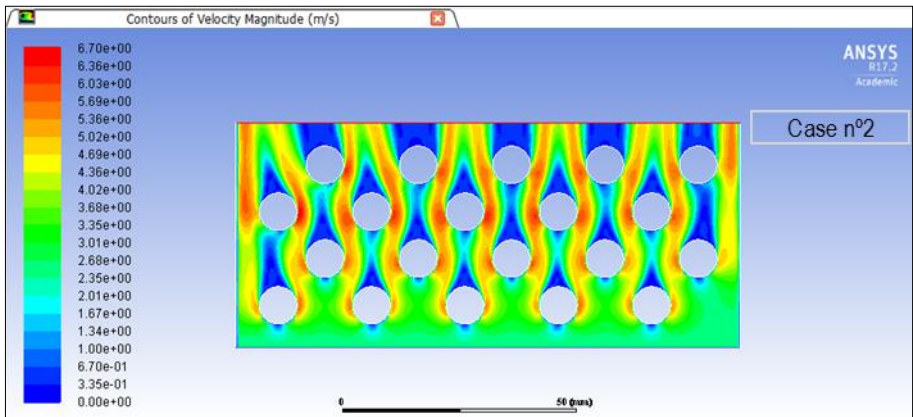
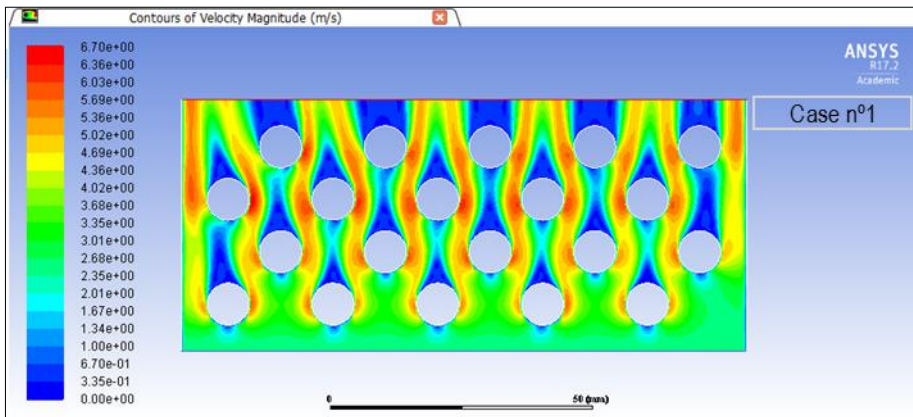


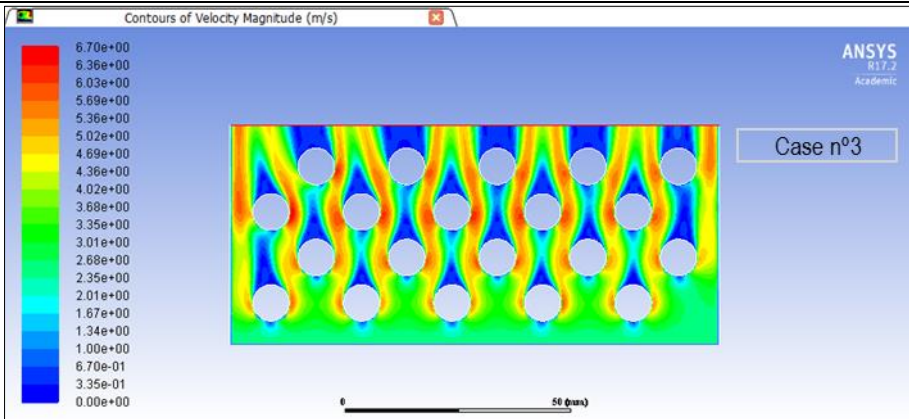
Design 2

Design 2 is made using the dimensions indicated in Table 4 arrangement B. It consists of a staggered tube bench, divided in four rows of five tubes, including 20 tubes in total. The diameter of the tubes is 8 mm.

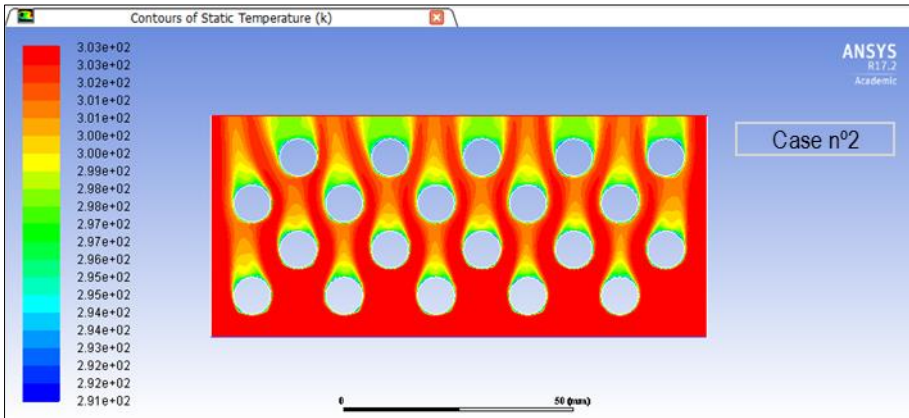
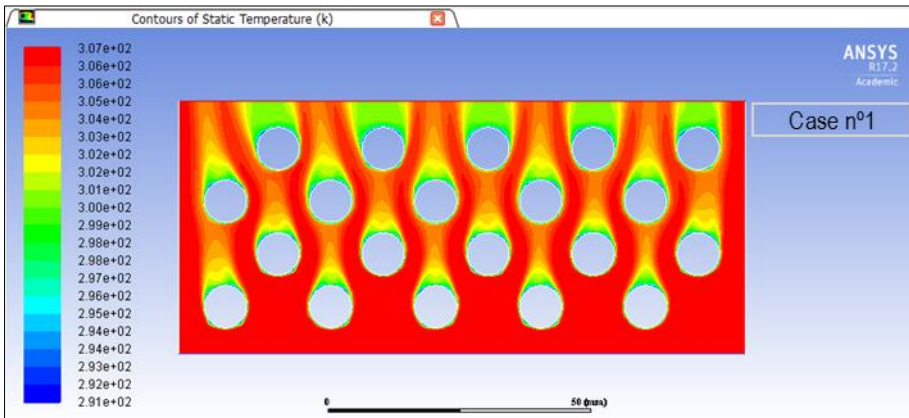
n° Design	Case n°	Mesh n° of nodes	v_i (m/s)	v_o (m/s)	T_i (°C)	T_o (°C)	ΔT (°C)	ΔP (Pa)
	1	49,335	2.5	2.7	34.0	29.8	4.2	18.0
2	2	49,335	2.5	2.7	30.0	26.9	3.1	18.0
	3	49,335	2.5	2.7	26.0	24.1	1.9	18.0

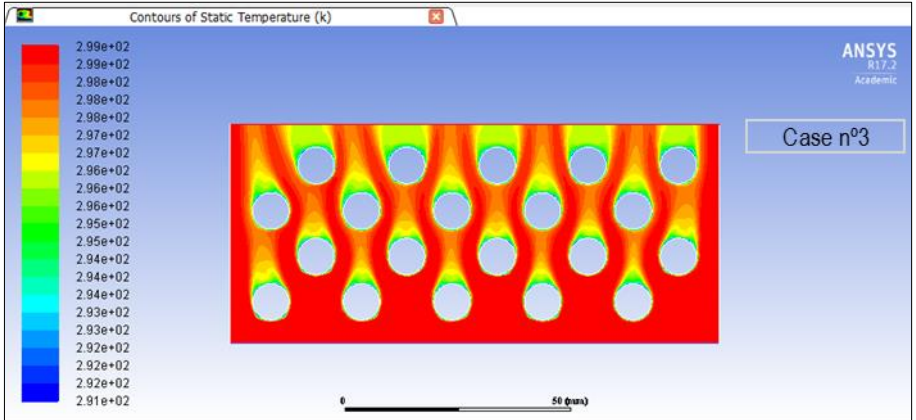
The velocity contour profile shows a similar behaviour as Design 1 with the creation of low velocity zones behind each tube, and preferential paths on both sides. Once again, the different inlet temperatures do not affect significantly the velocity



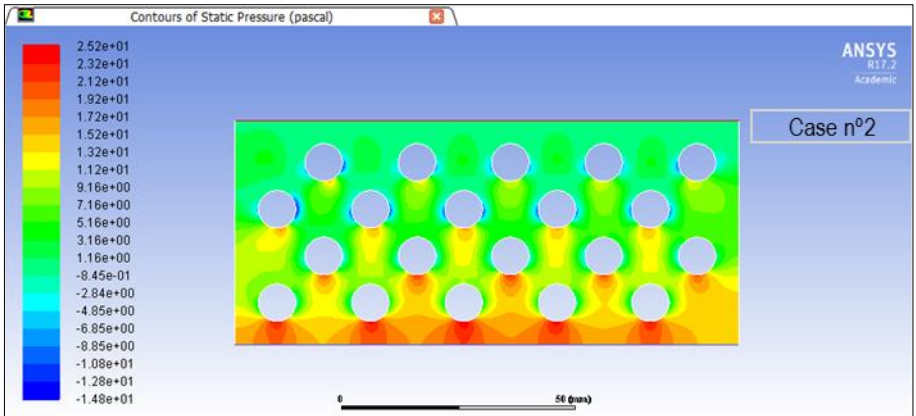
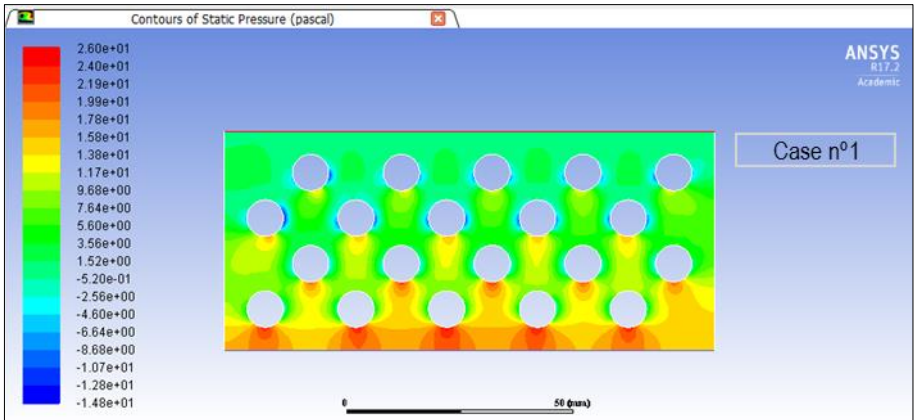


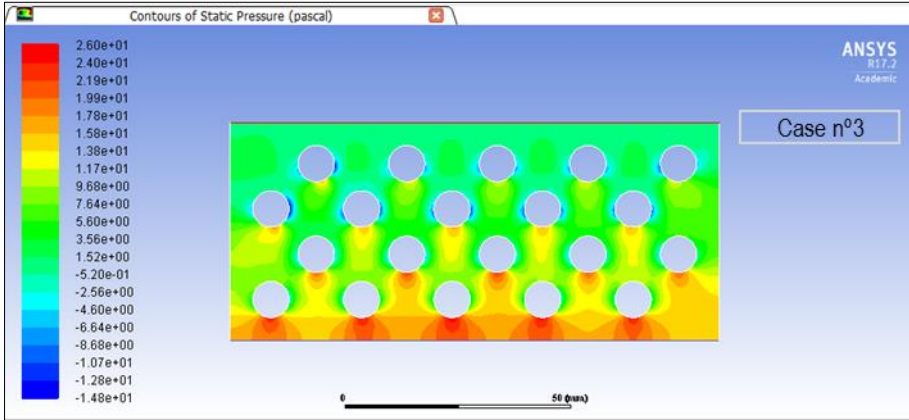
As for the temperature, the system is not able to reach the temperature of 25 °C





The pressure drop of the designs is even lower than in Design 1, only 18 Pa due to the disposition of the tubes and the absence of baffle.



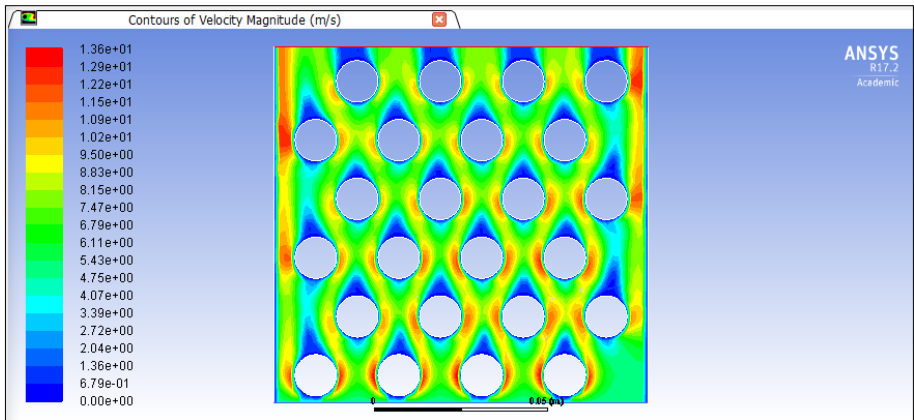


Design 3

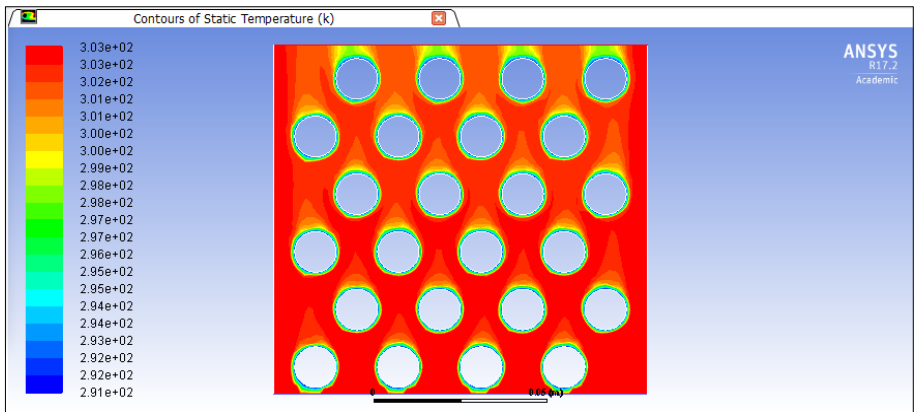
Design 3 was made in an attempt to determine if adding an additional row to Design 1; the system was able to reach the temperature of 25°C.

n° Design	Mesh n° of nodes	v_i (m/s)	v_o (m/s)	T_i (°C)	T_o (°C)	ΔT (°C)	ΔP (Pa)
3	12,578	5.0	5.4	30.0	27.5	2.5	$1.2 \cdot 10^2$

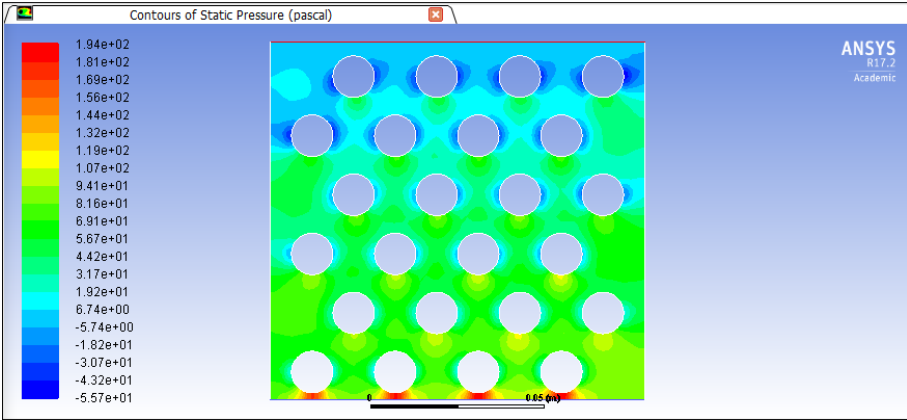
The velocity contour shows that the low velocity zones behind each tube are reduced, but in this case, the preferential paths that appeared in Design 1 are not accentuated, though on both sides of the design the preferential path are still present, and the velocity is gradually increased.



The temperature profile shows that the system is unable to reach the temperature of 25 °C at the outlet. Notice that behind each tube, a lower temperature zone is created which matches with the low velocity zones.



The pressure contour shows a gradual lowering of the pressure from the inlet to the outlet, though it is relatively low.

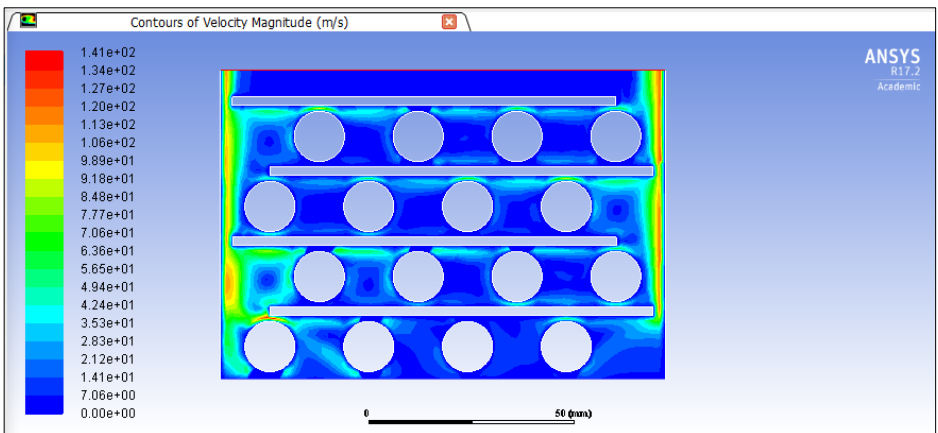


Design 4

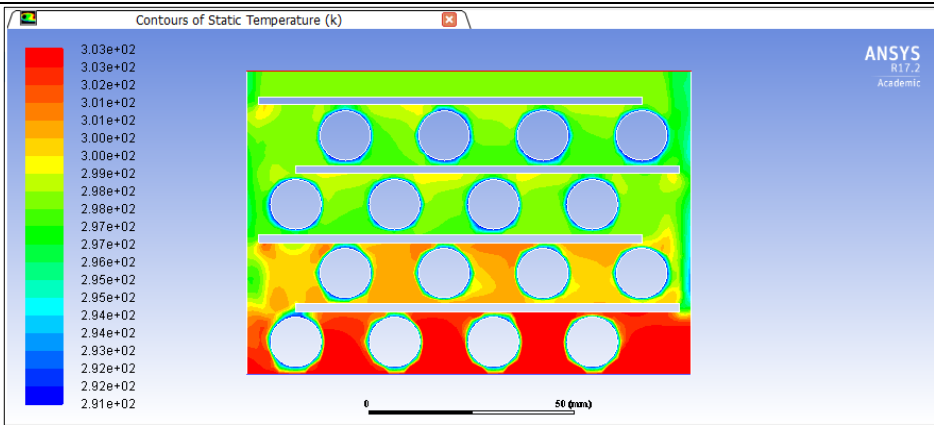
Design 4 introduces for first time the horizontal baffles in the design. In this case, 1 mm width baffles were added at Design 1. The distance between the tube and the baffle in this case is 1.5 mm to provide the best heat exchange possible. The baffle guide the air flow through each row of the tube bench. As the baffle is not attached to the wall, a space is created where the air is expanded and cooled.

n° Design	Mesh n° of nodes	v_i (m/s)	v_o (m/s)	T_i (°C)	T_o (°C)	ΔT (°C)	ΔP (Pa)
4	11,116	6.5	9.3	30.0	24.8	5.2	$2.0 \cdot 10^4$

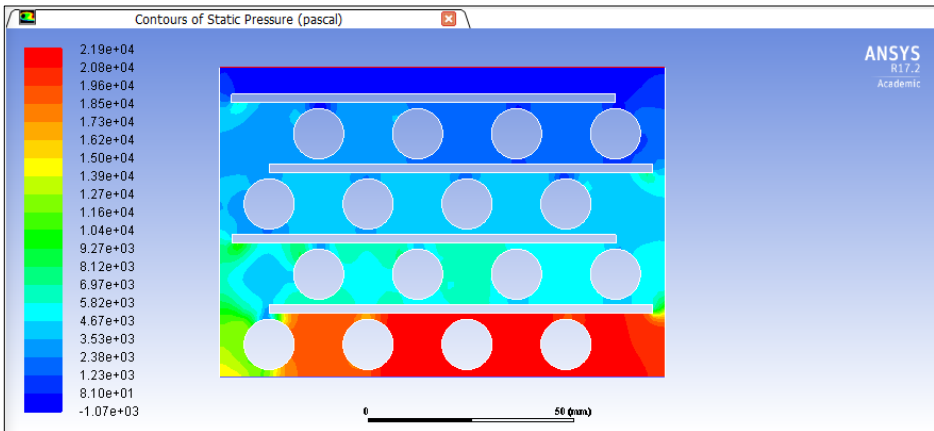
The velocity contour shows two high-speed paths in the design, one at the right and another at the left where the air goes through the space created between the wall and the baffle. The velocity in the rest of the design remains low, creating zones between the baffle and the tube where the velocity is increased.



The addition of the baffles provide a significant change on the temperature contour. In this case, the action of the wall-baffle space highly contributes on the cooling of the air. The deflectors guide the air in every row severely increasing the heat exchanged.



However, the design has an important pressure drop of $2.0 \cdot 10^4$ Pa due to the several expansions the gas suffers from the inlet to the outlet in the different zones described before. This is because an alternative solution was meant to be found in order to find a balance between pressure drop and the outlet temperature

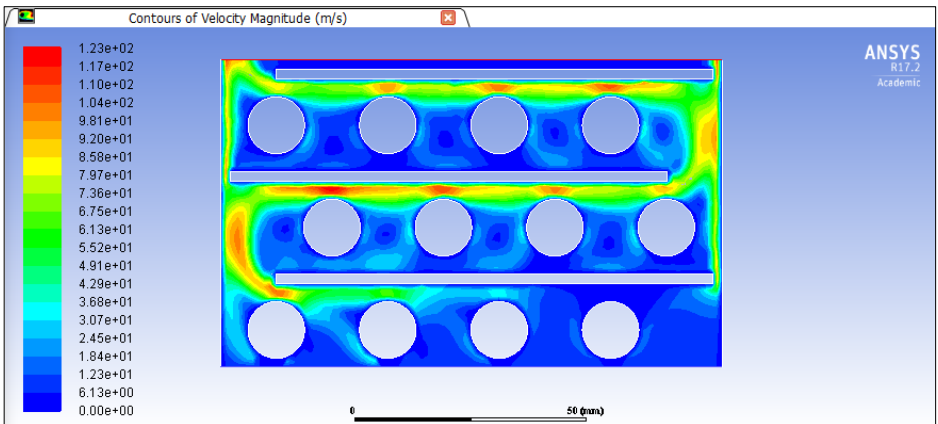


Design 5

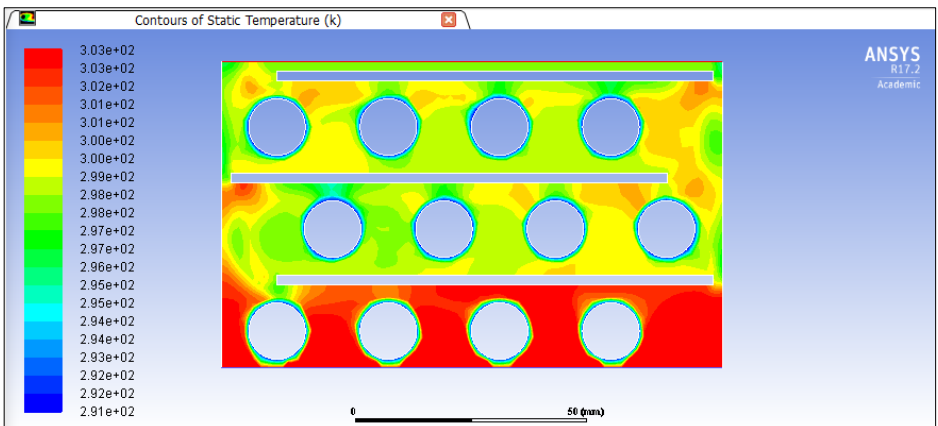
In Design 5, the space between the tube and the baffle was increased in order to decrease the pressure drop created between the tube and the baffle.

n° Design	Mesh n° of nodes	v_i (m/s)	v_o (m/s)	T_i (°C)	T_o (°C)	ΔT (°C)	ΔP (Pa)
5	10,819	6.5	8.8	30.0	24.9	5.1	$1.7 \cdot 10^4$

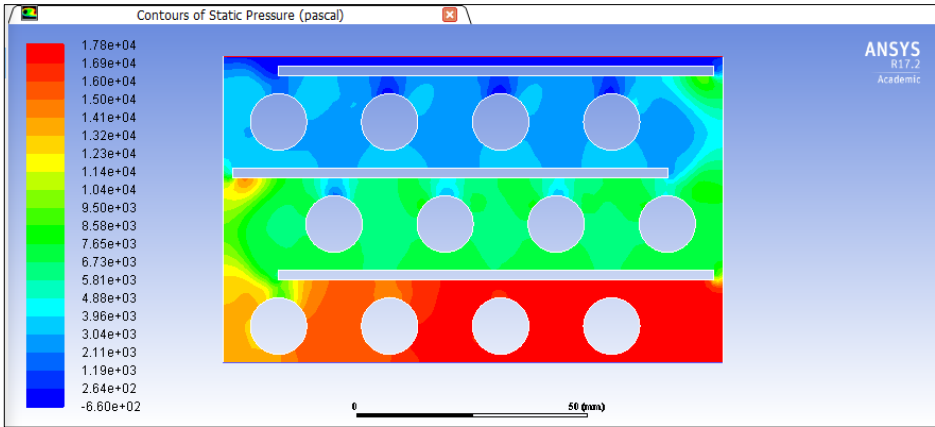
The velocity contour profile shows the appearance of a high-speed preferential path. This preferential path begins on top of the second tube of the first row (green profile zone), and crosses the second and the third row on the upper side.



The temperature profile is strongly influenced by the velocity profile as for the change of direction of the airflow could be also seen in the temperature profile. Because of the preferential path, higher temperature zones appear where the velocity is lower.



The pressure drop in this case is divided in three zones where the air gradually losses its pressure.

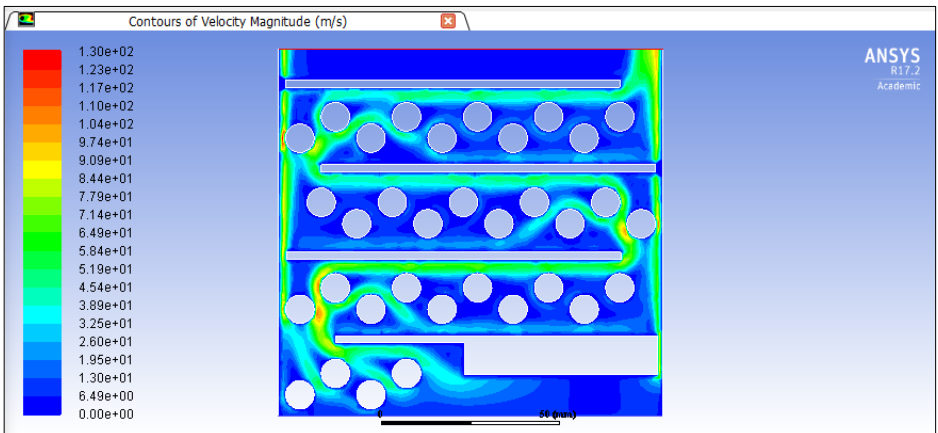


Design 6

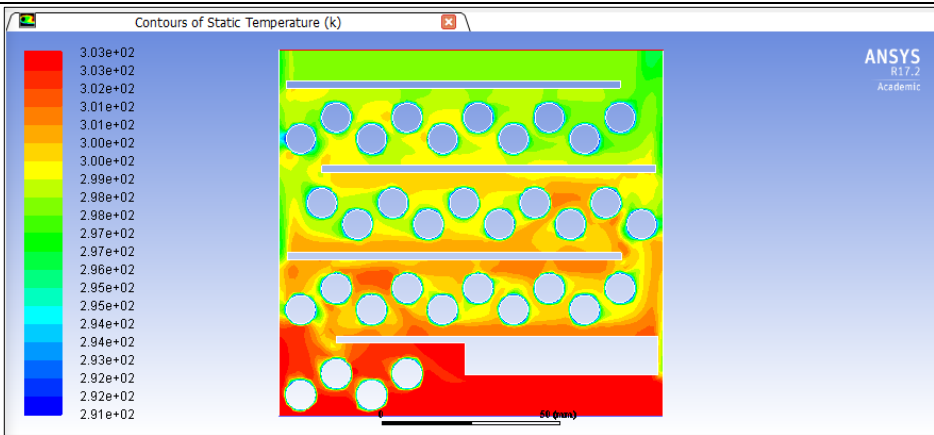
It was found that the contribution of the first tubes of the left side was not significant. Therefore, the tubes were eliminated and a rectangular baffle was added in the first row. The result is shown in Design 6. In addition, the diameter of the tubes changed to 8 mm and an additional row was added forming a staggered tube bench with five tubes per row.

n° Design	Mesh n° of nodes	v_i (m/s)	v_o (m/s)	T_i (°C)	T_o (°C)	ΔT (°C)	ΔP (Pa)
6	21,369	6.5	9.7	30.0	24.9	5.1	$1.9 \cdot 10^4$

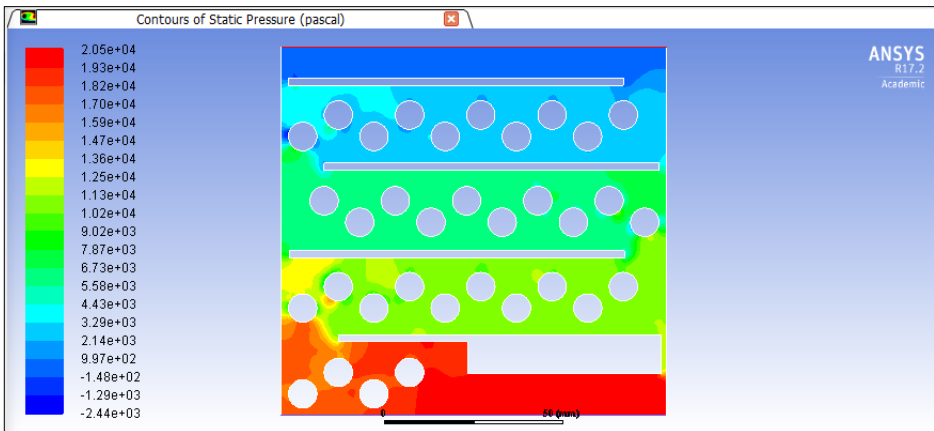
As for the velocity contour, preferential paths are still created flowing on the upper side of every row. The rectangular baffle divides the flow in two streams, one that goes through the baffle-wall space and another that goes directly to the tube bench.



The temperature profile shows a progression in the cooling of the air, but because of the preferential paths, hot air zones are created. The temperature reached at the outlet though is acceptable.



In the pressure contour, different pressure zones are created depending on the tube bench and the distance from the inlet. In this case, the pressure drop is considerably high.



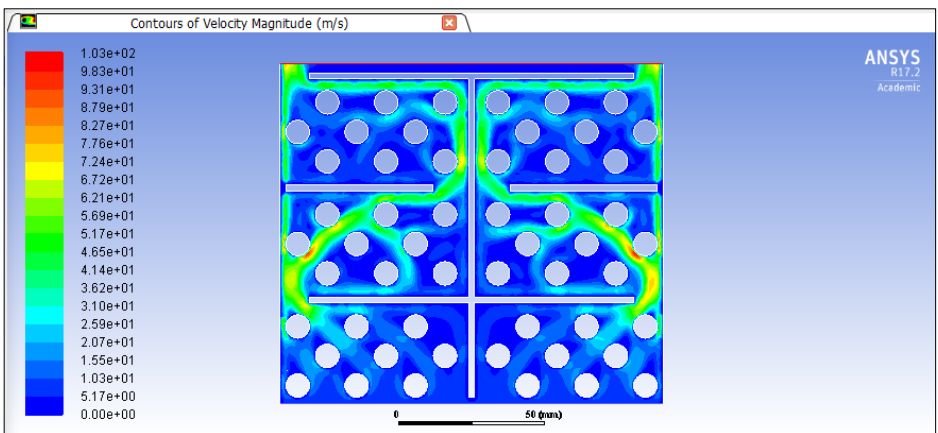
Design 7

Design 7 is the first attempt of the second final design. The design is composed by 6 zones delimited by vertical and horizontal deflectors, each zone has a staggered tube bench composed of three rows of three tubes.

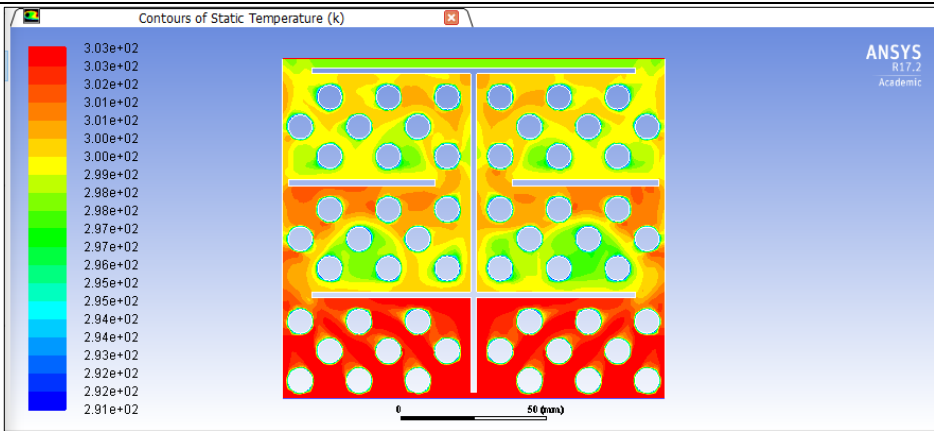
With the appearance of the vertical deflector, the problem of the prior tubes is solved. The airflow is now divided in two different parts, and goes through each tube bench until reaches the outlet. Notice that in the outlet, a horizontal deflector is added to force the airflow to cross the entire tube bench in order to reach the exit

n° Design	Mesh n° of nodes	v_i (m/s)	v_o (m/s)	T_i (°C)	T_o (°C)	ΔT (°C)	ΔP (Pa)
7	11,836	6.5	8.5	30.0	25.0	5.0	$8.7 \cdot 10^4$

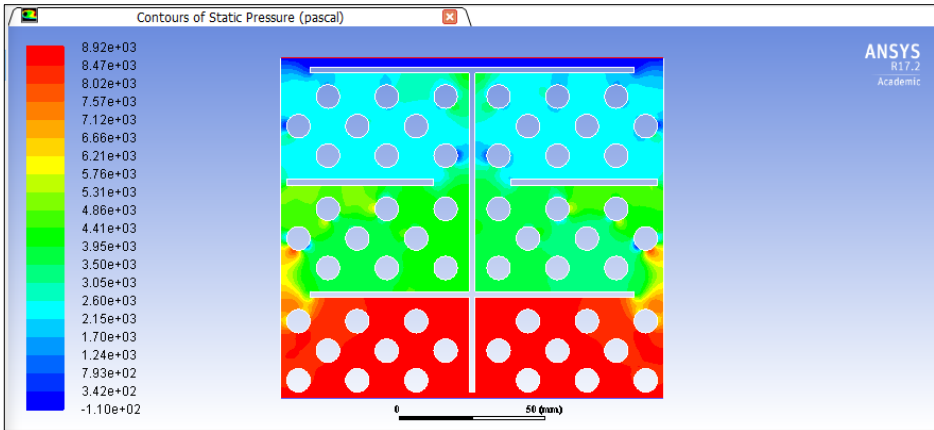
The velocity contour shows the creation of preferential paths (green) all over the design. At the inlet, the different paths the air follows converge at the end of the first tube bench, increasing the velocity and creating a preferential path that crosses the second tube bench straight. At the third tube bench, the airflow goes straight to the outlet striking directly on the vertical and horizontal baffles.



The temperature contour shows a progressive cooling through the design, reaching an outlet temperature of 25 °C. Here, the geometry of the tubes and its arrangement has a great influence in the temperature.



As for the pressure contour, different pressure zones are created on each zone. Most of the pressure drop is due to the wall-deflector spaces.

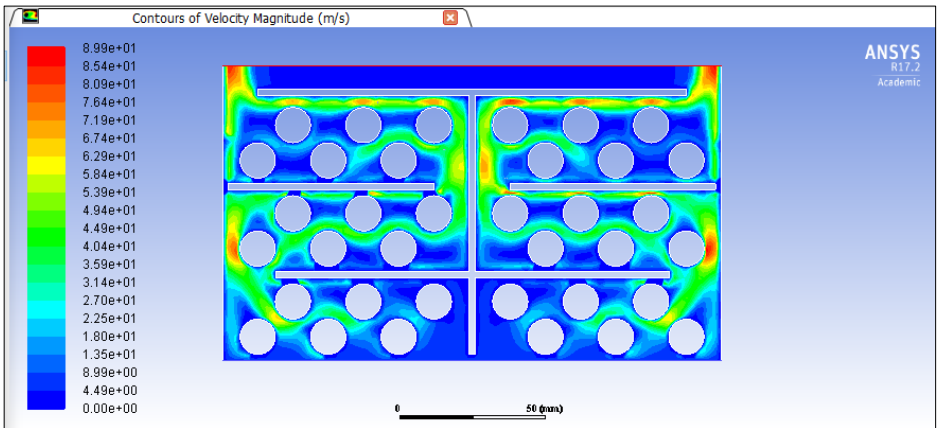


Design 8

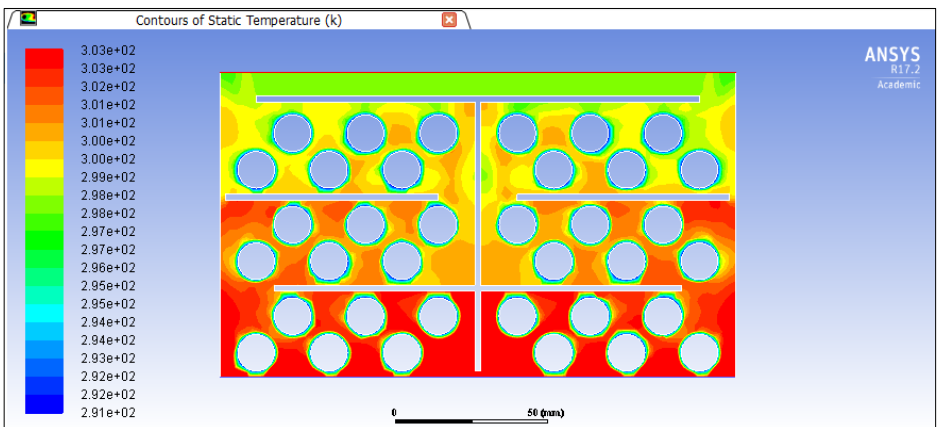
Design 8 consist of a modification of design 7. The diameter tube was increased to 12 mm and one row on each section was eliminated.

n° Design	Mesh n° of nodes	v_i (m/s)	v_o (m/s)	T_i (°C)	T_o (°C)	ΔT (°C)	ΔP (Pa)
8	14,360	6.5	8.5	30.0	25.0	5.0	$1.2 \cdot 10^4$

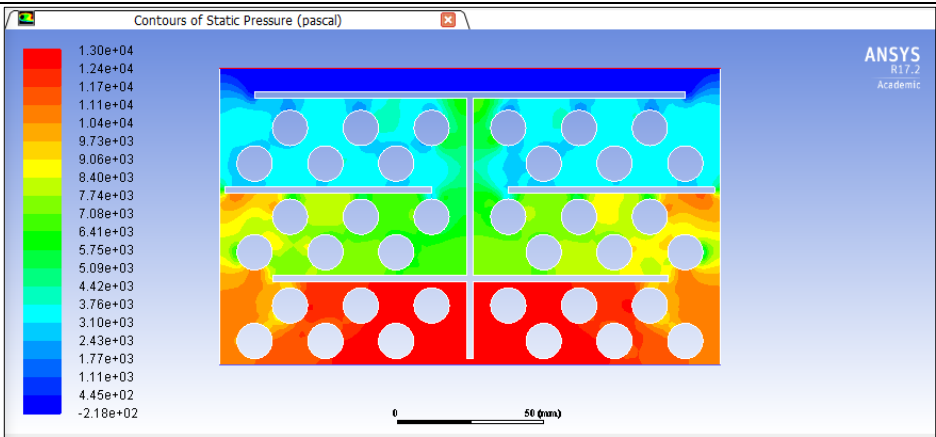
The velocity profile is similar to the velocity profile of Design 7. In this case, the preferential path on the second section is located between the tubes. In the third row, the preferential path is partially divided and joined in the outlet.



The temperature profile shows a progressive cooling of the air. However, different hot zones are created because low velocity and the creation of the preferential path.



In this case, the pressure loss is lower than Design 7 and has a similar behaviour, creating different pressure zones on each section.

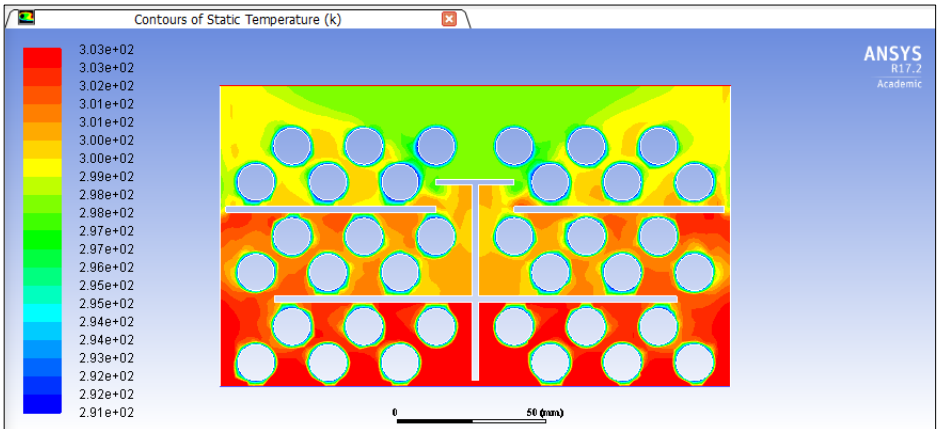
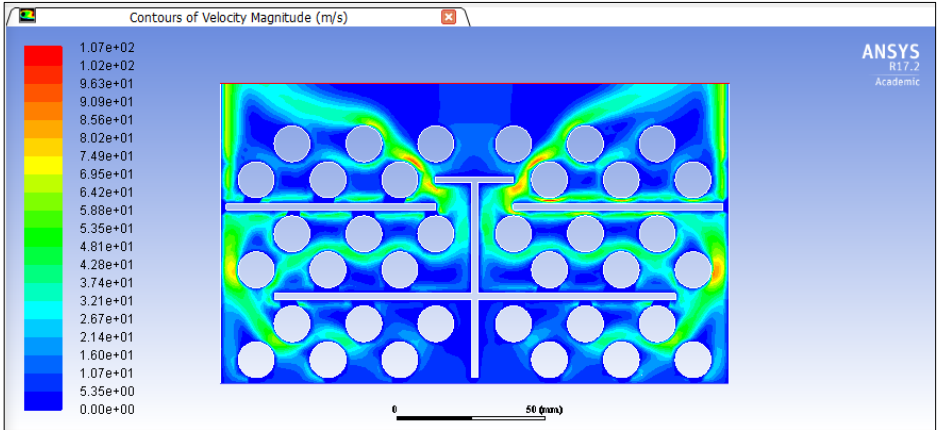


Design 9

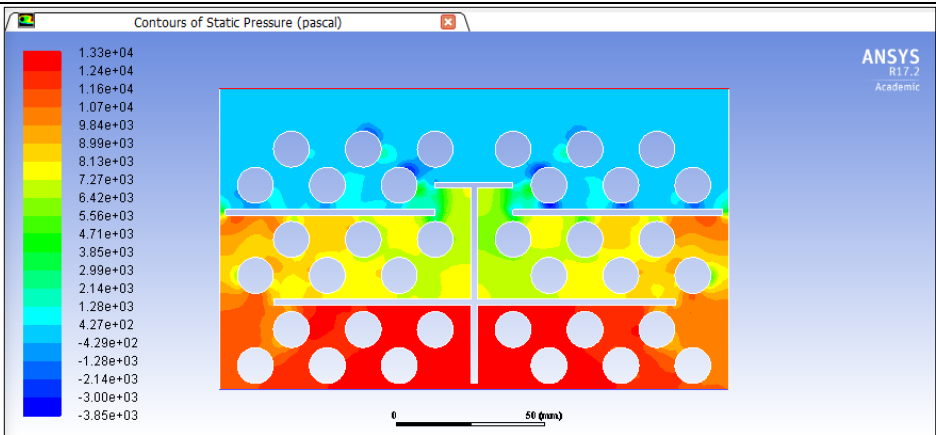
In an attempt to eliminate the problem of the preferential paths created in the previous design and guide the airflow through the entire tube bench in the last row, Design 9 was proposed.

n° Design	Mesh n° of nodes	v _i (m/s)	v _o (m/s)	T _i (°C)	T _o (°C)	ΔT (°C)	ΔP (Pa)
9	14,406	6.5	15.9	30.0	25.3	4.7	1.2·10 ⁴

Unfortunately, as shown in the velocity contour, most of the airflow is not redirected and goes straight to the outlet at the same temperature that has at the exit of the second tube bench



As for the pressure drop, the value remains constant if we compare with Design 8



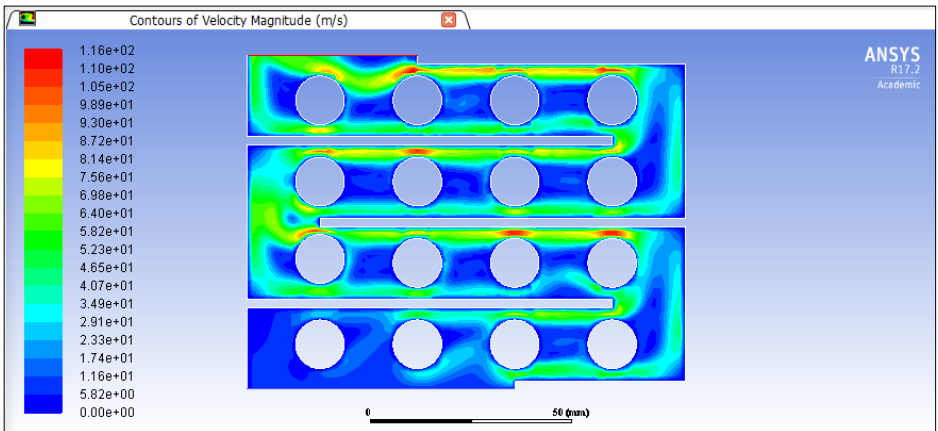
Design 10

Design 10 is one of the final variations of Design 1. In Design 10 the wall-baffle space disappears and now the deflector is joined to the wall.

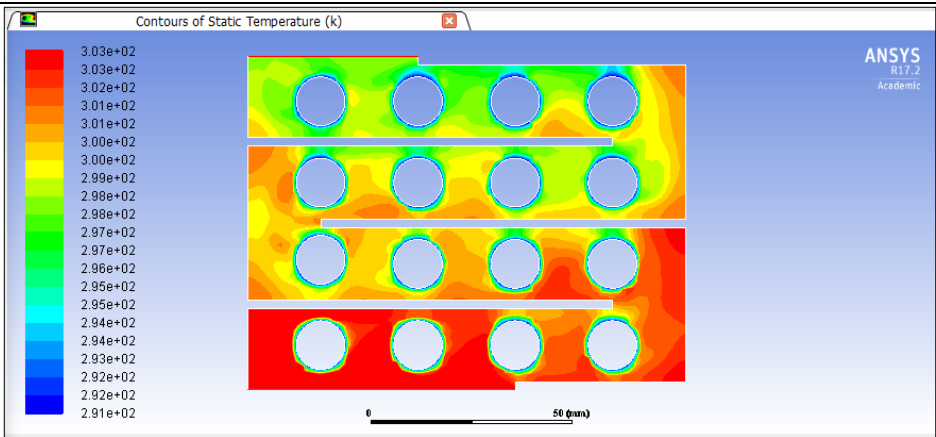
By eliminating this space, all the airflow is forced to cross the entire each row in order to reach the outlet. By adding two barriers at the inlet and at the outlet, the heat transfer of the first and last row is highly increased.

n° Design	Mesh n° of nodes	v _i (m/s)	v _o (m/s)	T _i (°C)	T _o (°C)	ΔT (°C)	ΔP (Pa)
10	12,576	6.5	33.2	30.0	24.8	5.2	2.5·10 ⁴

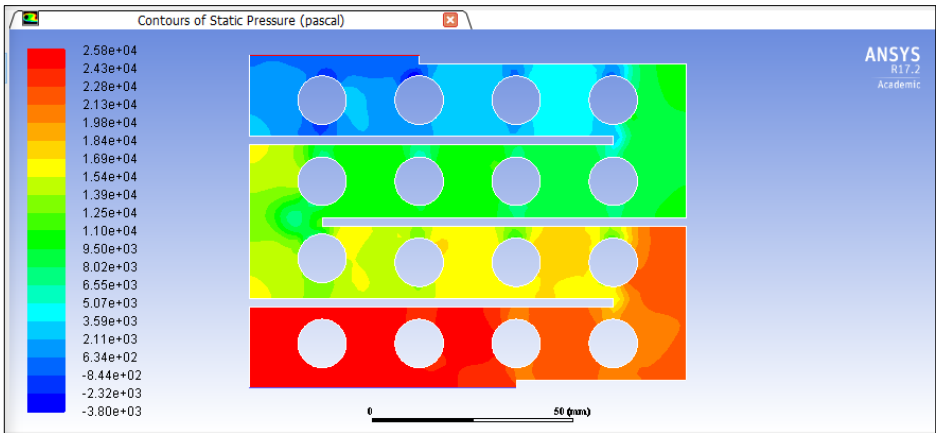
The velocity contour shows the creation of two preferential paths for the airflow. It could be also noticed that in the corners of the design the velocity is 0, meaning that the air is not being renovated.



As for the temperature profile, it is important to notice the creation of dead spaces in the corners of the walls of the designs because of the preferential paths. These hot spaces of null speed difficult the calculation of the solution.



The pressure drop in this design is mostly due to the different changes of the course of the airflow.

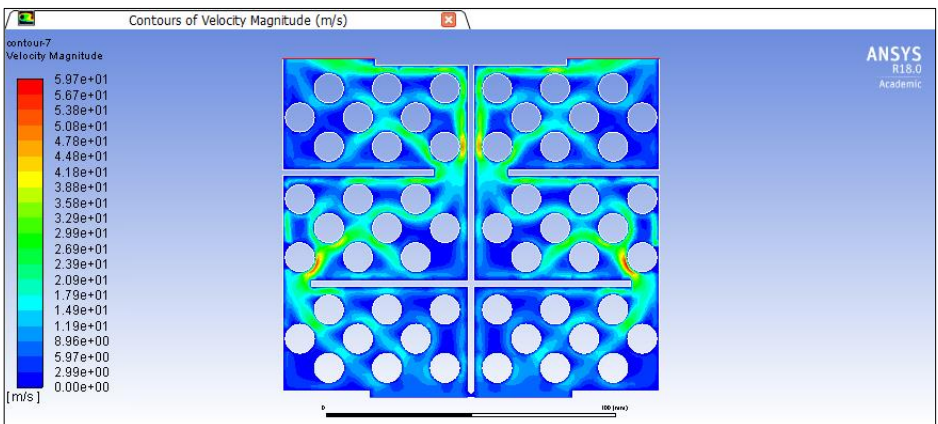


Design 11

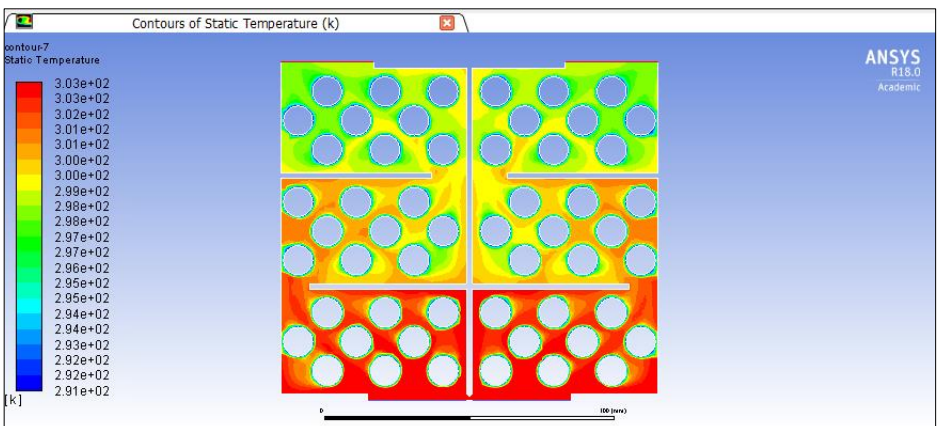
Design 11 is a modification of Design 7 including the baffles attached to the wall and the barriers in the inlet and outlet. Design 11 is considered a previous version of the second final design.

n° Design	Mesh n° of nodes	v _i (m/s)	v _o (m/s)	T _i (°C)	T _o (°C)	ΔT (°C)	ΔP (Pa)
11	18,552	6.5	17.2	30.0	25.3	4.7	3.6·10 ³

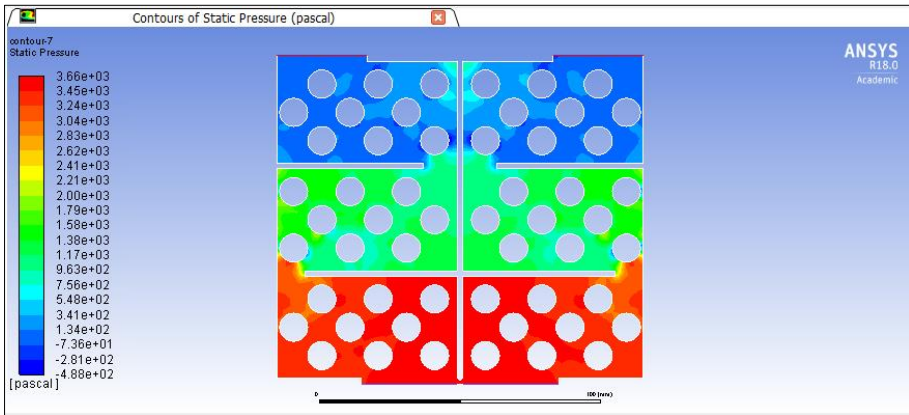
By joining the baffle to the wall, the air is forced to change its direction, increasing the heat transferred with the tubes, though it creates dead zones where the air is not being renovated. The airflow in the last zone goes straight to the outlet and only a small part is divided from the main flow and goes through the tube bench.



As for the temperature contour, it important to notice the creation of hot spaces in the corners of the design.



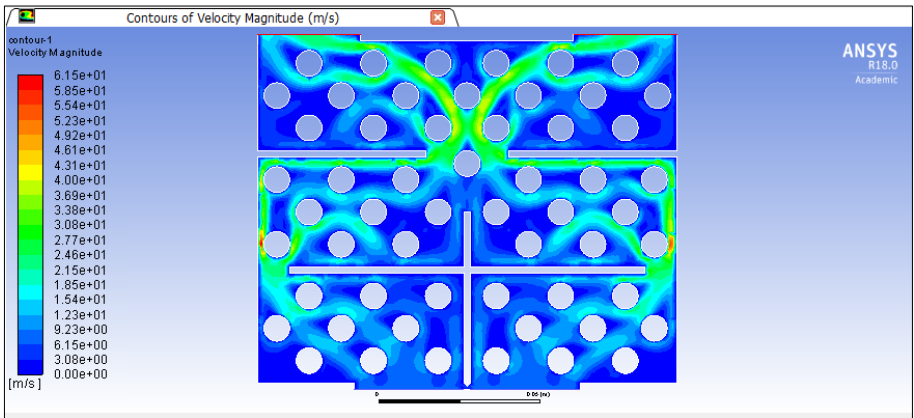
The pressure contour shows the different zones from the inlet to the outlet in descending order because of the changes of direction of the airflow. Notice that the pressure remains constant in each stage and is only perturbed when the air crosses from one section to another.



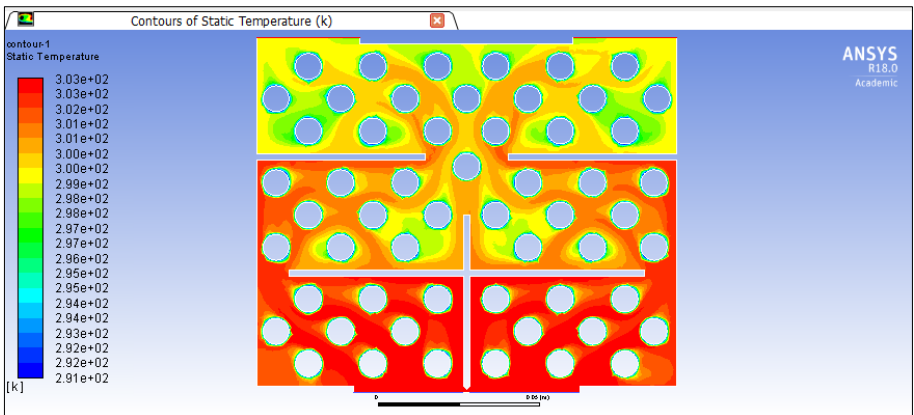
Design 12

Design 12 consist of a variation of design 11, where the vertical deflector is partially eliminated and substituted with two new tubes in order to eliminate the preferential path. However, instead of decreasing the effect of the preferential path, it was intensified as illustrated in the velocity contour.

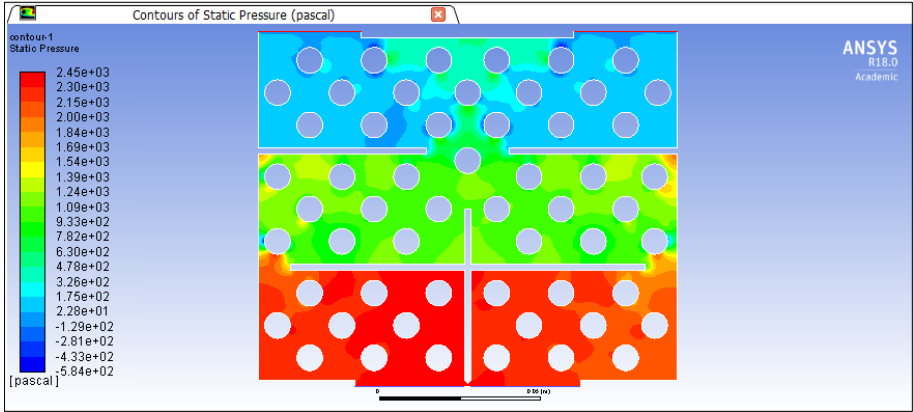
n° Design	Mesh n° of nodes	v_i (m/s)	v_o (m/s)	T_i (°C)	T_o (°C)	ΔT (°C)	ΔP (Pa)
12	39,677	6.5	16.0	30.0	25.8	4.2	$2.3 \cdot 10^3$



The temperature at the outlet was also increased due to this preferential path



The pressure drop though, decreased from Design 11.

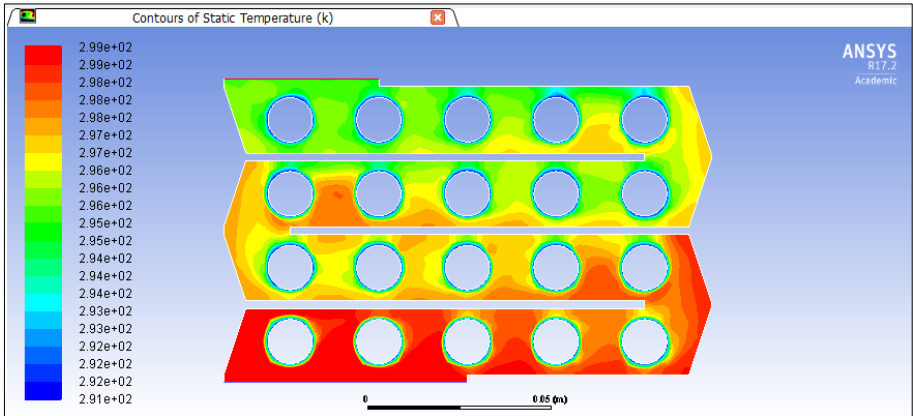
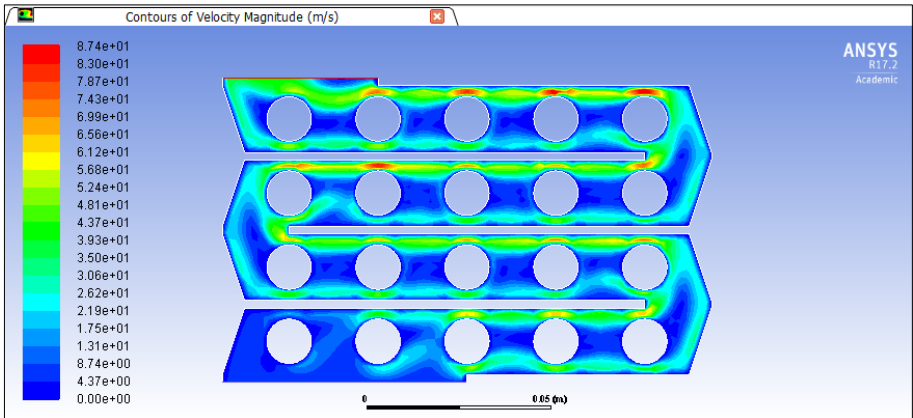


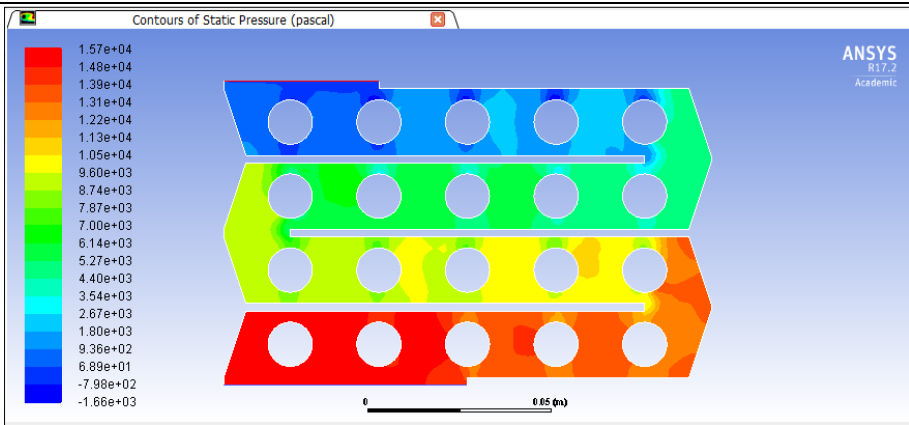
APPENDIX 3. FINAL DESIGN 13 USING ANSYS®

This appendix is divided in the different cases carried out.

Case 1. 26 °C to 23 °C and $v_i = 5$ m/s

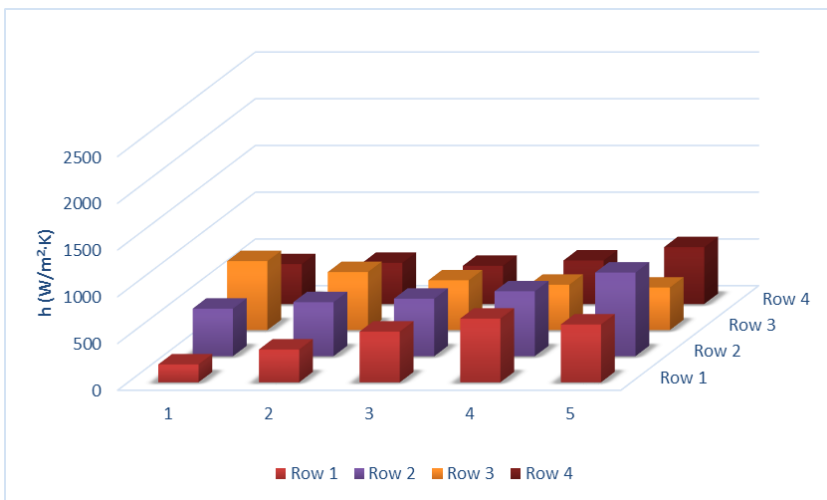
The velocity, temperature and pressure contours are shown in the subsequent Figures.





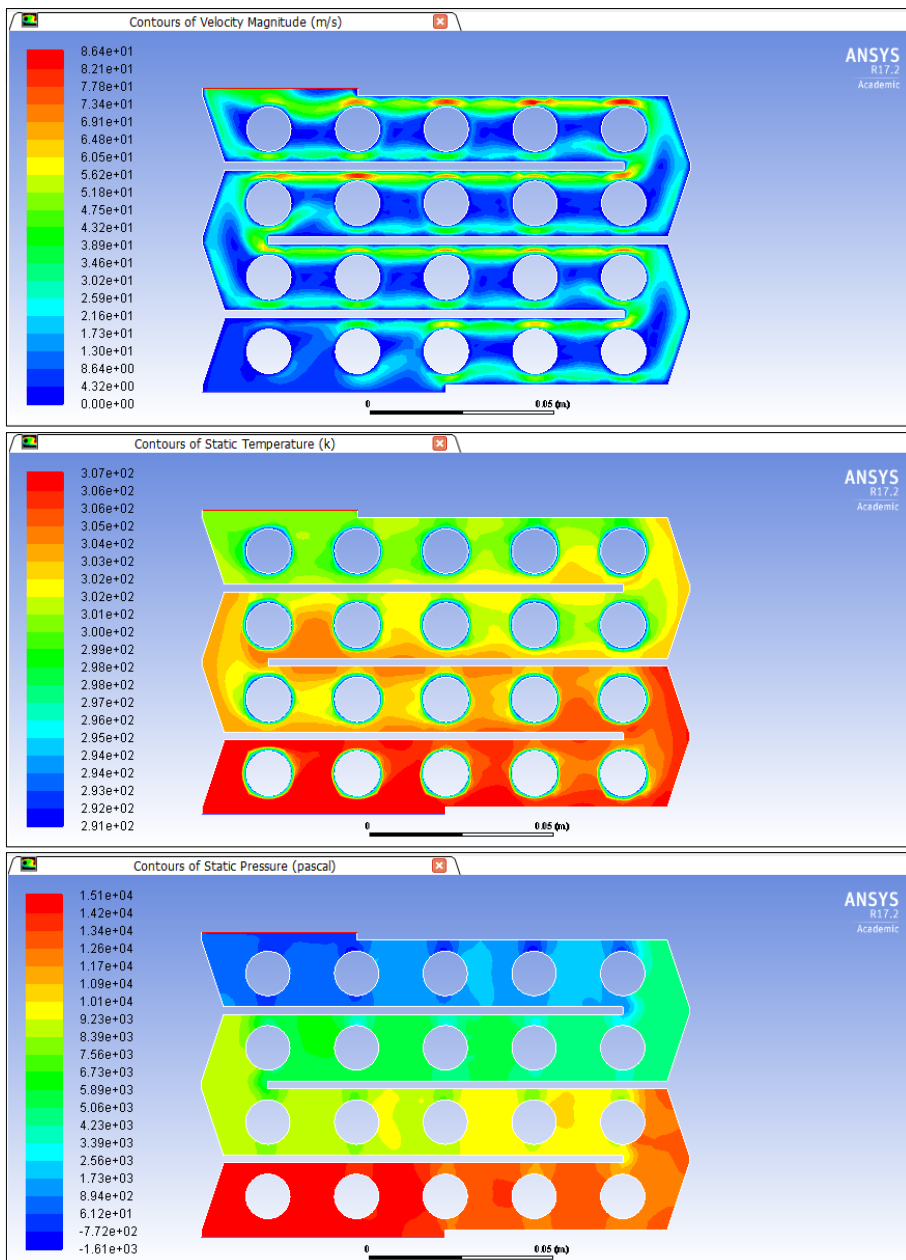
The values of h on each tube of the design are listed and illustrated in the table and figure below. The values of h in this conditions are low because the inlet temperature and the temperature of the tubes are close to each other.

h (W/m ² ·K)	Row 1	Row 2	Row 3	Row 4
1	191.5	509.2	738.0	426.2
2	351.0	577.8	620.9	439.8
3	542.6	615.2	532.3	408.4
4	681.9	694.5	485.3	465.4
5	618.8	894.6	455.2	608.2



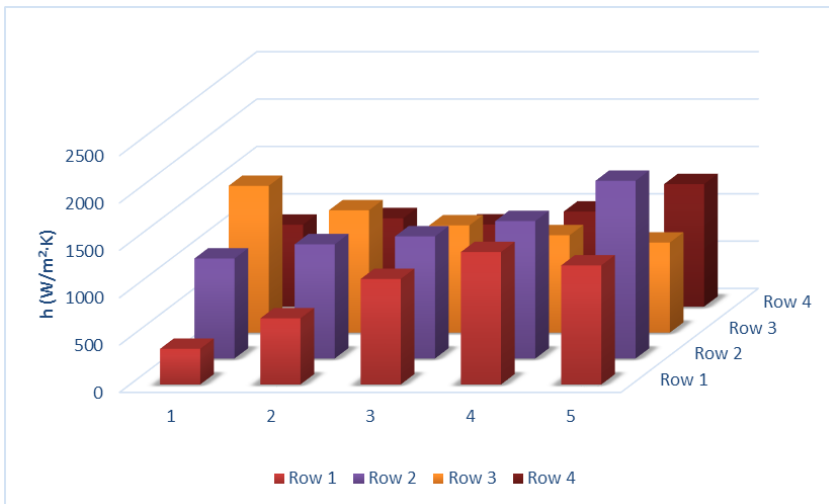
Case 2. 34 °C to 27 °C and $v_i= 5 \text{ m/s}$

The velocity, temperature and pressure contours are shown in the subsequent Figures.



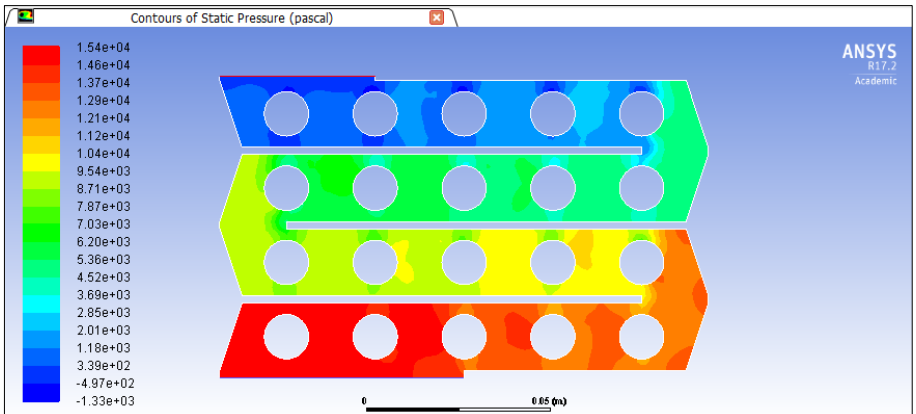
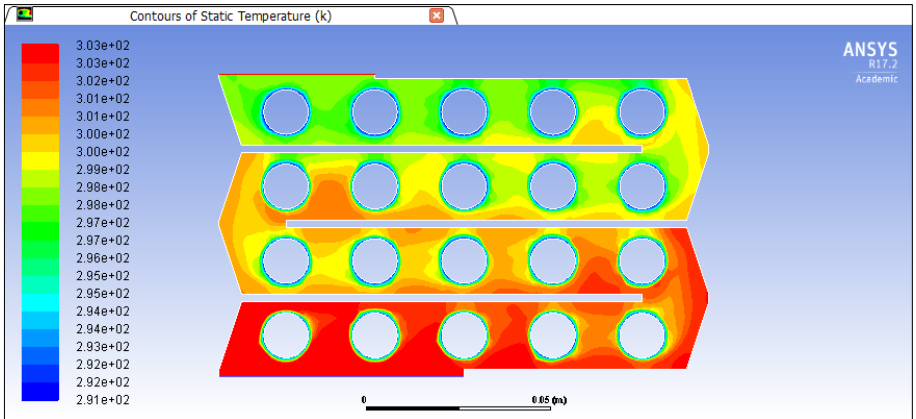
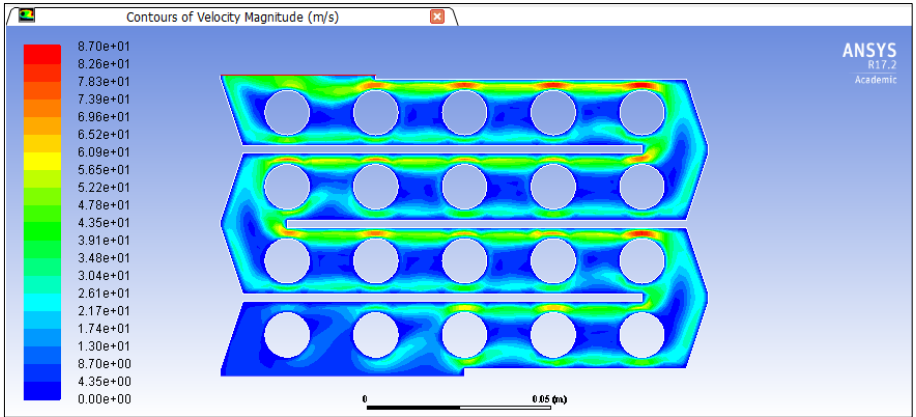
The values of h on each tube of the design are listed and illustrated in the table and figure below. By increasing the difference between the inlet temperature, the system is capable to increase the heat exchanged. The values of h here are increased if we compare them with case 2.

h (W/m ² ·K)	Row 1	Row 2	Row 3	Row 4
1	376.2	1056.3	1549.4	865.3
2	698.7	1206.7	1291.7	933.8
3	1113.8	1290.0	1131.9	867.8
4	1398.4	1451.3	1027.7	1003.9
5	1257.0	1876.9	950.2	1294.0



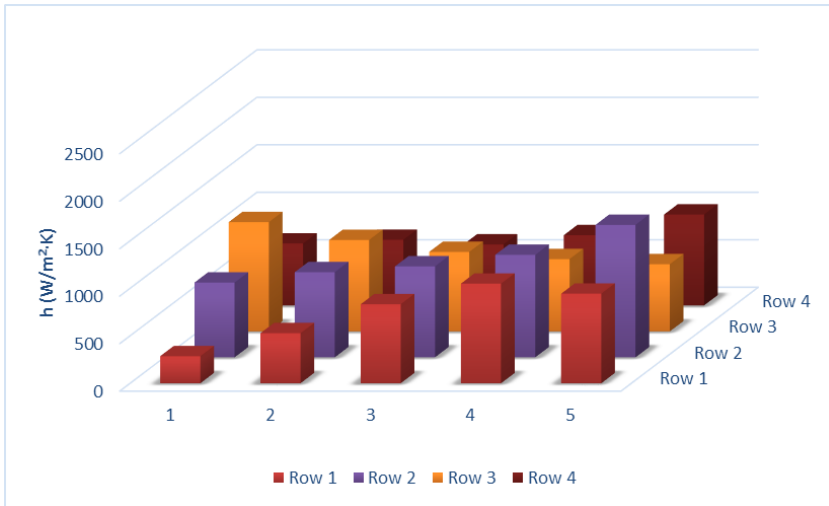
Case 3. 30 °C to 25 °C and $v_i=5$ m/s

The velocity, temperature and pressure contours are shown in the subsequent Figures.



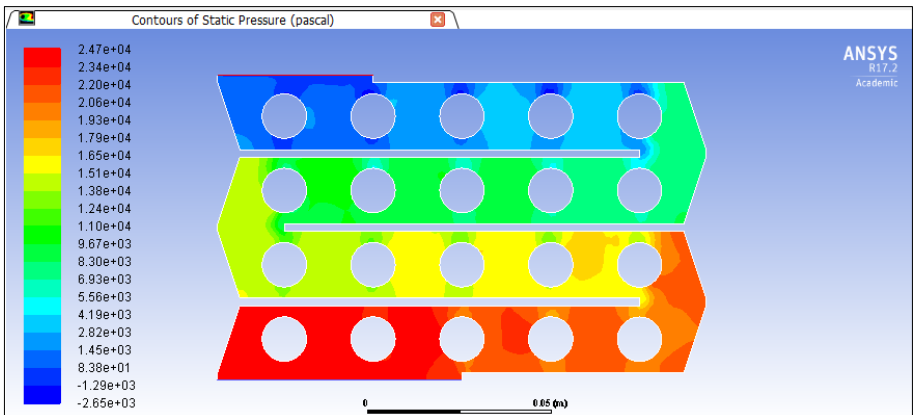
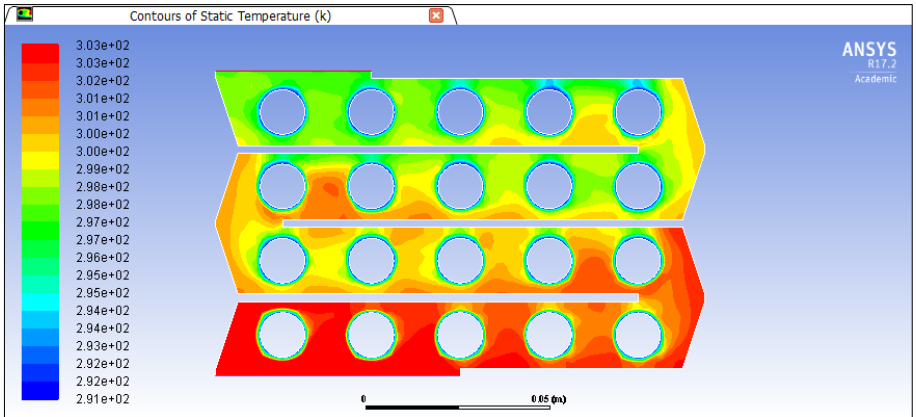
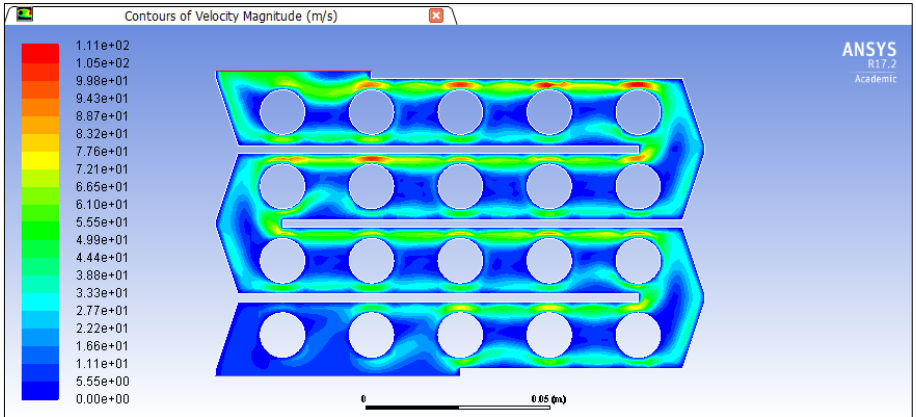
The values of h on each tube of the design are listed and illustrated in the table and figure below.

h ($W/m^2 \cdot K$)	Row 1	Row 2	Row 3	Row 4
1	284.8	786.7	1150.3	652.0
2	527.1	896.6	961.7	690.7
3	832.1	957.9	836.7	641.8
4	1048.6	1079.4	760.6	739.3
5	943.1	1394.4	706.5	956.8



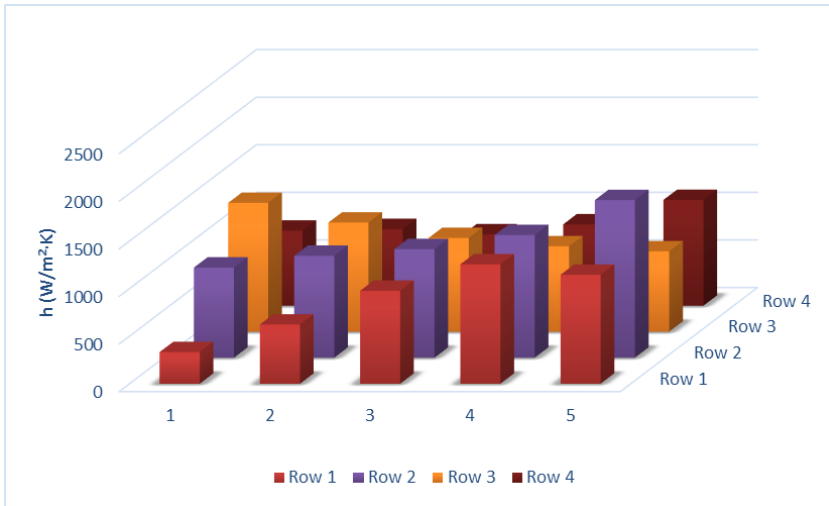
Case 4. 30 °C to 25 °C and $v_i=6$ m/s

The velocity, temperature and pressure contours are shown in the subsequent Figures.



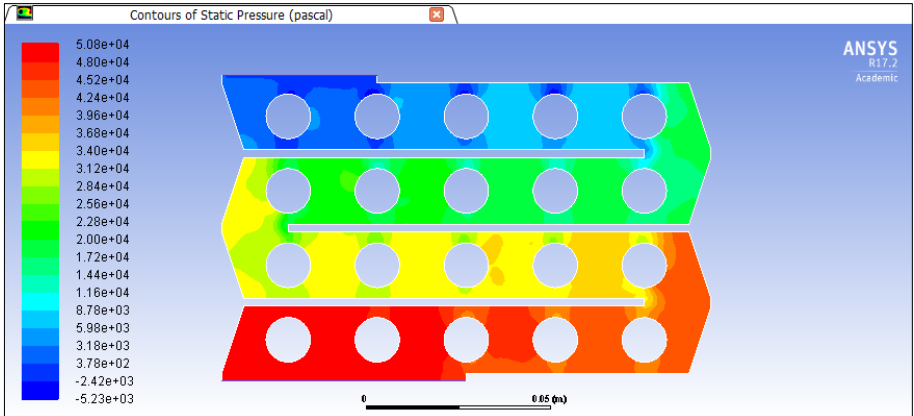
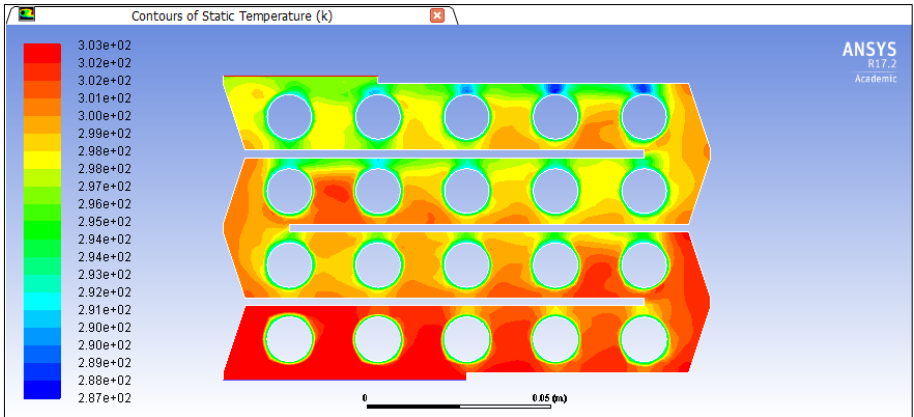
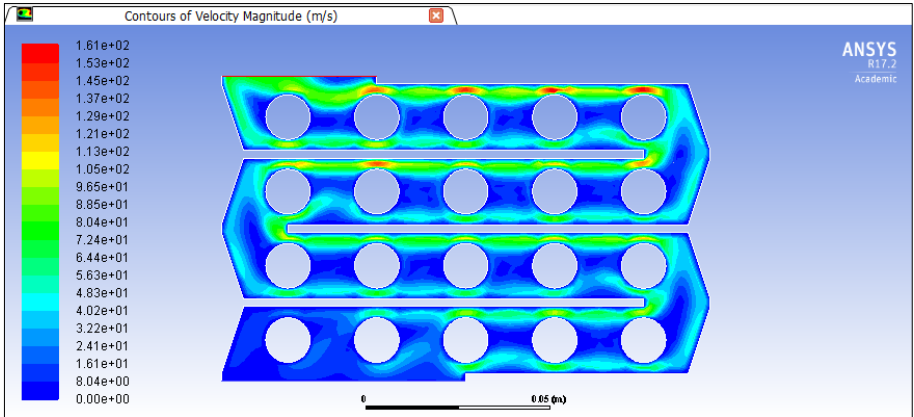
The values of h on each tube of the design are listed and illustrated in the table and figure below.

h ($W/m^2 \cdot K$)	Row 1	Row 2	Row 3	Row 4
1	332.6	947.2	1354.5	788.5
2	622.0	1070.9	1147.0	805.2
3	976.7	1141.3	985.3	749.6
4	1254.7	1289.2	897.5	854.7
5	1144.8	1656.9	844.3	1111.0



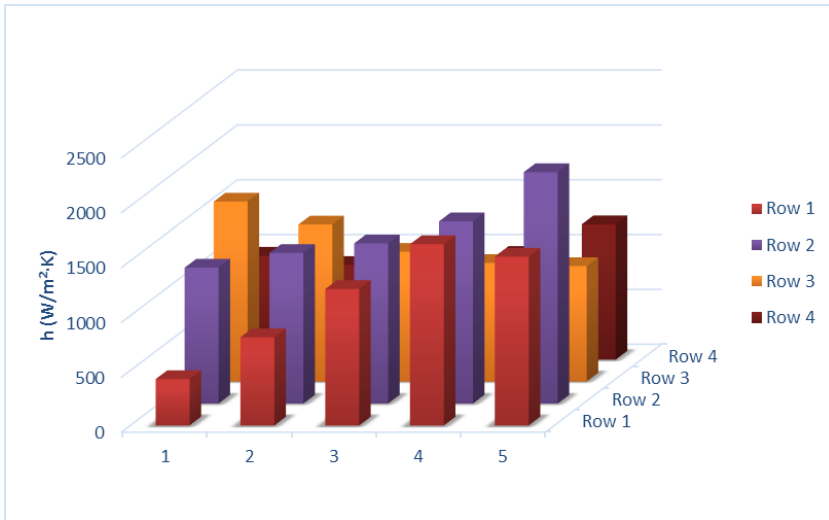
Case 5. 30 °C to 25 °C and $v_i=7.5$ m/s

The velocity, temperature and pressure contours are shown in the subsequent Figures.



The values of h on each tube of the design are listed and illustrated in the table and figure below.

h ($W/m^2 \cdot K$)	Row 1	Row 2	Row 3	Row 4
1	422.6	1239.0	1640.9	947.5
2	803.8	1373.0	1431.7	863.3
3	1244.1	1459.9	1182.9	849.2
4	1652.7	1661.0	1081.3	955.2
5	1539.1	2109.0	1052.9	1234.1

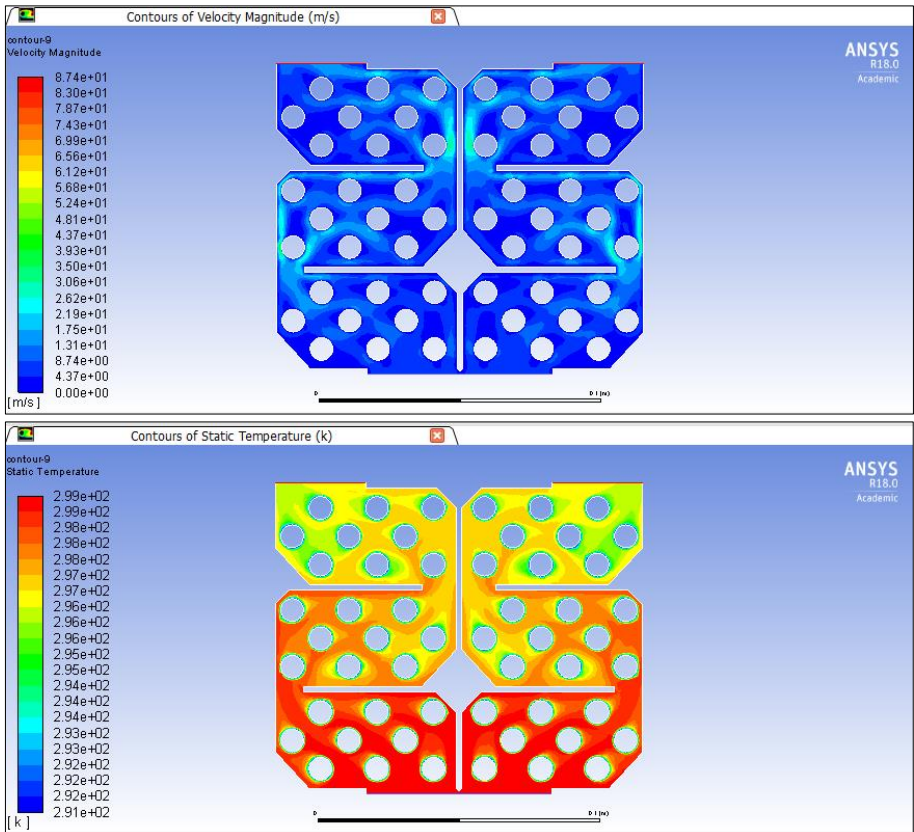


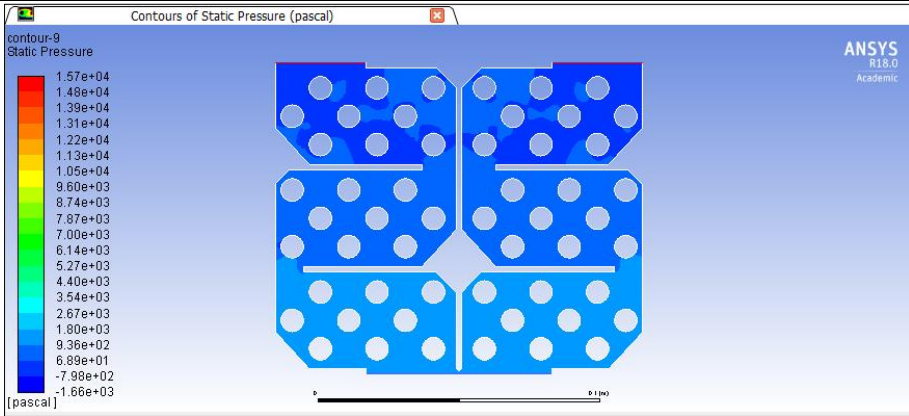
APPENDIX 4. FINAL DESIGN 14 USING ANSYS®

This appendix is divided in the different boundary conditions used on each case.

Case 1. 26 °C to 23 °C and $v_i = 5$ m/s

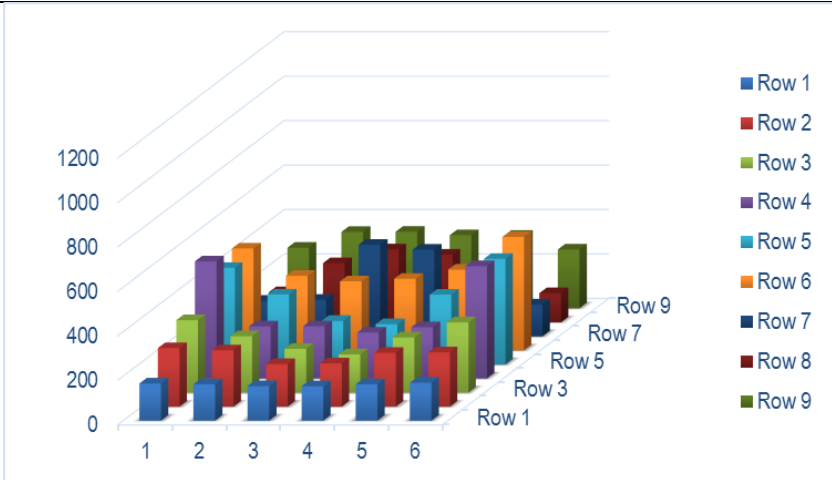
The velocity, temperature and pressure contours are shown in the subsequent Figures.





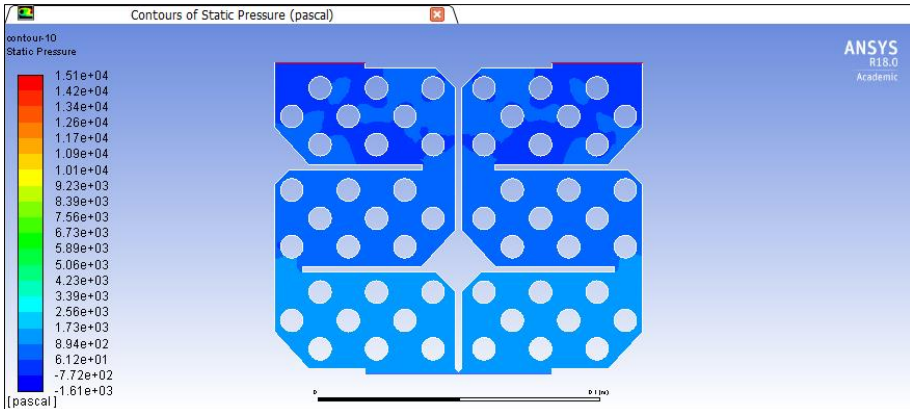
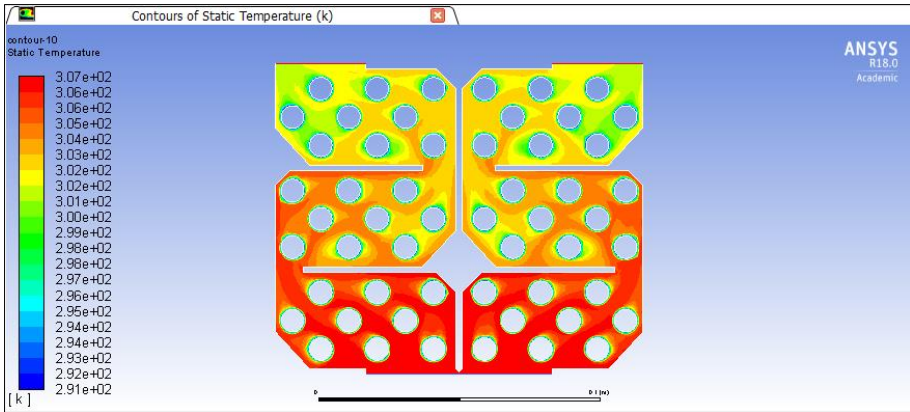
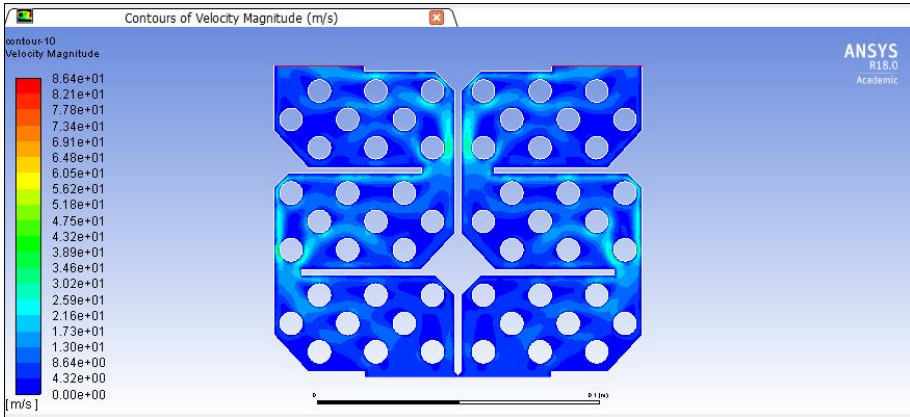
The values of h on each tube of the design are listed and illustrated in the table and figure below.

h (W/m ² ·K)	Row 1	Row 2	Row 3
1	167.3	263.1	325.8
2	163.9	253.4	253.2
3	155.4	191.4	196.8
4	154.7	194.6	171.6
5	163.8	242.0	247.7
6	170.2	244.2	315.5
h (W/m ² ·K)	Row 4	Row 5	Row 6
1	526.8	434.4	458.5
2	234.4	314.8	335.6
3	234.8	196.0	310.9
4	206.8	181.3	322.1
5	230.8	314.2	363.4
6	505.4	475.1	510.7
h (W/m ² ·K)	Row 7	Row 8	Row 9
1	160.3	135.6	272.4
2	165.0	266.3	343.9
3	411.8	328.5	344.4
4	390.0	304.4	328.9
5	146.1	257.4	326.1
6	142.9	131.1	264.6



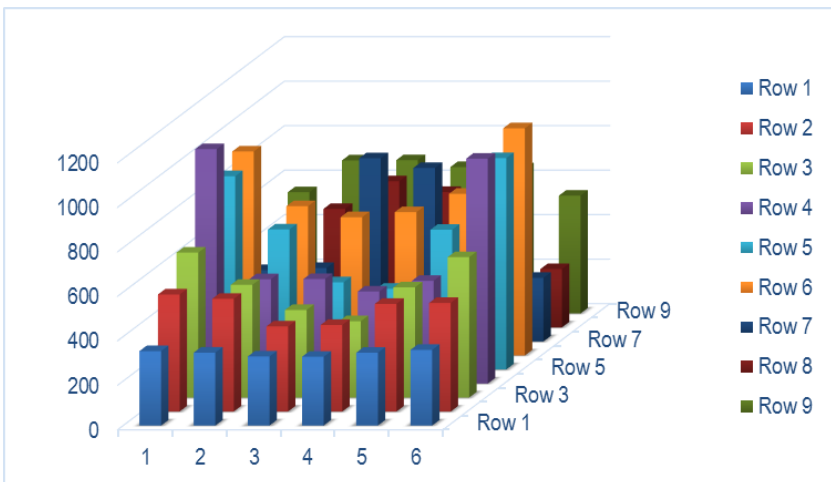
Case 2. 34 °C to 27 °C and $v_i=5$ m/s

The velocity, temperature and pressure contours are shown in the subsequent Figures.



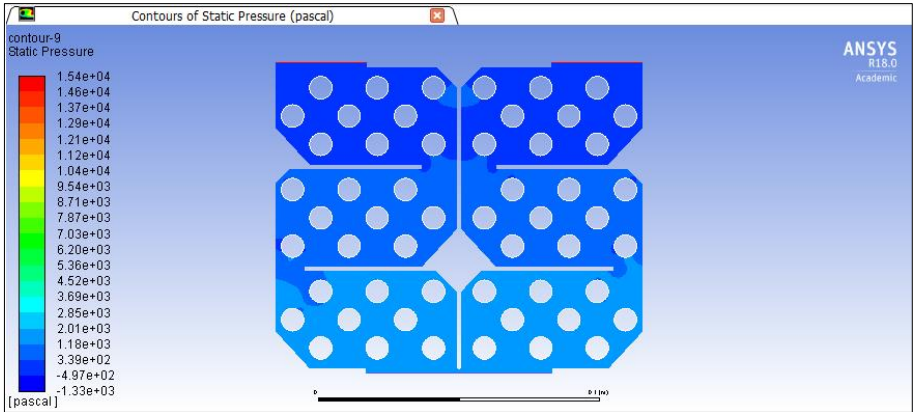
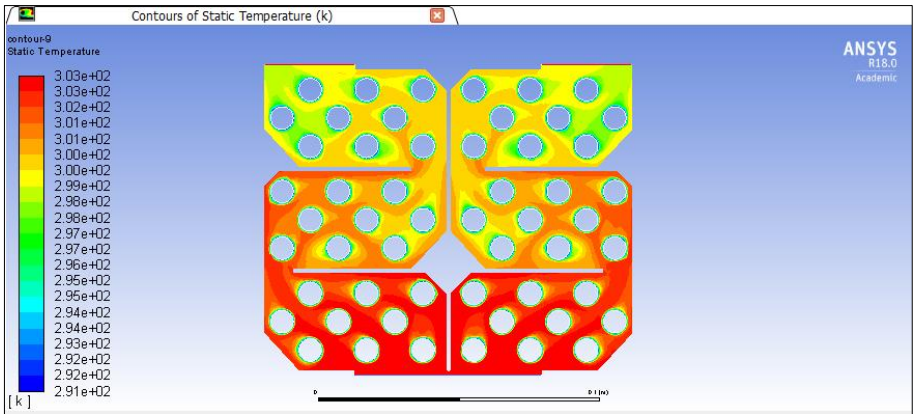
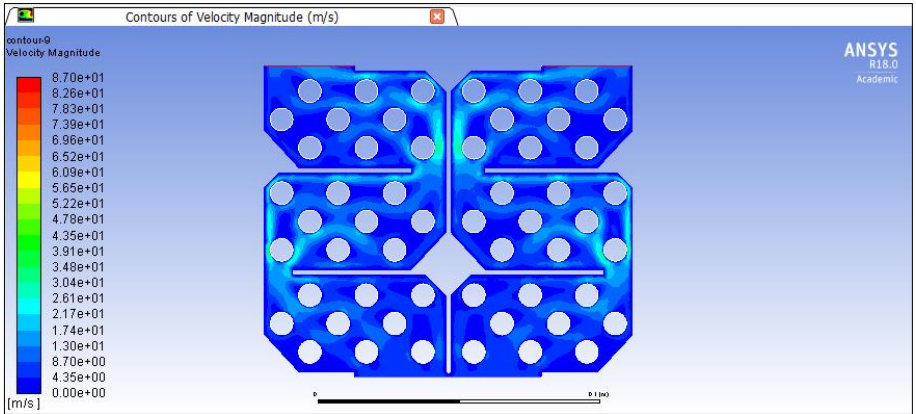
The values of h on each tube of the design are listed and illustrated in the table and figure below

h ($W/m^2 \cdot K$)	Row 1	Row 2	Row 3
1	334.5	526.3	651.5
2	327.8	506.7	506.5
3	310.8	382.8	393.6
4	309.4	389.2	343.2
5	327.5	483.9	495.4
6	340.3	488.4	631.0
h ($W/m^2 \cdot K$)	Row 4	Row 5	Row 6
1	1053.6	868.8	917.0
2	468.7	629.6	671.3
3	469.6	392.1	621.7
4	413.5	362.6	644.5
5	461.6	628.3	726.9
6	1010.8	950.3	1021.4
h ($W/m^2 \cdot K$)	Row 7	Row 8	Row 9
1	320.6	271.2	544.8
2	330.0	532.6	687.8
3	823.6	657.0	688.8
4	779.9	608.7	657.8
5	292.2	514.7	652.3
6	285.7	262.3	529.3



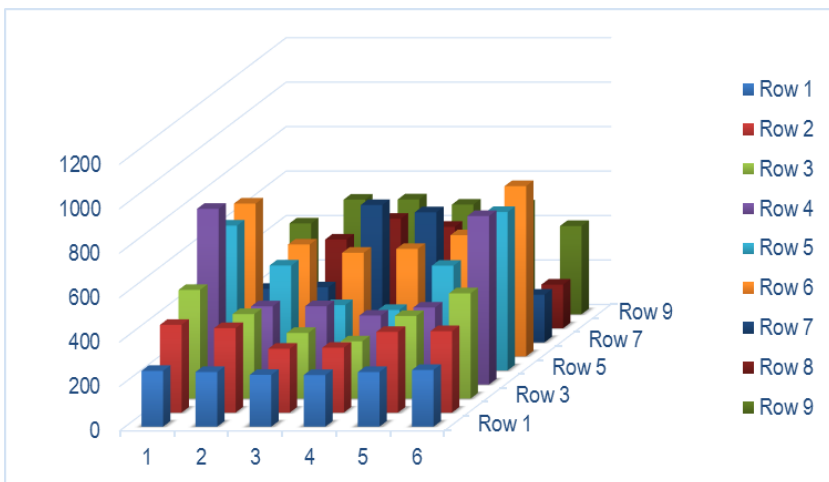
Case 3. 30 °C to 25 °C and $v_i = 5 \text{ m/s}$

The velocity, temperature and pressure contours are shown in the subsequent Figures.



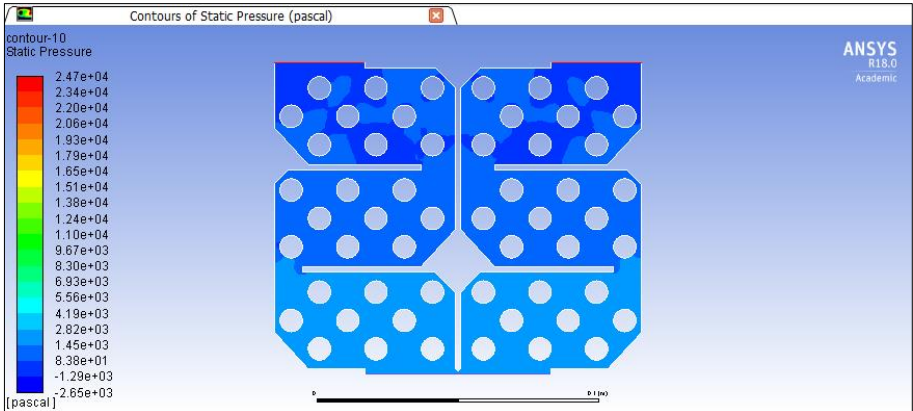
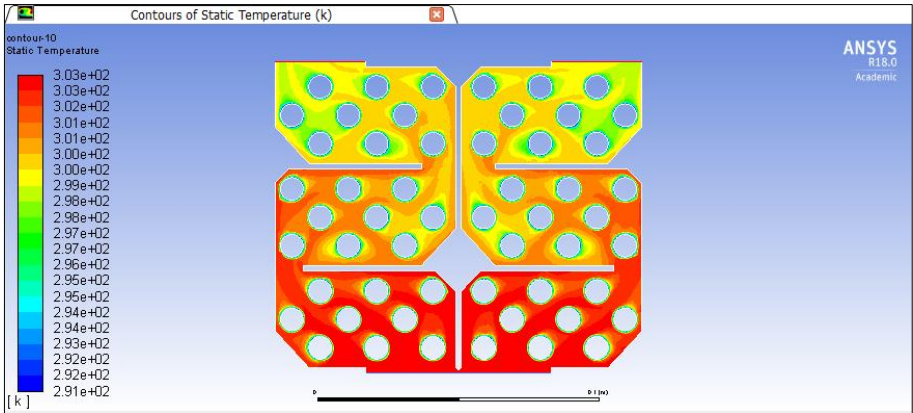
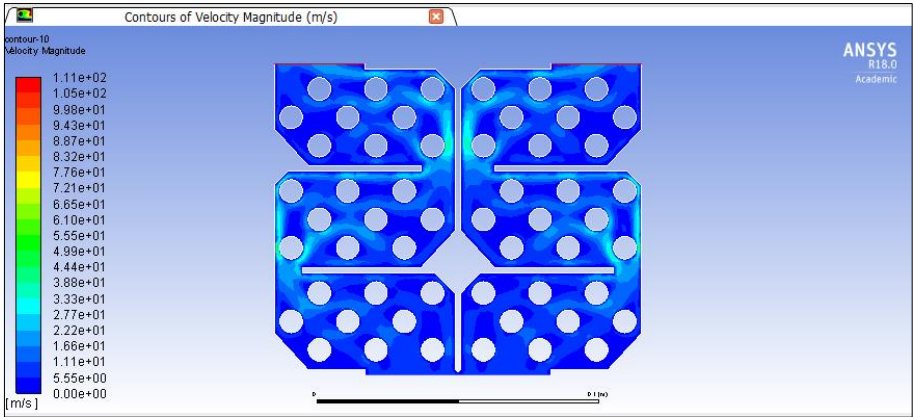
The values of h on each tube of the design are listed and illustrated in the table and figure below

h ($W/m^2 \cdot K$)	Row 1	Row 2	Row 3
1	250.9	394.7	488.6
2	245.9	380.1	379.9
3	233.1	287.1	295.2
4	232.0	291.9	257.4
5	245.7	362.9	371.6
6	255.2	366.3	473.2
h ($W/m^2 \cdot K$)	Row 4	Row 5	Row 6
1	790.2	651.6	687.7
2	351.5	472.2	503.4
3	352.2	294.1	466.3
4	310.2	272.0	483.3
5	346.2	471.2	545.2
6	758.1	712.7	766.0
h ($W/m^2 \cdot K$)	Row 7	Row 8	Row 9
1	240.5	203.4	408.6
2	247.5	399.4	515.8
3	617.7	492.8	516.6
4	584.9	456.6	493.4
5	219.1	386.1	489.2
6	214.3	196.7	396.9



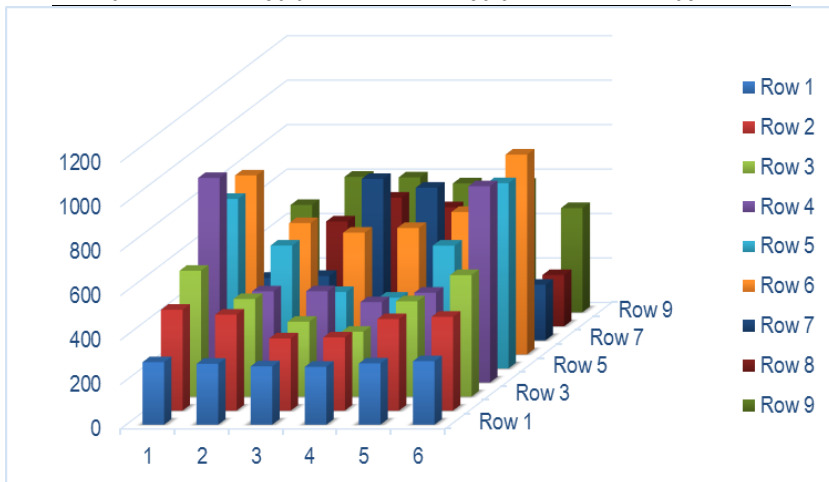
Case 4. 30 °C to 25 °C and $v_i=6$ m/s

The velocity, temperature and pressure contours are shown in the subsequent Figures.



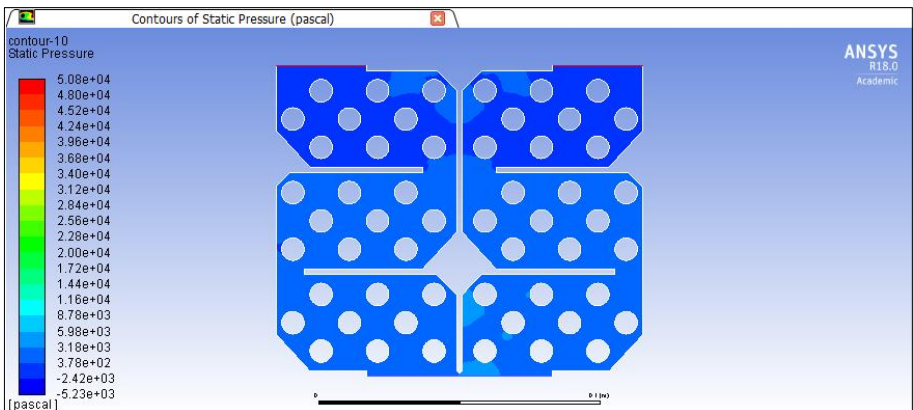
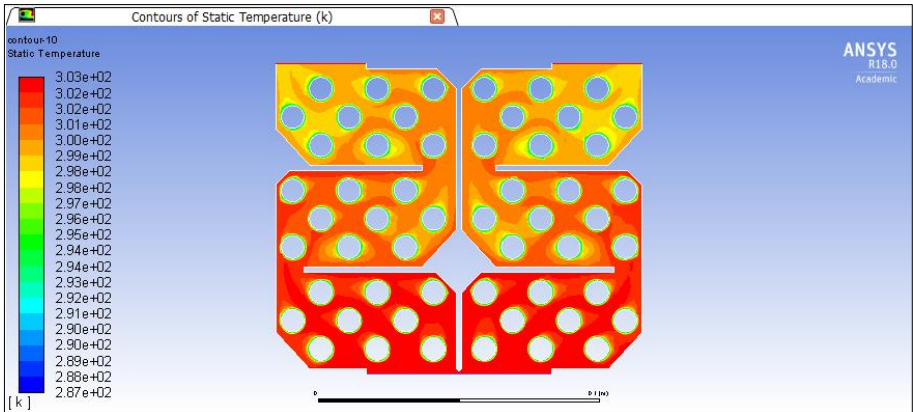
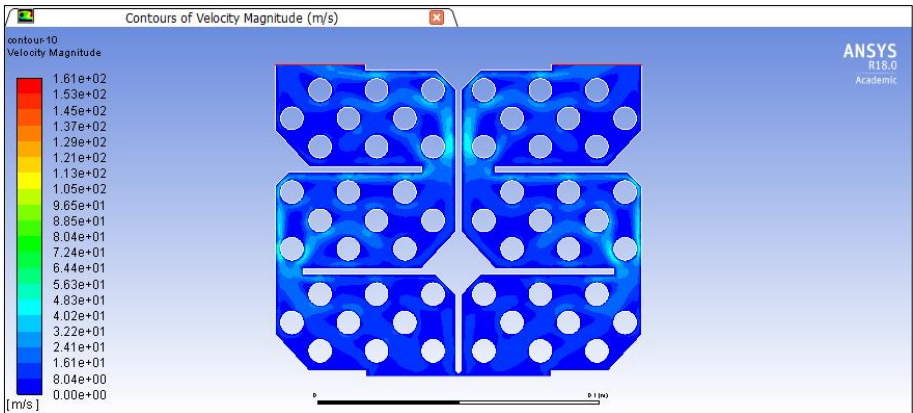
The values of h on each tube of the design are listed and illustrated in the table and figure below

h ($W/m^2 \cdot K$)	Row 1	Row 2	Row 3
1	281.0	453.7	565.9
2	273.8	431.5	438.9
3	262.3	324.7	336.6
4	260.1	329.3	291.6
5	275.3	411.5	428.4
6	285.4	421.7	546.4
h ($W/m^2 \cdot K$)	Row 4	Row 5	Row 6
1	920.2	762.7	805.0
2	409.9	552.9	590.6
3	410.5	343.7	547.5
4	361.2	318.3	568.7
5	403.8	552.6	640.9
6	883.0	833.5	898.7
h ($W/m^2 \cdot K$)	Row 7	Row 8	Row 9
1	281.0	238.3	482.6
2	289.8	471.3	609.5
3	726.4	578.5	606.7
4	686.5	535.4	579.5
5	256.0	455.2	577.6
6	250.0	230.6	468.7



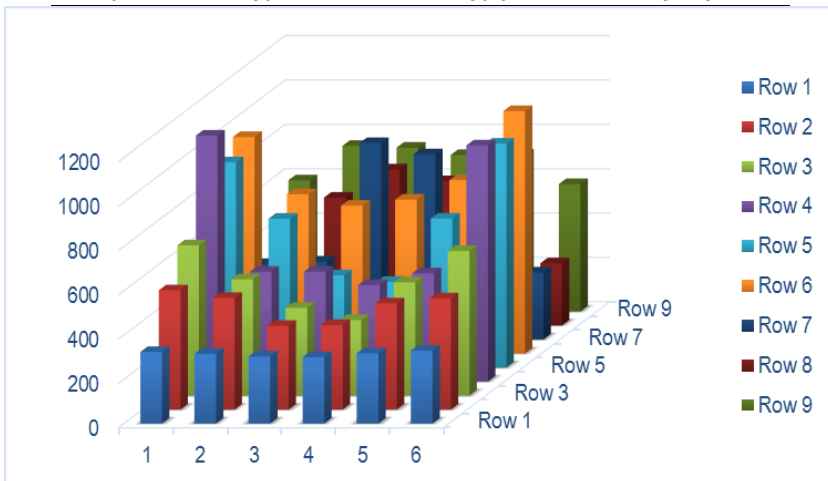
Case 5. 30 °C to 25 °C and $v_i=7.5$ m/s

The velocity, temperature and pressure contours are shown in the subsequent Figures.



The values of h on each tube of the design are listed and illustrated in the table and figure below

h ($W/m^2 \cdot K$)	Row 1	Row 2	Row 3
1	323.0	537.9	677.8
2	314.7	503.8	524.3
3	302.8	377.6	395.4
4	299.7	381.5	340.6
5	316.8	479.2	510.6
6	328.7	501.7	652.1
h ($W/m^2 \cdot K$)	Row 4	Row 5	Row 6
1	1109.6	925.6	976.7
2	495.4	671.2	718.6
3	495.4	416.3	667.0
4	435.3	386.3	694.3
5	488.1	672.0	781.9
6	1065.2	1010.4	1093.5
h ($W/m^2 \cdot K$)	Row 7	Row 8	Row 9
1	340.3	289.5	591.6
2	352.1	577.0	747.5
3	886.2	704.2	738.9
4	835.5	651.1	705.9
5	310.3	557.1	707.9
6	302.2	280.6	574.5



APPENDIX 5. NON-CONVERGING RESULTS

The results of the non-converging simulations carried out when the element size was decreased are shown below.

